AFRL-RH-FS-TR-2018-0025

Simulated Supercontinuum Generation in the Human Eye from 1200 nm to 1400 nm

Christopher B. Marble
Consortium Research Fellows Program

Andrew W. Wharmby
711th Human Performance Wing
Airman Systems Directorate
Bioeffects Division
Optical Radiation Bioeffects Branch

October 2018

Interim Report - April 1, 2018 to October 15, 2018

<u>**DESTRUCTION NOTICE**</u> **- Destroy by any method that will prevent disclosure of contents or reconstruction of this document.**

Distribution A: Approved for public release; distribution unlimited. PA Case No: TSRL-PA-2019-0114

Air Force Research Laboratory
711th Human Performance Wing
Airman Systems Directorate
Bioeffects Division
Optical Radiation Bioeffects Branch
JBSA Fort Sam Houston, Texas 78234

NOTICE AND SIGNATURE PAGE

"Simulated Supercontinuum Generation in the Human Eye from 1200 nm to 1400 nm"

(AFRL-RH-FS-TR- 2018 - 0025) has been reviewed and is approved for publication in accordance with assigned distribution statement.

Digitally signed by SHORTER.PATRICK.D.1023156390
Date: 2018.11.19 14:17:26 -06'00'

PATRICK SHORTER, Major, USAF
Chief, Optical Radiation Bioeffects Branch

PUTNAM.CHRISTOPHER.M.1273958769

Digitally signed by PUTNAM.CHRISTOPHER.M.1273958769
Date: 2018.12.03 14:11:18 -06'00'

CHRISTOPHER M. PUTNAM, Lt Col, USAF, BSC
Deputy Chief, Bioeffects Division
Airman Systems Directorate
711th Human Performance Wing
Air Force Research Laboratory

REPORT DOCUMENTATION PAGE

Form Approved OMB No. 0704–0188

1. REPORT DATE *(DD–MM–YYYY)*	2. REPORT TYPE	3. DATES COVERED *(From — To)*
10/01/2018	Interim Report	April 1, 2018 to October 15, 2018

4. TITLE AND SUBTITLE

Simulated Supercontinuum Generation in the Human Eye from 1200 nm to 1400 nm

5a. CONTRACT NUMBER
FA8650-14-D-6519

5b. GRANT NUMBER

5c. PROGRAM ELEMENT NUMBER

6. AUTHOR(S)

Christopher B Marble, Andrew W. Wharmby

5d. PROJECT NUMBER

5e. TASK NUMBER

5f. WORK UNIT NUMBER
H0RY

7. PERFORMING ORGANIZATION NAME(S) AND ADDRESS(ES)
Air Force Research Laboratory
711th Human Performance Wing
Airman Systems Directorate
Bioeffects Division
Optical Radiation Bioeffects Branch

8. PERFORMING ORGANIZATION REPORT NUMBER

9. SPONSORING / MONITORING AGENCY NAME(S) AND ADDRESS(ES)
Air Force Research Laboratory
711th Human Performance Wing
Airman Systems Directorate
Bioeffects Division
Optical Radiation Bioeffects Branch

10. SPONSOR/MONITOR'S ACRONYM(S)
711 HPW/RHDO

11. SPONSOR/MONITOR'S REPORT NUMBER(S)
AFRL-RH-FS-TR-2018-0025

12. DISTRIBUTION / AVAILABILITY STATEMENT

Distribution A: Approved for public release; distribution unlimited. PA Case No: TSRL-PA-2019-0114

13. SUPPLEMENTARY NOTES

14. ABSTRACT

To understand the possible eye safety implications of supercontinuum generation in the human eye, a one-dimensional simulation was created by extending a femtosecond wave propagator previously used by the Air Force Research Lab to incorporate phase-modulation and self-focusing effects. Simulation of femtosecond MPE limit pulses propagating in the human eye demonstrate multiple hazards not anticipated from longer pulse duration studies including: a hazard from the broad pulse bandwidth required to form femtosecond pulses, self-phase modulation generating shorter frequency light, and self-focusing generating plasma near the retina. These results provide guidance for future experimental studies of retinal exposure to femtosecond pulses and lay the foundation for future two-dimensional modeling of nonlinear effects in the human eye.

15. SUBJECT TERMS

16. SECURITY CLASSIFICATION OF: a. REPORT	b. ABSTRACT	c. THIS PAGE	17. LIMITATION OF ABSTRACT	18. NUMBER OF PAGES	19a. NAME OF RESPONSIBLE PERSON / 19b. TELEPHONE NUMBER *(include area code)*
U	U	U	U	95	Andrew Wharmby / 210-539-8284

This Page Intentionally Left Blank

TABLE OF CONTENTS

LIST OF FIGURES

LIST OF TABLES

LIST OF EQUATIONS

ACKNOWLEDGEMENTS

The authors thank Dr. Benjamin Rockwell, Dr. Robert Thomas, and Mr. Gary Noojin for their helpful comments and advice. Christopher Marble thanks his advisor at Texas A&M University, Dr. Vladislav Yakovlev, for his guidance on this project.

This research was supported by the Consortium Research Fellows Program, Texas A&M University and the United States Air Force Research Laboratory.

1.0 SUMMARY

The American National Standards Institute (ANSI) Z136.1-2014 eye safety standards have been determined from experimental studies of laser exposure with pulse durations ranging from 100 femtosecond (fs) to several seconds [1]. A previous experimental study propagated 35 fs, 1200 to 1400 nanometer (nm) pulses with pulse energies under the ANSI Maximum Permissible Exposure (MPE) limit in water [2]. The propagated pulses were observed to undergo supercontinuum generation including a visible wavelength component. Since the aqueous and vitreous humors of the eye are, to a first approximation, water this experiment raised concerns that supercontinuum generation could occur in the eye for infrared pulses under the MPE limit. To understand the possible eye safety implications of supercontinuum generation in the human eye, a one-dimensional simulation was created by extending a femtosecond wave propagator previously used by the Air Force Research Laboratory (AFRL) to incorporate phase-modulation and self-focusing effects. By incorporating these nonlinear optical effects, it was found that the strong visible light generation reported in the water experiment was a result of the pulse self-focusing until ionizing the water into plasma. Simulation of femtosecond MPE limit pulses propagating in the human eye demonstrate multiple hazards not anticipated from longer pulse duration studies including: a hazard from the broad pulse bandwidth required to form femtosecond pulses, self-phase modulation generating shorter frequency light, and self-focusing generating plasma near the retina. These effects result in hazardous retinal exposures for 35 fs to 100 fs pulses with wavelengths from 1350 nm to 1399 nm. MPE pulses from 1200 nm to 1300 nm are not observed to be retinal hazards for pulse durations as small as 35 fs. Pre-focusing the pulse resulted in worse retinal exposures including plasma generation near the retinal plane for 100 fs pulses from 1300 nm to 1399 nm. Negatively chirping the pulse to correct for chromatic dispersion did not result in an increased retinal hazard. These results will provide guidance for future experimental studies of retinal exposure to femtosecond pulses and lay the foundation for future two-dimensional modeling of nonlinear effects in the human eye.

In Section 2, the current MPE limits under the ANSI standard are discussed and results of the previous water experiment summarized. The nonlinear optical properties of water are briefly introduced in Section 2.1. In Section 2.2, the reduced eye model is introduced and the importance of the chromatic aberration in understanding infrared pulse focusing in the eye is discussed. In Section 2.3, phase modulation and supercontinuum generation are outlined and the expected frequency broadening is solved for a simplified analytical case. Self-focusing and plasma generation are the subject of Section 2.4 which becomes relevant when interpreting the water experiment and reduced eye model in the results section. Sections 2.5 and 2.6 outline the previous pulse propagation model and current model respectively. The sections that follow discuss effects that are not simulated such as thermal effects (Section 2.7) and other nonlinear effects (Section 2.8). The introduction then concludes with a review of eye safety hazards (Section 2.9). The methods section is separated into sub-sections discussing general propagation methods (Section 3.1), simulation set-up for comparison against the water experiment (Section 3.2), and the reduced eye model using unchirped and chirped pulses (Sections 3.3 and 3.4). A method to "score" eye hazards from the simulation is presented in Section 3.5. The methods section concludes with the description of two convergence tests performed to determine the sensitivity of the simulation results to a change in simulation parameters (Section 3.6). The results are similarly divided into sub-sections regarding simulation of the water experiment (Section 4.1), simulation of a MPE pulse entering the eye (Section 4.2), and the results of the convergence tests (Section 4.3). The overall report concludes with further discussion of the risks of unexpected eye hazards from ultrashort, femtosecond pulses and proposes areas of interest for future experiments and simulation. Tables documenting the pulse characteristics at the retinal plane under different simulated conditions are provided in Appendix A. The MATLAB simulation code for the water experiment and human eye are provided in Appendix B.

2.0 INTRODUCTION

The laser eye safety standard ANSI Z136.1 was updated in 2014 in response to experimental studies of retinal hazards ranging from continuous wave exposures of multiple seconds to ultrashort 100 fs pulses [1]. In these studies, the minimum exposures for visible lesions to appear in retinal tissues were measured. One result of the 2014 update was the increase in minimum permissible exposures in the 1300 nm to 1400 nm region by as much as three orders of magnitude. This decision was based on studies of nanosecond to second pulses in the 1300 nm to 1400 nm region [1]. Shorter pulse duration studies were limited to wavelengths less than or equal to 1064 nm and have not been studied in the 1300 nm to 1400 nm region [3]–[17]. Intense, ultrashort (< 100 ps) pulses can undergo nonlinear processes resulting in unanticipated retinal hazards [18]. Due to the high pulse intensities required for nonlinear processes to occur, concerns about nonlinear effects have been raised for wavelengths above 1200 nm. Wavelengths above 1200 nm have higher MPEs in nanosecond to second studies due strong absorption by the aqueous and vitreous humors of the eye [2]. Of concern are nonlinear processes such as supercontinuum generation and harmonic generation where an incident infrared pulse can be converted into a visible pulse that can reach the retina without being absorbed. A preliminary study of supercontinuum generation in water was conducted (Figure 1) [2] in response to this concern. Results from this study suggested that laser pulses in the 1200 nm to 1400 nm region (Figure 2 top) could be spectrally broadened into visible pulses (Figure 2 bottom) resulting in retinal damage. The supercontinuum threshold reported was far below the ANSI MPE for 100 fs pulses (Equation 1) in the near-infrared (near-IR) (Figure 3). The study was complicated by the effects of other nonlinear processes in the media, particularly self-focusing which will be addressed in section 2.4.

$$MPE = 0.1 * (8 + 10^{0.04(\lambda - 1250)})\ uJ/cm^2, 1200\ nm \leq \lambda < 1400\ nm \qquad (1)$$

Equation 1. ANSI MPE for 100 fs to 10 ps Pulses from 1200 nm to 1400 nm

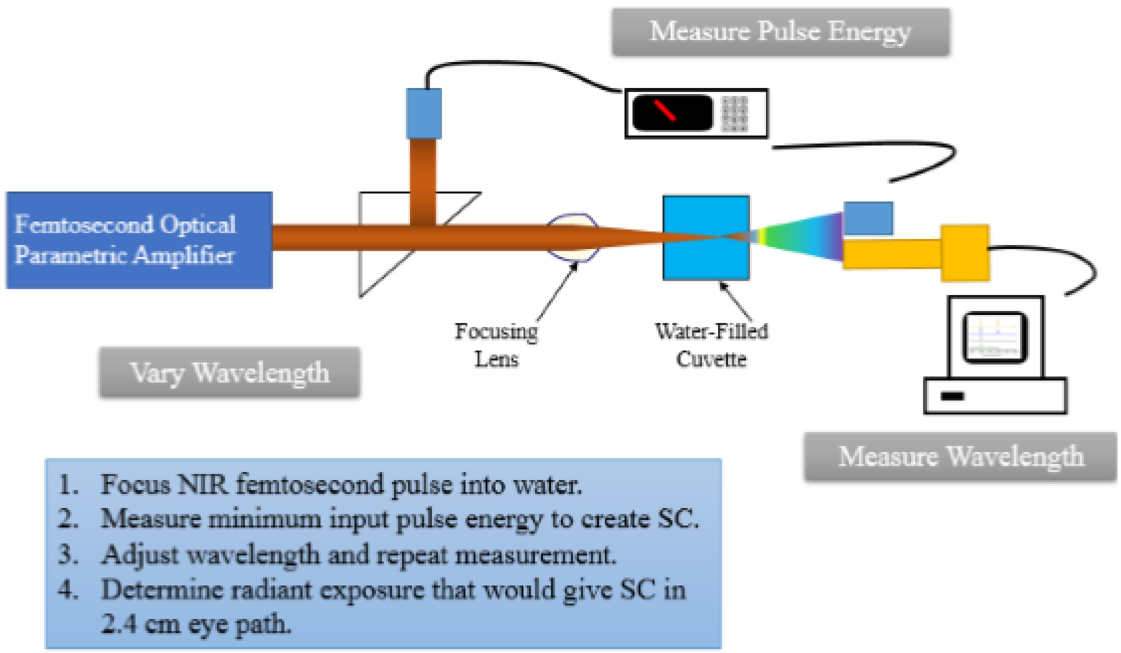

Figure 1. Set-up of Water Experiment. Figure 7.1 from [2].

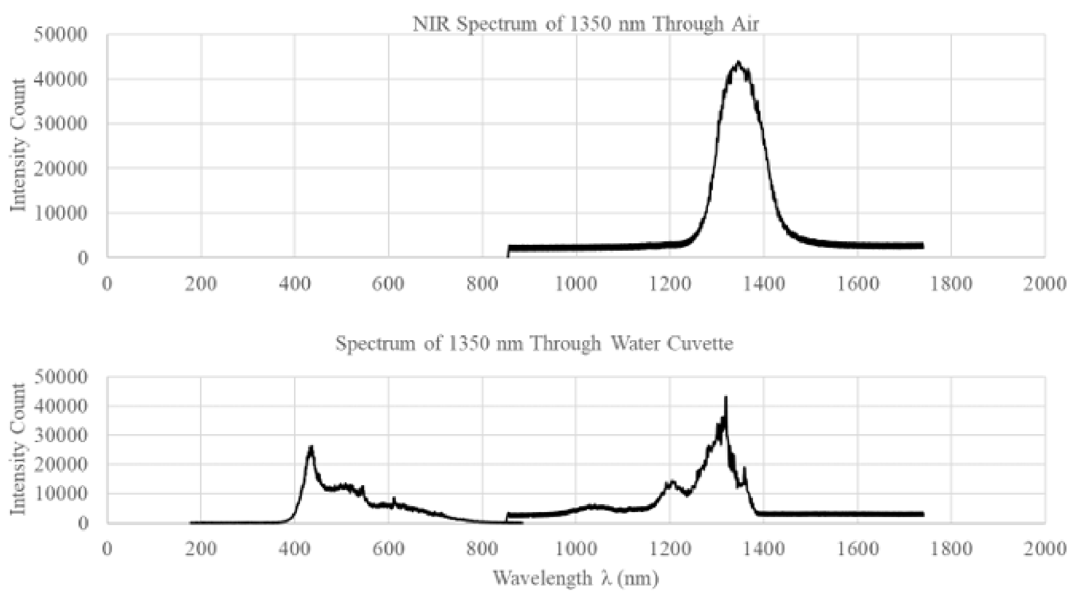

Figure 2. Visible Light Generation Due to Supercontinuum in Water [2]. The top graph shows the pulse spectra prior to entering the water medium. The bottom graph shows the spectra after passing through the water medium.

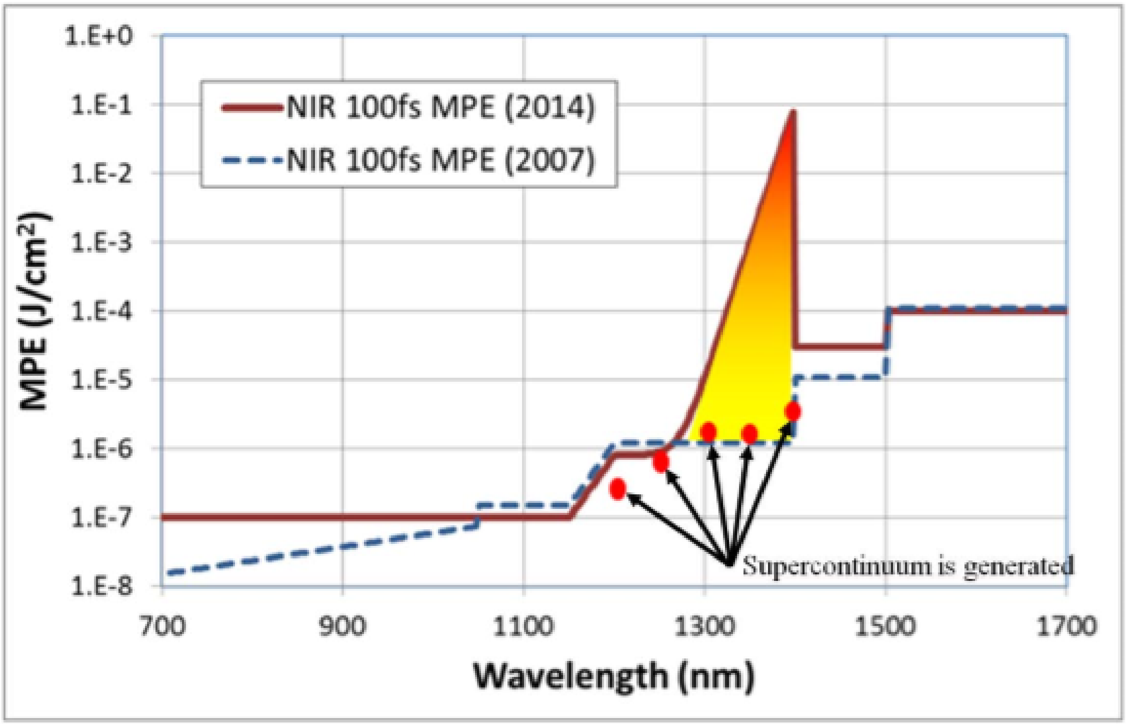

Figure 3. ANSI MPE Limits Versus Experimental Supercontinuum Thresholds. The ANSI-Z136.1-2007 and -2014 MPE limits for 100 fs pulses compared to the supercontinuum generation thresholds for 35 fs pulses. Figure is a reprint of Figure 9.15 in [2].

2.1 Nonlinear Optical Properties

Nonlinear optical effects such as supercontinuum generation and harmonic generation are byproducts of the dependence of the optical properties of media on the electric field strength of the pulse propagating through the medium. For a pulse propagating in a centrosymmetric medium like liquid water, the index of refraction and absorption coefficient can be approximated by [19]

$$n(I) \approx n_0 + n_2 I \tag{2}$$

Equation 2. Approximate Index of Refraction of Water

$$\alpha(I) \approx \alpha_0 + \beta I \tag{3}$$

Equation 3. Approximation of Absorption in Water

using linear refractive index (n_0), linear absorption (α_0), nonlinear refractive index (n_2), and nonlinear absorption (β).

The linear optical properties of water (n_0 and α_0) have been well studied in the 1200 nm – 1400 nm region [20]. In a previous report, the authors measured the nonlinear optical properties of water (n_2 and β), in the 1150 nm – 1400 nm region using 90 fs to 120 fs pulses [21].

2.2 The Reduced Eye Model

The human eye is a complex organ. To make computer simulations feasible the structure of the human eye must be simplified. The reduced eye model (REM) approximates the focusing components of the eye using a hemi-spherical lens with a radius of curvature (r_c) of 0.61 cm [22]. The REM reduces the tissues in the path length to four layers: the cornea (0.05 cm), aqueous humor (0.31 cm), lens (0.36 cm), and vitreous humor (1.72 cm) with the retinal layer located 2.44 cm [22].

To use the REM model to simulate near-IR light propagation to the retina, we must account for pulse dispersion, chromatic aberration, and absorption. A Sellmeier equation fit for the refractive index of REM tissues has been made that includes the wavelengths of interest [23]. To a reasonable approximation, the refractive index of the REM tissues can be estimated to be the refractive index of pure water [24]. The focal length of the eye is then be estimated to be

$$f_{lens} \approx r_c \frac{n(\lambda)}{n(\lambda) - 1} \tag{4}$$

Equation 4. Focal Length of Eye as a Function of Wavelength

It is critical to account for chromatic aberration in the eye since nonlinear optical processes are dependent on the beam intensity through the beam path. The human eye brings light with wavelength of 589 nm to a focus at the retinal plane. Chromatic aberration results in infrared pulses being focused beyond the retinal plane [23]. The resulting correction to the focusing geometry increases the beam diameter at the retinal plane. For example, assuming no aberrations for a 589 nm pulse with an initial diameter of 4.24 mm, the 589 nm pulse would focus to a beam diameter of 4.3 µm at the retinal plane. A 1400 nm pulse would only focus to a beam diameter of 190 µm before reaching the retinal plane as the focal point for mid-IR radiation is behind the retina. Failure to account for chromatic aberration would result in a three order of magnitude overestimate of beam intensity at the retinal plane.

Absorption in the REM tissues prior to the retina transitions from negligible to strong in the 1200 nm to 1400 nm region. The absorption coefficients of the cornea, aqueous humor, lens and vitreous humor have been measured in the 1200 nm to 1400 nm range [25]. Like the refractive index, the absorption coefficients of the cornea, aqueous and vitreous humors can be approximated to be water's absorption coefficient for all wavelengths of interest. The exception is the lens of the eye which is less strongly absorbing than other

REM tissues [20], [24], [25].

2.3 Phase Modulation and Supercontinuum Generation

The absorptive nature of the eye above 1200 nm reduces the beam power by orders of magnitude prior to reaching the retina. This fact underlies the generally higher MPE for near-IR pulses than visible pulses of equivalent pulse duration. Self-phase modulation (SPM) and cross-phase modulation (XPM) are nonlinear processes than can convert near-IR radiation to shorter, less strongly absorbed, wavelengths. In the case of SPM, a high intensity pulse modifies the refractive index of the media it is passing through (neglecting absorption for simplicity). The time varying refractive index of the media then in turn modifies the constituent frequencies of the pulse resulting in frequency broadening [26].

For a pulse propagating through a medium with a uniform linear and nonlinear refractive index we recall the phase of the pulse (ϕ) with a central frequency (ω_0) (and central wavelength (λ_0)) to be

$$\phi(t,L) = \omega_0 t - kL = \omega_0 t - \frac{2\pi}{\lambda_0} n(t)L \tag{5}$$

Equation 5. Phase of Pulse

where L is the distance to the point in the medium you are observing and k is the wavenumber. Hence the instantaneous frequency shift ($\Delta\omega$) can be calculated from

$$\omega(t) = \frac{d\phi}{dt} = \omega_0 - \frac{2\pi L}{\lambda_0}\frac{dn}{dt} \tag{6}$$

Equation 6. Pulse Frequency

For an oversimplified example of the effect, we can assume a Gaussian intensity distribution $I(t) = I_0 Exp[-\frac{t^2}{\tau^2}]$ where τ is determined by the time duration. From this assumption and Equation 2 the frequency shift can be calculated

$$\Delta\omega(t) = \omega(t) - \omega_0 = -\frac{2\pi L n_2 I_0}{\lambda_0} Exp[-\frac{t^2}{\tau^2}] \tag{7}$$

Equation 7. Pulse Frequency Shift

The maximum frequency shift occurs at $t = \pm\frac{\tau}{\sqrt{2}}$. We observe from equation Equation 7 that the frequency shift broadens the pulse frequency towards longer and shorter wavelengths. The maximum frequency shift would be

$$\Delta\omega_{max} = \frac{4\pi L n_2 I_0}{\lambda_0 \sqrt{2}} Exp[0.5] \tag{8}$$

Equation 8. Maximum Frequency Shift

This would result in a shift in wavelength toward the visible spectrum of

$$\Delta\lambda_{max} = \frac{2\pi\Delta\omega_{max}}{\omega_0(\omega_0 + \Delta\omega_{max})} \tag{9}$$

Equation 9. Maximum Wavelength Shift

As previously stated, the calculation greatly oversimplifies the problem. For femtosecond pulses group velocity dispersion (GVD) alters the intensity distribution of the pulse as it propagates through media [27]. If this dispersion is combined with SPM, the resulting broadband pulse can separate into distinct visible and near-IR pulses. At this point, the pulses would propagate independently. This is not true for high intensity pulses due to their influence on the refractive index of the media allowing for interaction between pulses. This interaction between two co-propagating pulses is called cross-phase modulation and results in additional frequency broadening beyond the anticipated SPM broadening [26].

2.4 Self-Focusing

Self-focusing can be viewed as a spatial analogue of SPM. In the case of SPM, the pulse frequency is modified due to the change in refractive index as a function of time. In contrast, self-focusing alters the beam width and focal point due to change in refractive index as a function of radial distance from the center of the pulse [19]. Consider a radial cross-section of a pulse propagating a length through water

$$\phi(r) = \frac{2\pi}{\lambda_0} n(r) L = \frac{2\pi}{\lambda_0} n_0 L + \frac{2\pi}{\lambda_0} n_2 I(r) L. \tag{10}$$

Equation 10. Radial Phase of Pulse

We can compare this radial phase to the radial phase imparted by a lens ($\phi_{lens}(r) = \frac{2\pi}{\lambda_0} n_{lens} L(r) + \frac{2\pi}{\lambda_0}(L - L(r))$). Rewriting the radial phase of the lens to isolate the radially dependent term ($\phi_{lens}(r) = \frac{2\pi}{\lambda_0} L + \frac{2\pi}{\lambda_0}(n_{lens} - 1)L(r)$). Neglecting the constant phase terms, we observe the $\frac{2\pi}{\lambda_0} n_2 I(r) L$ phase shift is mathematically equivalent to light propagating through a lens with a pathlength of $L(r) = \frac{n_2}{n_{lens}-1} I(r) L$.

We previously noted that chromatic dispersion results in near-IR pulses having much larger beam widths at the retina compared to visible pulses. Additionally, chromatic dispersion results in the beam not reaching its focal point where the beam would be more intense (resulting in more SPM). Hence, it is crucial to determine if self-focusing alters the beam path. The importance of self-focusing in the eye for ultrashort pulses has been the subject of previous research [28], [29]. Self focusing will also need to be considered when simulating the previous water study as the input pulse power in the study was above the critical power that is defined as

$$P_{crit} = \frac{\pi(0.61)^2 {\lambda_0}^2}{8n_0n_2} \tag{11}$$

Equation 11. Critical Power (SI Units)

Unfortunately for numerical simulation, self-focusing is an unstable phenomenon which cannot be easily controlled and is susceptible to random defects in the beam profile [26]. Calculations of self-focusing are limited in nature and simulations of laser pulse propagation can deviate from experimental studies where small irregularities in the beam are magnified through nonlinear processes [19].

The relationship between the beam power (P) and the critical power dictates which of three cases the beam path will follow. If the beam power is less than the critical power, the beam width at the focus (w_0) is decreased by [30]

$$w_{sf} \approx w_0\sqrt{1 - P/P_{crit}} \tag{12}$$

Equation 12. Beam Width at Focal Point with Self-Focusing

The focusing angle from self-focusing ($\theta_{nonlinear}$) can be estimated [19]

$$\theta_{nonlinear} = \sqrt{2n_2I/n_0} \tag{13}$$

Equation 13. Self-Focusing Angle

and the combined focusing angle from linear focusing (θ_{linear}) and self-focusing can also be estimated [19]

$$\theta_{total} = \sqrt{{\theta_{nonlinear}}^2 + {\theta_{linear}}^2}. \tag{14}$$

Equation 14. Total Focusing Angle

In the second case, $P \approx P_{crit}$, the beam initially focuses like case one but eventually becomes self-trapped. In this case, upon reaching a critical beam width (w_{crit}), the beam will propagate forward with a constant beam width. Self-focusing can move the focal point of the beam forward if $z_{sf} < z_{focus}$. Here, the position of the focus can be calculated using the beam width entering the media (w) and beam width at the low intensity focus (w_0) to be [19]

$$z_{sf} = \frac{0.5kw^2}{\sqrt{P/P_{crit} - 1} + z_{focus}/(0.5kw_0^2)}, \; P > P_{crit} \tag{15}$$

Equation 15. Distance to Self-Focusing Point

In the third case, $P >> P_{crit}$, irregularities in the beam profile are amplified by nonlinear processes such as four wave mixing which results in the beam breaking up into small, high intensity regions (filaments). This process is very dependent on the beam quality as a "clean" beam will have a much higher threshold to filament compared to a "dirty" beam resulting in an inherent beam factor (G) with values commonly between 3 and 10. The threshold for filamentation occurring prior to self-trapping is then $P/P_{crit} = 4G^2$ and the distance to the filamentation point is [19]

$$z_{fil} = \frac{G}{n_2 k_0 I}, \; P \gg P_{crit} \tag{16}$$

Equation 16. Distance to Filamentation Point

Despite the filamentation threshold, in water in the near-IR, experimental observations support plasma clamping as the dominate mechanism halting beam collapse with filamentation being only a minor contributor. These observations suggest plasma formation due to multi-photon ionization occurs when the pulse intensity reaches $2 \times 10^{17} W/m^2$ to $3 \times 10^{17} W/m^2$ consistent with Keldysh theory [31].

2.5 Simulation Background

The standard approach to simulating supercontinuum generation is to propagate the laser pulse using the nonlinear Schrödinger equation (NLSE) or, if necessary, the generalized nonlinear Schrödinger equation (GNLSE). The NLSE and GNLSE assume that the pulse can be represented using a slowly evolving envelope function or by taking the paraxial approximation [32]. The slowly varying envelope approximation holds for pulse durations much longer than an optical cycle ($t = \frac{2\pi}{\omega}$), an assumption that ceases to be valid for pulse durations under 100 fs [32]. The paraxial approximation is also problematic for simulating the human eye since the paraxial approximation results in errors for waves propagating at large angles with respect to the propagation axis. In the case of the human eye, these errors compound as the pulse propagates and affect both the spatial [33] and temporal [34] properties of the pulse. Neglecting the issues inherent with a slowly evolving envelope approximation, strong absorption in the infrared and substantial dispersion due to the wide bandwidth of ultrashort pulses would require use of a more numerically complex GNLSE model over the NLSE which assumes negligible absorption and limited pulse bandwidth [32].

Recognizing the difficulties of ultrashort pulse propagation, a method based on the principles of Fourier optics was proposed that incorporated absorption and group velocity dispersion and higher order dispersion effects [24]. This method allowed for a two-dimensional ultrashort pulse propagation that incorporated focusing and aberrations. The propagator solves the scalar wave equation in two dimensions. Pulse propagation is performed in five steps. In Equation 17a, the pulse's electric field (E) is brought into the frequency domain via Fourier transform. In Equation 17b, a Hankel transform is used to replace the radial coordinate (r) with ν which is related to r through the Bessel function solution to the scalar wave equation $J_0(\nu r)$. In the transformed $\Psi(\omega,\nu,z_0)$ space, the scalar wave equation is a second order constant coefficient differential equation whose solutions are known, hence in Equation 17c the pulse can be propagated forward directly using the complex refractive index $n^*(\omega)$ via $k^*(\omega) = n^*(\omega)\omega/c$ where c is the speed of light in vacuum. In Equation 17d and Equation 17e the pulse is converted back into the time-space domain at a coordinate Δz deeper in the medium [24].

$$E(\omega,r,z_0) = \frac{1}{\sqrt{2\pi}}\int_{-\infty}^{\infty} E(t,r,z_0)Exp[-i\omega t]dt \tag{17a}$$

$$\Psi(\omega,\nu,z_0) = \int_{0}^{\infty} E(\omega,r,z_0)J_0[\nu r]rdr \tag{17b}$$

$$\Psi(\omega,\nu,z_0+\Delta z) = \Psi(\omega,\nu,z_0)\times Exp[-i\sqrt{[k(\omega)]^2-\nu^2}\Delta z] \tag{17c}$$

$$E(\omega,r,z_0+\Delta z) = \int_{0}^{\infty} \Psi(\omega,\nu,z_0+\Delta z)J_0[\nu r]rdr \tag{17d}$$

$$E(t,r,z_0+\Delta z) = \frac{1}{\sqrt{2\pi}}\int_{-\infty}^{\infty} E(\omega,\nu,z_0+\Delta z)Exp[+i\omega t]dt \tag{17e}$$

Equation 17. Two-Dimensional Pulse Propagation using Fourier Optics [24].

Despite the success of this method, this type of simulation incorporates only linear optical effects and incorporating nonlinear optical effects was not explored.

2.6 Simulation Theory

Extending prior work on the ultrashort pulse propagator, a simple method to incorporate SPM and XPM into the one-dimensional propagator is devised. From Equation 17c above, one observes that for one-dimensional propagation in the frequency domain the linear propagator equation simplifies to

$$\Psi(\omega, z_0 + \Delta z) = \Psi(\omega, z_0) \times Exp[-ik(\omega)\Delta z] \tag{18}$$

Equation 18. One-Dimensional Pulse Propagator

To incorporate the nonlinear effects, one must now simply include the nonlinear refractive index and absorption coefficient as $n^*(\omega,t) = n_0^*(\omega) + \Delta n^*(t)$ for intense pulses. The problem with this approach is handling $\Delta n^*(t)$. By the same logic employed to solve the NLSE via the split-step Fourier method [32], the split step method is used to separate the nonlinear and nonlinear effects. If we view this problem in terms of operators we have

$$\Psi(\omega, z_0 + \Delta z) = \Psi(\omega, z_0) \times Exp[\widehat{D} + \widehat{N}] \tag{19}$$

Equation 19. One-Dimensional Pulse Propagator with Operator Notation

where $\widehat{D} = -in_0^*(\omega)\omega\Delta z/c$ and $\widehat{N} = -i\Delta n^*(t)\omega\Delta z/c$. The propagator is then divided up with an error of $O(\Delta z^3)$ to be [32], [35]

$$Exp[\widehat{D} + \widehat{N}] = Exp[\widehat{N}/2]Exp[\widehat{D}]Exp[\widehat{N}/2] + O(\Delta z^3) \tag{20}$$

Equation 20. Symmetric Decomposition of the Exponential Operator

The linear operator $\widehat{D}$ is applied in the frequency domain such as in Equation 17c; however, the nonlinear operator $\widehat{N}$ should be applied in the time domain. Using the split-step approach:

$$\tilde{E}(t,z_0) = E(t,z_0) \times Exp[-(i\frac{\omega_0}{c}n_2(z_0) + \frac{1}{2}\beta(z_0))I(t,z_0)(\frac{\Delta z}{2})] \tag{21a}$$

$$\Psi(\omega,z_0) = \frac{1}{\sqrt{2\pi}}\int_{-\infty}^{\infty}\tilde{E}(t,z_0)Exp[-i\omega t]dt \tag{21b}$$

$$\Psi(\omega,z_0+\Delta z) = \Psi(\omega,z_0) \times Exp[-(i\frac{\omega_0}{c}n_0(\omega,z_0) + \frac{1}{2}\alpha_0(\omega,z_0))\Delta z] \tag{21c}$$

$$\tilde{E}(t,z_0+\Delta z) = \frac{1}{\sqrt{2\pi}}\int_{-\infty}^{\infty}\Psi(\omega,z_0+\Delta z)Exp[+i\omega t]dt \tag{21d}$$

$$E(t,z_0+\Delta z) = \tilde{E}(t,z_0+\Delta z) \times Exp[-(i\frac{\omega_0}{c}n_2(z_0) + \frac{1}{2}\beta(z_0))I'(t,z_0)(\frac{\Delta z}{2})] \tag{21e}$$

Equation 21. One-Dimensional Nonlinear Pulse Propagation

The methods section discusses the process in which Equation 21a-e is numerically solved. By solving the one-dimensional case, the pulse is propagated using a single machine instead of a computational cluster. In exchange for discarding the radial coordinate, one must make simplifying assumptions about the radial pulse distribution as well as add in the focusing behavior of the pulse. These assumptions and their validity are addressed in the methods section. This section concludes with observing three details that will be applied in addressing these issues. The first is how the profile of the Gaussian laser pulse is initialized. For a Gaussian pulse with a time duration of τ_p and chirp b the electric field is [33]

$$E(t,x_0) = Constant \times Exp[-(\frac{2ln(2)}{\tau_p^2} - ib)t^2] \times Exp[i\omega_0 t] \tag{22}$$

Equation 22. Electric Field of a Gaussian Pulse in the Time Domain

The constant represents the amplitude of the electric field and is discussed in section 3.1. The second is that the pulse intensity is calculated from the electric field by [36]

$$I(t,x_0) = \frac{cn_0\varepsilon_0}{2}|E(t)|^2 \tag{23}$$

Equation 23. Pulse Intensity

where ε_0 is the permittivity of vacuum. Lastly, the beam width of a Gaussian beam focusing into a medium, neglecting self-focusing, is calculated with [36]

$$w(z) = w_0 \times \sqrt{1 + \frac{(z - z_{focus})^2}{(z_{Rayleigh})^2}} \tag{24}$$

Equation 24. Beam Width of a Focusing Gaussian Pulse

where $w_0 = \frac{2\lambda_0 f_{lens}}{\pi(2w_{lens})}$, $z_{Rayleigh} = \pi w_0^2/\lambda_0$, w_{lens} is the beam width at the lens and f_{lens} is the focal length of the lens.

2.7 Thermal Lensing

In the previous sections, we neglected the temperature dependence of n and α which can complicate pulse simulation. For a long duration, spatially Gaussian laser pulse, the temperature at each point in the medium will be dependent on the radial distance of that point from the pulse resulting in a radially dependent refractive index change. By the same argument as self-focusing, the radially dependent refractive index causes beam focusing or defocusing called thermal lensing. The rise time of a thermal lens can be calculated based on the ratio of beam radius to velocity of sound in the medium. For water, assuming a worst-case beam radius of 5 µm provides a rise time on the order of nanoseconds [37]. Since this report focuses on pulse durations of 100 fs or less we conclude that the thermal lens generated by a femtosecond pulse can be neglected.

Thermal lensing for multi-pulse exposures cannot be neglected as the thermal lens created by one pulse may alter the propagation of later pulses. Multi-pulse exposures are beyond the scope of this report; however, the minimum repetition rate for the thermal lens of one pulse to affect later pulses can be estimated by finding the characteristic time. The characteristic time depends on the thermal conductivity, density, specific heat capacity and beam radius (K_{therm}, ρ, C_p, and $w(z)$) of the media by [38], [39]

$$t_c = \frac{[w(z)]^2}{4}\frac{\rho C_p}{K_{therm}} \tag{25}$$

Equation 25. Characteristic Time for a Thermal Lens to Dissipate by Conduction

For further discussion of the retinal safety implications of thermal lensing see [24].

2.8 Nonlinear Effects Not Simulated

There are other nonlinear effects that affect pulse propagation beyond SPM, XPM, and self-focusing. These effects fall outside the capabilities of the one-dimensional wave propagator and will require different simulation approaches outside the scope of this project. Stimulated inelastic scattering processes such as stimulated Brillouin scattering (SBS) and stimulated Raman scattering (SRS) fall outside of the propagator model. Both processes can transfer pulse energy to other wavelengths and create co-propagating pulses that interact with the original pulse through XPM resulting in further broadening. SBS can be ignored since SBS occurs via acoustic vibrations which occur at the speed of sound in the media, which is slower than the femtosecond pulse timescale [32]. SRS is a much faster process and will broaden the pulse further into the IR regime [32]. Previous authors have argued that for water in the near-IR the Raman effects of the stretch resonance of the OH bond are weak enough to justify neglecting SRS [31].

A separate concern is harmonic generation at the interfaces between the different layers of the eye (air-cornea, cornea-aqueous humor, aqueous humor-lens, etc.). Harmonic generation poses similar retinal safety hazards as supercontinuum generation since harmonic generation also converts near-IR pulses to shorter wavelengths that can propagate to the retina with negligible absorption. Harmonic generation in REM tissues is not speculation, harmonic generation at the interface of biological tissues is the basis of biological imaging techniques such as multiphoton microscopy [40]–[42]. Second and third harmonic generation has been used to image the cornea of the eye [43] and second harmonic generation in the eye has been achieved using nanosecond near-IR laser pulses [44].

2.9 Retinal Damage Risks

As discussed previously, retinal damage of sub-100 fs pulses have not been studied in the 1200 nm - 1400 nm region. Multiple damage mechanisms such as photo-thermal, microcavitation, and laser induced breakdown (LIB) can occur at the retinal epithelium layer [29]. In this report, an attempt to simulate these damage mechanisms is not made. An effort is instead made to determine if nonlinear effects modify the pulse properties prior to reaching the retinal epithelium and the pulse characteristics at the retinal plane are reported.

Four risks with femtosecond pulses that are atypical of longer pulse durations are identified. The first risk is referred to as ”bandwidth risk.” Gaussian pulses 1 ps or longer have narrow transform-limited bandwidths of 1 nm or smaller. Shortening the pulse width to 100 fs, the transform-limited bandwidth broadens to 20 nm - 30 nm for 1200 nm - 1400 nm pulses. For pulses in the 1300 nm - 1400 nm region, the shorter wavelength components of the pulse are much less strongly absorbed than the longer wavelength components. The longer wavelengths will be absorbed in the aqueous humor of the eye, but the remaining shorter wavelengths will propagate to the retinal plane possibly with energies per area above the energy per area MPE limit set using visible pulses which propagate the retina with little absorption. For this risk, the ANSI MPE limit in the visible of 0.1 $\mu J/cm^2$ (corresponding to 38 nJ for a pulse with an initial radius of 3.5 mm) is considered to be the retinal injury threshold since it is (a) lower than the infrared threshold, (b) is based on the assumption that almost the entire pulse reaches the retina, and (c) visible eye safety limits have been more thoroughly studied at femtosecond time scales.

The second risk is broadband SPM converting the pulse from a strongly absorbed near-IR pulse to shorter wavelength weakly absorbed near-IR and/or visible pulses. Much like the case with bandwidth risk, the concern is that the energy per unit area at the retinal plane will exceed the threshold to cause eye injury via the effects discussed above. This risk is considered for supercontinuum generation with and without self-focusing since self-focusing can reduce the area of the pulse at the retinal plane as well as indirectly enhance the supercontinuum by raising the pulse intensity (via reducing the pulse area during propagation).

The third risk factor is self-focusing until plasma generation occurs. As discussed in section 2.2, the eye focuses near-IR pulses behind the retinal plane, which greatly reduces the pulse intensity at the retinal plane compared to comparable visible pulses. However, if the pulse power exceeds the critical power, self-focusing becomes dominant resulting in critical beam collapse. If beam collapse occurs, the pulse will continue to focus until it reaches the critical intensity needed for plasma formation (see section 2.4). Reaching the plasma generation threshold near the retina is believed to correspond with LIB injury (see Fig. 5 in [29] for a histopathology of a probable LIB injury).

The fourth risk is exclusive to wavelengths near the 1400 nm limit of our study. In a prior study conducted by the authors [21], nonlinear absorption transitioned to saturable absorption between 1350 nm and 1400 nm. The intensity threshold for absorption saturating at 1400 nm is expected on the order of 10^{16} W/m^2; however, saturable absorption could become problematic to simulate at intensities as low as 10^{15} W/m^2 if the pulse is broad enough to include wavelengths below 1350 nm. If this occurs in the human eye, a pulse near the 1400 nm limit could propagate to the retinal plane exceeding the ANSI limit by orders of magnitude.

3.0 METHODS AND PROCEDURES

3.1 Simulation Setup

For both simulation of pulse propagation in water and the human eye, temporally Gaussian pulses were initialized using Equation 23. For numerical simulation a discrete space/-time step (dx/dt) had to be chosen. Spatial steps were chosen to be 50 nm, one-tenth of the smallest wavelength of interest (500 nm) as recommended by reference [24]. The time step was then set to be consistent with the spatial step $dt = dx/c$ (also recommended for the SPLIT propagator [24]). Due to the limitations of one-dimensional simulation, the pulse was treated as a spatially flat top pulse (pulse intensity is a Heaviside function to a beam width w) where the beam width is calculated using Equation 24. The initial pulse intensity was calculated from the input pulse energy, time duration and pulse area and used to determine the constant in Equation 22. In both the water and human eye simulations, a look-up table was used for the linear refractive index/absorption coefficient of water where values for each simulated wavelength were interpolated from adjacent wavelength values in the same table. The nonlinear refractive index/absorption coefficients were taken from reference [21] for the central wavelength being simulated.

The pulse was propagated through the simulated water medium using Equation 21 with fast Fourier transform/inverse transform functions acting in place of Equation 21b and d respectively. At each step the pulse intensities were found using the pulse areas calculated from Equation 24. At the end of simulation, the output intensities and spectral powers were returned as data files for each wavelength of interest.

In both the water and eye simulations, a second set of simulations were run with self-focusing effects. For the self-focusing simulation, the beam width $w(z)$ was computed at each step from the previous beam width $w(z-\Delta z)$ using the focusing angle (Equation 14) where the nonlinear angle (Equation 13) was computed using the maximum pulse intensity at the previous step and the linear angle $\theta_{linear}(z) = \arctan\left(\frac{w(z)-w(z-\Delta z)}{\Delta z}\right)$ was computed from the original beam widths found from Equation 24. To prevent the beam width from collapsing to zero in the strong focusing case of self-focusing, a minimum radius (r_{min}) was specified (the procedures used to find r_{min} is discussed in the following sections).

3.2 Simulation Of Previous Water Experiment

In the water experiment, 35 ± 5 fs pulses were focused into a quartz cuvette of water (10.0 mm path length) and the resulting was spectra measured. For the simulation, Gaussian near-IR pulses with central wavelengths consistent with the input wavelengths reported in the experiment were propagated through 10.0 mm of water. The original spectra from the experiment were recovered; however, the spectra were not intensity calibrated in the original report (see Figure 2 for uncalibrated spectra) preventing comparison with the numerical simulation. A relative intensity calibration of the NIR-512 and USB-2000+ spectrometers was performed by coupling an LS-1 light source into the NIR-512 and USB-2000+ with an optical fiber. After calibration, the central wavelength for each input pulse was determined and used as the central wavelength in the simulation (see Table 1). Simulated beam parameters reported from the original experiment were used for the pulse duration, pulse energy, beam width (beam radius), distance to the focus, and Rayleigh range (see Table 1 for parameters).

Table 1. Water Simulation Parameters for Each Wavelength

Central Wavelength (nm)	**1185**	**1225**	**1310**	**1350**	**1400**
Pulse Time (fs)	35	35	35	35	35
Pulse Energy (μJ)	1.928	1.653	1.616	1.994	1.956
$\mathbf{n_2 (10^{-20}\ m^2/W)}$	4.5	9.3	6.8	9.0	7.5
$\boldsymbol{\beta} \mathbf{(10^{-14}\ m/W)}$	9.3	12.9	8.2	15.8	-7.7 **or** 0.0
Beam Radius at Focus (μm)	34.1	34.1	34.1	34.3	34.3
Distance to Focus (mm)	7.781	7.103	7.273	5.918	7.442
Rayleigh Range (mm)	3.049	2.927	2.814	2.731	2.634

After simulating pulse propagation in water using Gaussian beam focusing, self-focusing needed to be incorporated into the model to determine if it affected supercontinuum broadening. A simplified simulation was ran where only self-focusing and absorption were included. From this simulation, a study of worst-case self-focusing was conducted with the self-focusing contribution added to the Gaussian focusing using Equation 14. In this worst-case study, the beam propagates without dispersion, SPM, or nonlinear absorption. From this study, we see that the pulse is prone to self-focusing until reaching the plasma generation threshold discussed in section 2.4. The beam widths corresponding to plasma generation according to Keldysh theory were estimated from this worst-case simulation [31].

After estimating the minimum beam widths, the full beam propagation in water simulation was repeated with self-focusing included. At each propagation step, the beam width was checked against the minimum beam width found in the simplified simulation. If the beam width was found to be less than the allowed minimum value, the beam width was replaced with the minimum value, effectively acting in place of the plasma clamping process discussed in [31].

3.3 Simulation Of Reduced Eye Model

To simulate supercontinuum generation in the human eye, 1200 nm - 1400 nm pulses with pulse durations from 10 fs to 1 ps were propagated through a REM model of the eye. In place of the five layers of the eye (including the retinal tissue), the simulation incorporated four layers with pathlengths of 4.0 mm, 4.0 mm, 16.4 mm and 1.6 mm representing the aqueous humor, lens, vitreous humor, and post retinal epithelium region respectively. The first, third, and fourth layers were given the optical properties of water. In the second layer, the absorption coefficient was reduced to 40% of the absorption of water similar to the absorption reported in the lens of the eye [25]. Since the nonlinear properties of the lens are unknown, we choose to treat the nonlinear properties of the lens to be the same as water. The fourth layer was included in the simulation so that it could simultaneously be used to study the case of pre-focused pulses (where the pulse is deliberately focused in front of the retinal plane to maximize harm to retinal tissues). The linear focusing behavior of the beam was modeled using Equation 24. The beam width and focal length for each wavelength were calculated using the Sellmeier equation and assuming that the eye is a hemi-spherical lens using as discussed in [23]. The pulse was propagated 24.4 mm through the model to the simulated retinal plane (and then 1.4 mm beyond the retinal plane) using the parameters in Table 2. The pulse intensity as a function of time and pulse spectra at the retinal plane and 1.4 mm beyond the retinal plane were recorded for analysis. In the case of a MPE 1399 nm pulse, it was observed that the propagation method could result in unphysical energy generation (due to the high MPE and β being negative) so the 1399 nm pulses were simulated with β at its experimentally measured value [21] and β set to zero. Energy generation was observed not to be an issue for 1400 nm pulses since the MPE is orders of magnitude lower.

Table 2. Eye Simulation Parameters for Each Wavelength

Central Wavelength (nm)	**1200**	**1250**	**1300**	**1350**	**1375^**	**1399**	**1399***	**1400**
Pulse Energy (μJ)	0.305	0.346	4.16	385	3849	38485	38485	38.5
Refractive Index at λ_0	1.317	1.316	1.315	1.314	1.314	1.313	1.313	1.313
$n_2(10^{-20} m^2/W)$	4.45	9.26	6.8	9.0	8.3	7.5	7.5	7.5
$\beta(10^{-14} m/W)$	9.26	12.9	8.2	16	0	0	-7.7	-7.7
Beam Radius at Focus (μm)	2.77	2.89	3.01	3.13	3.19	3.25	3.25	3.26
Distance to Focus (cm)	2.53	2.54	2.55	2.55	2.55	2.56	2.56	2.56
Rayleigh Range (mm)	20.0	21.0	21.9	22.8	23.3	23.8	23.8	23.8

^ Nonlinear properties estimated based on wavelengths measured in [21].

* Propagated with the saturable absorption reported in [21].

As discussed above for the simulation of the water experiment, self-focusing effects must be considered. Repeating the same simulation parameters in Table 2, pulses at the MPE limit were propagated for each wavelength tested. Full simulations including self-focusing and plasma generation were also performed to determine if self-focusing or plasma effects could result in eye hazards.

3.4 Simulation Of Chirped Pulses

While the main study was of the retinal hazard of unchirped Gaussian pulses, real world pulses can be chirped. If negatively chirped, the chirp can correct for the dispersive effects of the water medium resulting in a more intense pulse at the retinal plane. To study the effect of chirp on the pulse properties, the simulation was repeated using pulses with a pre-computed chirp chosen to cancel the dispersion observed as the pulse propagates to the retinal plane.

3.5 Interpreting Retinal Exposures

The retinal hazards are ”scored” for each simulated run in terms of six risk factors. Risk factors one through four will be based on the total energy at the retinal plane between (1) 400 nm - 700 nm, (2) 700 nm - 1000 nm, (3) 1000 nm - 1200 nm, and (4) 1200 nm to 1400 nm. Three hazard levels are defined for this report. The lowest level labeled as ”concern”, is used for runs that are believed to be eye safe, but may be worth further study. Runs where wavelengths below 1000 nm reach the retinal plane are automatically defined as ”of concern” as well as any exposure above the 38 nJ limit for wavelengths above 1000 nm. The concern limit is set low for pulses under 1000 nm to highlight the threshold where supercontinuum broadening becomes measurable. The second hazard level labeled as ”hazard” is reserved for runs that likely represent a retinal hazard. For wavelengths under 1200 nm, 38 nJ is used as the hazard threshold (to be consistent with the current ANSI MPE limit of 0.1 $\mu J/cm^2$ for a 3.5 mm radius pulse). For wavelengths above 1200 nm, it is observed (through simulation) that exposures using 1300 nm, 1 ps pulses are allowed up to 210 nJ. Therefore, this is used as a probable damage threshold. The third damage threshold labeled as ”severe” is artificially set two orders of magnitude above the hazard threshold to highlight simulated exposures well above current ANSI MPE limits. These thresholds are tabulated in Table 3.

Table 3. Assumed Retinal Energy Exposure Limits Per Wavelength

Risk	(1) 400 nm to 700 nm	(2) 700 nm to 1000 nm	(3) 1000 nm to 1200 nm	(4) $>$ 1200 nm
Concern	Any	Any	38 nJ	38 nJ
Hazard	38 nJ	38 nJ	38 nJ	210 nJ
Severe	4 μJ	4 μJ	4 μJ	20 μJ

The fifth and sixth risk factors are calculated differently. The fifth factor is the total pulse energy per unit area at the retinal plane. Unfortunately, the current ANSI standard provides very different limits for different pulse wavelength. According to the standard, a 589 nm pulse at the MPE limit would result in a retinal exposure of 6.7 kJ/m^2 while a 1050 nm pulse would result in an exposure of only 1.1 J/m^2. To compare to the simulation, the 1.1 J/m^2 restriction is treated as the concern threshold for infrared pulses and the 6.7 kJ/m^2 as the threshold for a hazard. Again, any exposure more than 100 times the MPE limit is listed as severe. This fifth risk factor is important for interpreting pre-focused runs where the beam area can be greatly reduced by self-focusing.

The sixth risk factor is plasma generation prior to reaching the retina. While plasma beam propagation is beyond the scope of this simulation, the production of a plasma beam prior to the retinal plane should be treated as a probable retinal injury. For this report, reaching the plasma generation threshold prior to the retina will be treated as a severe LIB injury.

3.6 Convergence Tests Of Eye Simulation

In section 3.1, the spatial step was chosen to be 50 nm. The effect of changing the spatial step size was studied for a 50 fs, 1375 nm pulse using step sizes of 40 nm, 50 nm, 80 nm, 100 nm, and 160 nm. This pulse duration/wavelength combination was chosen since that pulse was found to be an eye hazard that did not self-focus into a plasma unless pre-focused. The resulting total energy, beam radius, and pulse energy in the visible, 700 nm - 1000 nm, 1000 nm - 1200 nm, and $>$ 1200 nm regions was recorded every four millimeters of propagation and at the retinal plane (24.4 mm). Since an analytical solution was not known, the error between each run and the 40 nm run was measured to determine the convergence of the method with respect to set size.

A second set of simulations were performed using a 50 fs, 1375 nm pulse where the total simulated time (T) was reduced to less than the total time of propagation in the eye. The simulations of pulses in the water cuvette and reduced eye model had a total simulated time that was always greater than the time required for the pulse to propagate to the end of the simulated pathlength. Reducing the total simulated time poses risks with the Fast Fourier Transform function in that the waves could ”wrap around” from the end of the simulation back to the beginning of the simulation (in the time domain) causing unphysical behavior. Reducing the total simulated time would greatly accelerate computation and will be of interest in future, more computationally intensive, two dimensional simulations. For this study the convergence of pulse properties (energy, radius, and energy fraction by wavelength) were studied for total simulated times of $T/2$, $T/4$, $T/8$, and $T/16$ to study the effect of allowing the pulse to ”wrap around” the simulation.

4.0 RESULTS AND DISCUSSION

4.1 Simulation Of Water Experiment

Simulated pulses were propagated through 10.0 mm of water and the resulting spectra compared to the intensity calibrated, experimentally measured spectra. The experimental calibrations were relative calibrations, therefore the experimental and simulated spectra differ by a numerical scaling factor. The numerical scaling factor for the infrared measurement was estimated by overlapping the experimental and simulated input spectra (Figure 5 - Figure 9). That scaling factor was then used to scale the simulated output spectra (Figure 5 - Figure 9 middle). The visible output spectra was scaled using the same factor since there was no visible input light to scale. It is important to note that the accuracy of the scaling is suspect since it is dependent on the collection efficiency of the experimental fiber alignments and the correlation between the calibration measurement taken by directly coupling the LS-1 into a collection fiber and collection of light focused in the experiment (refer to Figure 1 for the experimental diagram).

It is also important to note that the spectra of the experimental pulses used in the experiment were not transform-limited Gaussian pulses. The experimental pulses at 1225 nm and 1350 nm are approximately Gaussian while pulses at 1185 nm, 1310 nm and 1400 nm are not (Figure 5 - Figure 9 top). When the output spectra was compared to the simulation without self-focusing it was seen that the simulation and experiment are in agreement to within an order of magnitude near the original IR peak; however, simulation underestimates the amplitude of continuum generation for wavelengths approaching the visible region (Figure 5 - Figure 9 middle).

Figure 4 shows the results of the worst-case self-focusing study. It was seen that the pulse inevitably self-focuses to the plasma generation limit. Shown in Figure 5 - Figure 9 bottom are the output spectra plotted against the simulation with self-focusing incorporated. Improvements in matching the supercontinuum generation trend are seen; however, the simulation with self-focusing appears to underestimate the exiting pulse intensity by roughly one order of magnitude. The simplest explanation for this difference is that the scaling factor computed using the input spectra is not usable for the output spectra since self-focusing enhanced the output beam coupling with the collection optic (see Figure 1 for collection optic placement). Note that in Figure 9 bottom, we replaced the nonlinear absorption with zero since the (negative) nonlinear absorption at 1400 nm was stronger in the simulation than the linear absorption leading to unphysical energy generation.

Neither simulation explained the experimentally measured peaks in the 400 nm to 500 nm region though many possible explanations exist. For example, the peaks may be an artifact of the relative intensity calibration which is less precise at shorter wavelengths since the light source was approximated as a black body. Alternatively, the peaks could instead be real peaks from a nonlinear effect at the water/cuvette interface such as harmonic generation which was not simulated. The generation of light at 400 nm to 500 nm may be explained by plasma effects in the water or an SRS generated infrared pulse interacting with the main pulse as it propagates as well.

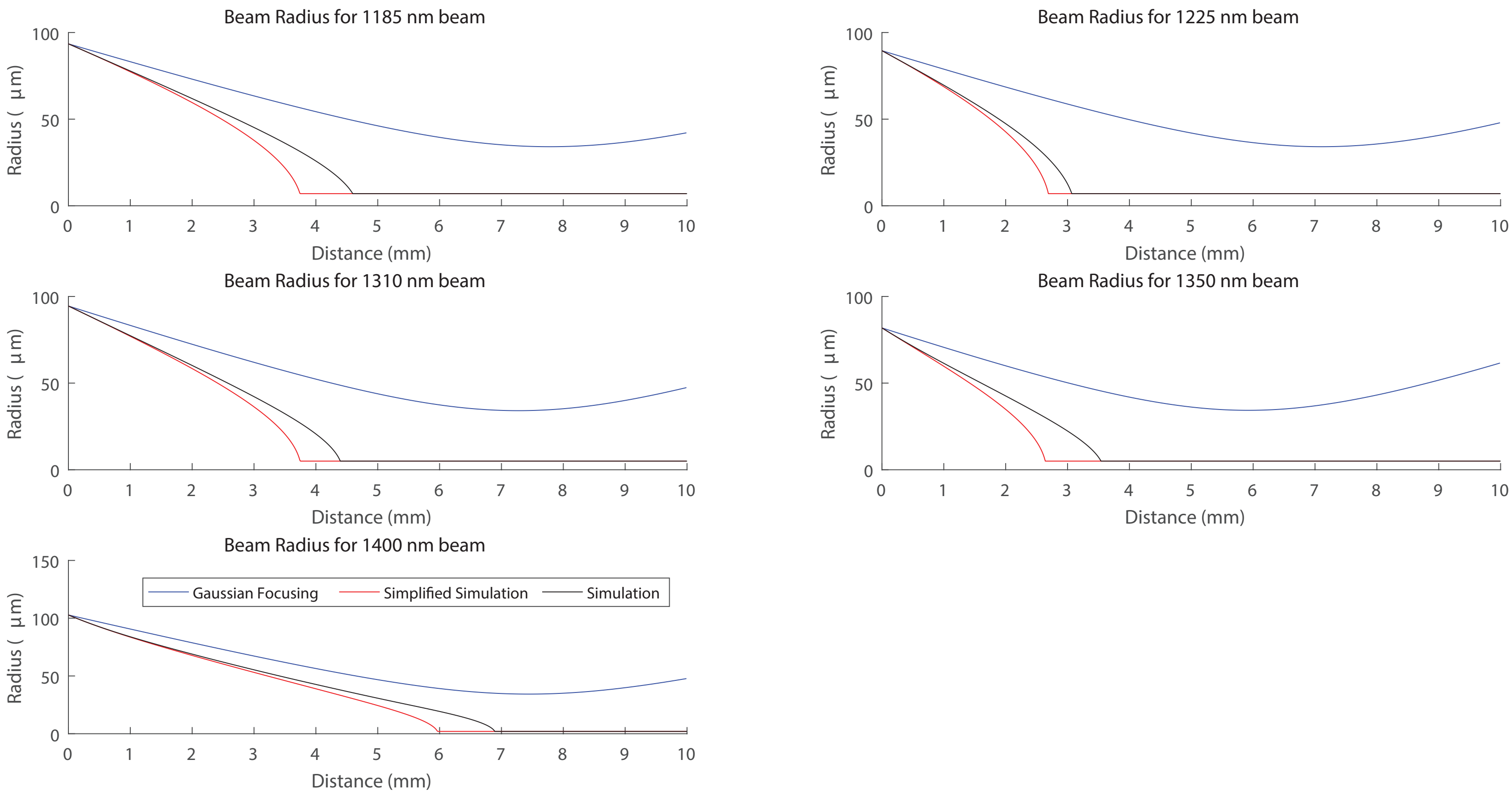

Figure 4. The beam radius as a function of distance into the water media. The blue line shows the radius for Gaussian beam focusing based on parameters in Table 1. The red line shows the result of a simplified simulation of self-focusing where only linear absorption was considered. The black line (between the red and blue lines) shows the radius in the full simulation. The minimum radii of the red and black lines was set to prevent the pulse intensity from exceeding the plasma generation threshold.

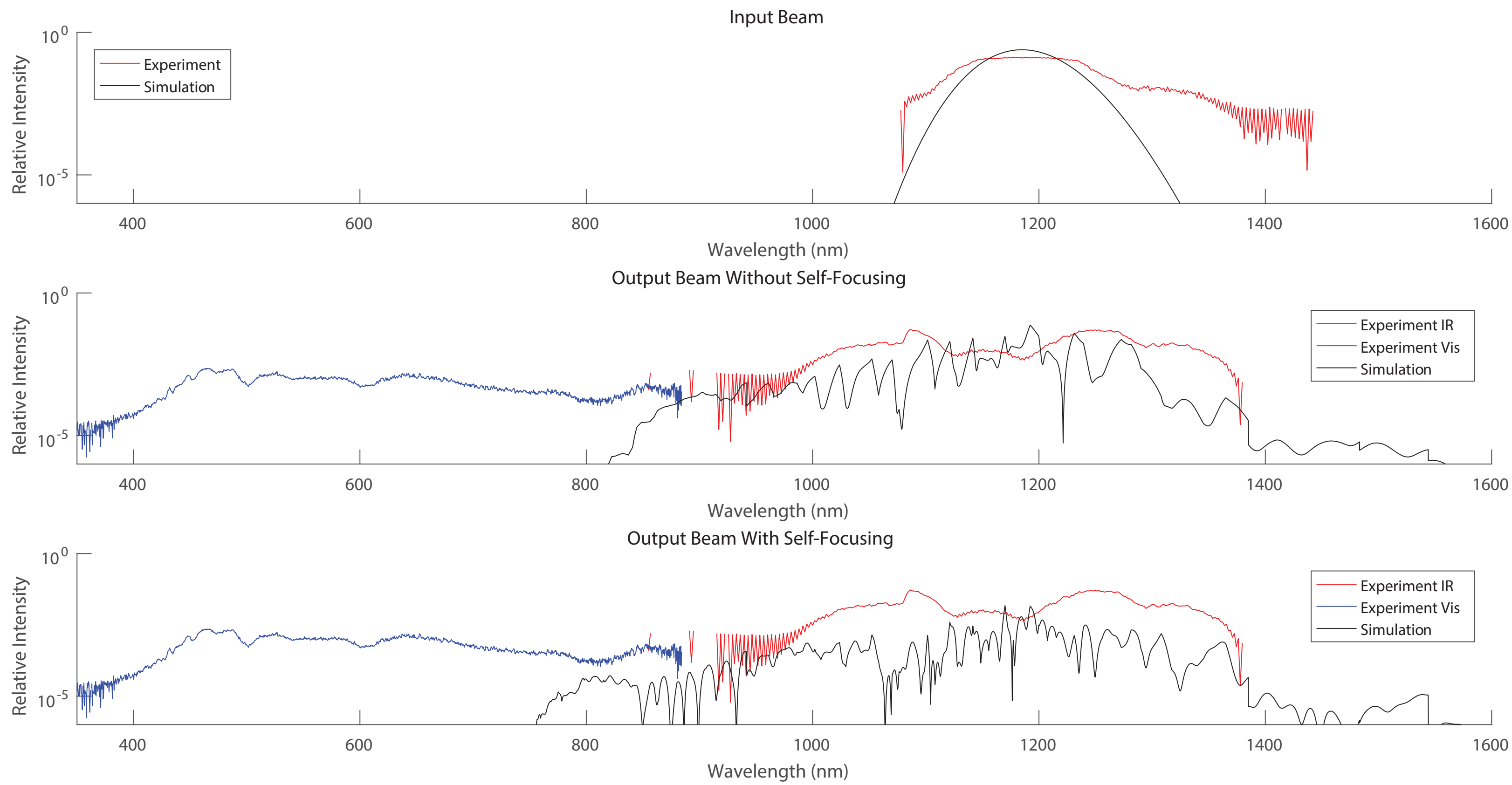

Figure 5. Comparison of "1200 nm" experimental run with a simulated beam at 1185 nm. The top graph compares input beam spectra. The middle graph compares beam spectra after passing through 10.0 mm of water assuming Gaussian beam focusing. The bottom graph compares beam spectra after passing through 10.0 mm of water with Gaussian beam focusing and self-focusing.

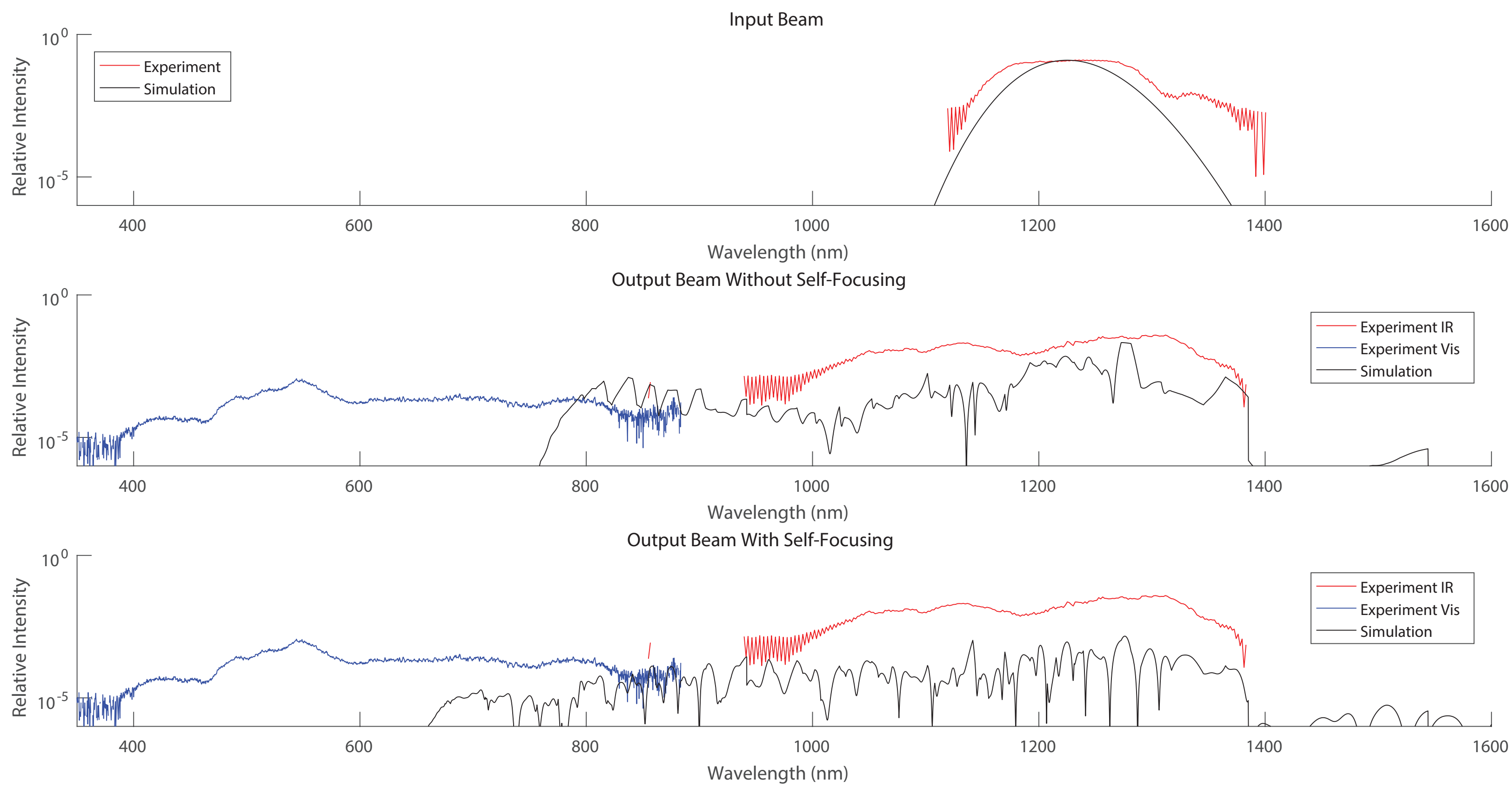

Figure 6. Comparison of "1250 nm" experimental run with a simulated beam at 1225 nm. The top graph compares input beam spectra. The middle graph compares beam spectra after passing through 10.0 mm of water assuming Gaussian beam focusing. The bottom graph compares beam spectra after passing through 10.0 mm of water with Gaussian beam focusing and self-focusing.

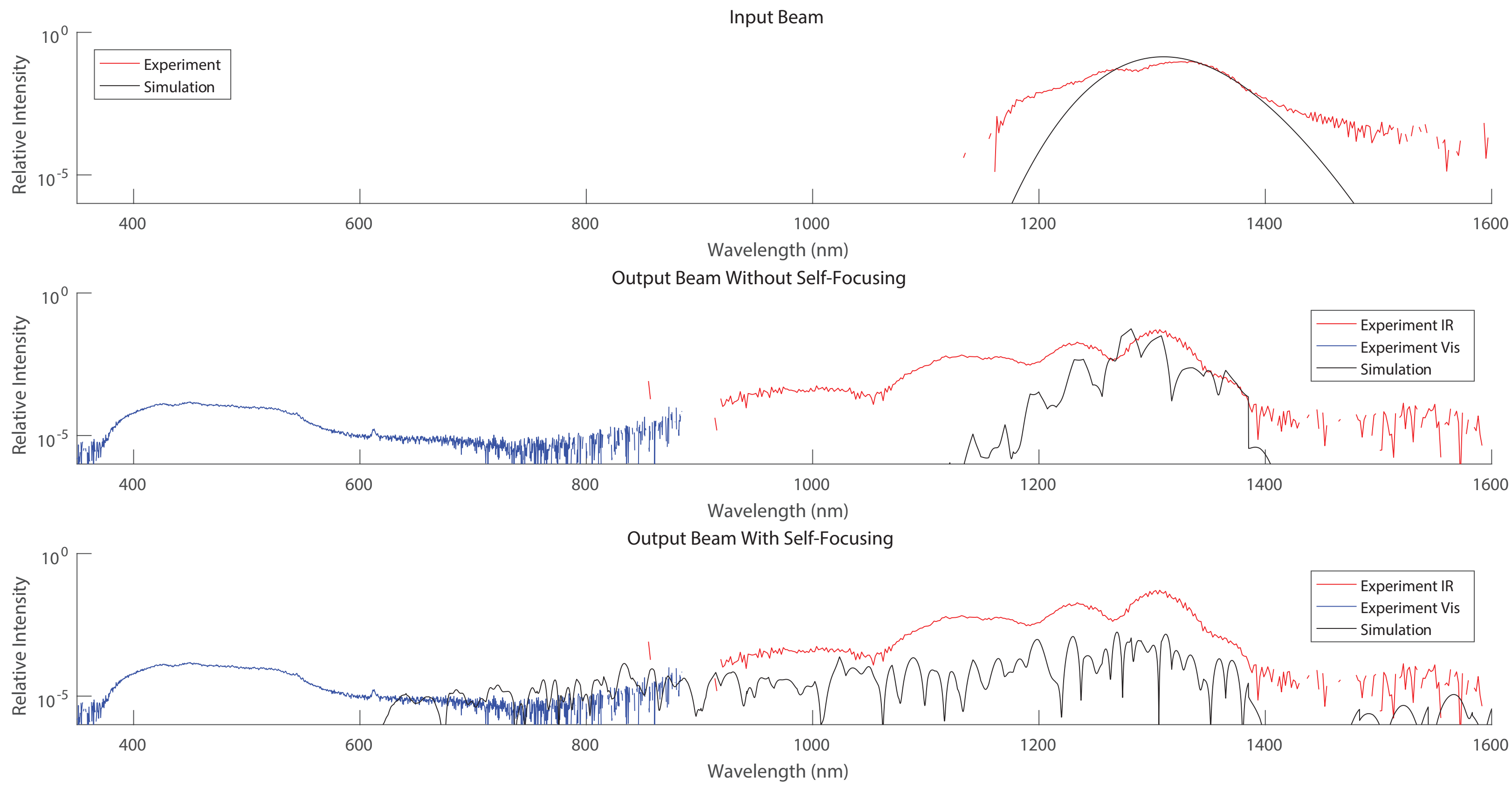

Figure 7. Comparison of "1300 nm" experimental run with a simulated beam at 1310 nm. The top graph compares input beam spectra. The middle graph compares beam spectra after passing through 10.0 mm of water assuming Gaussian beam focusing. The bottom graph compares beam spectra after passing through 10.0 mm of water with Gaussian beam focusing and self-focusing.

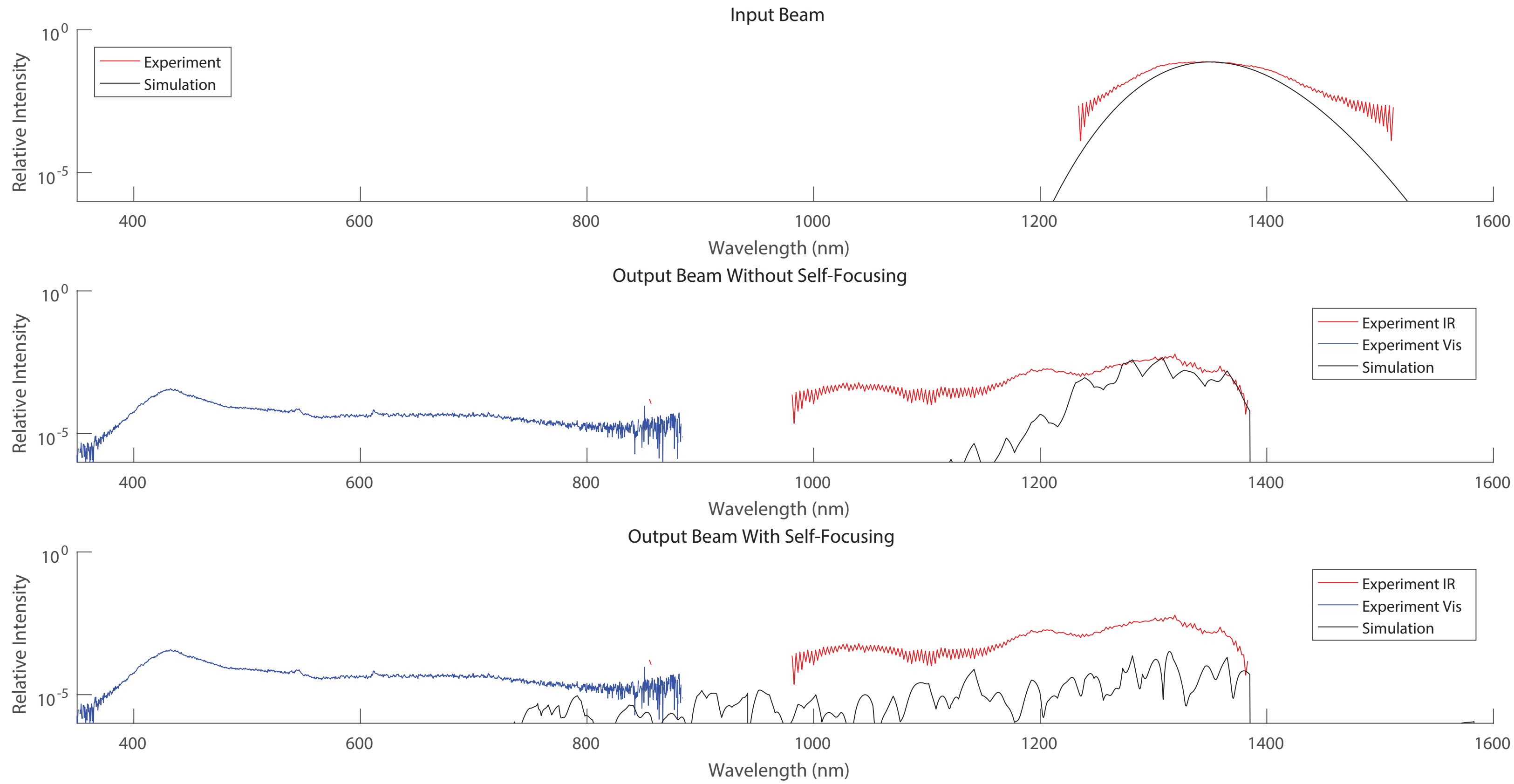

Figure 8. Comparison of "1350 nm" experimental run with a simulated beam at 1350 nm. The top graph compares input beam spectra. The middle graph compares beam spectra after passing through 10.0 mm of water assuming Gaussian beam focusing. The bottom graph compares beam spectra after passing through 10.0 mm of water with Gaussian beam focusing and self-focusing.

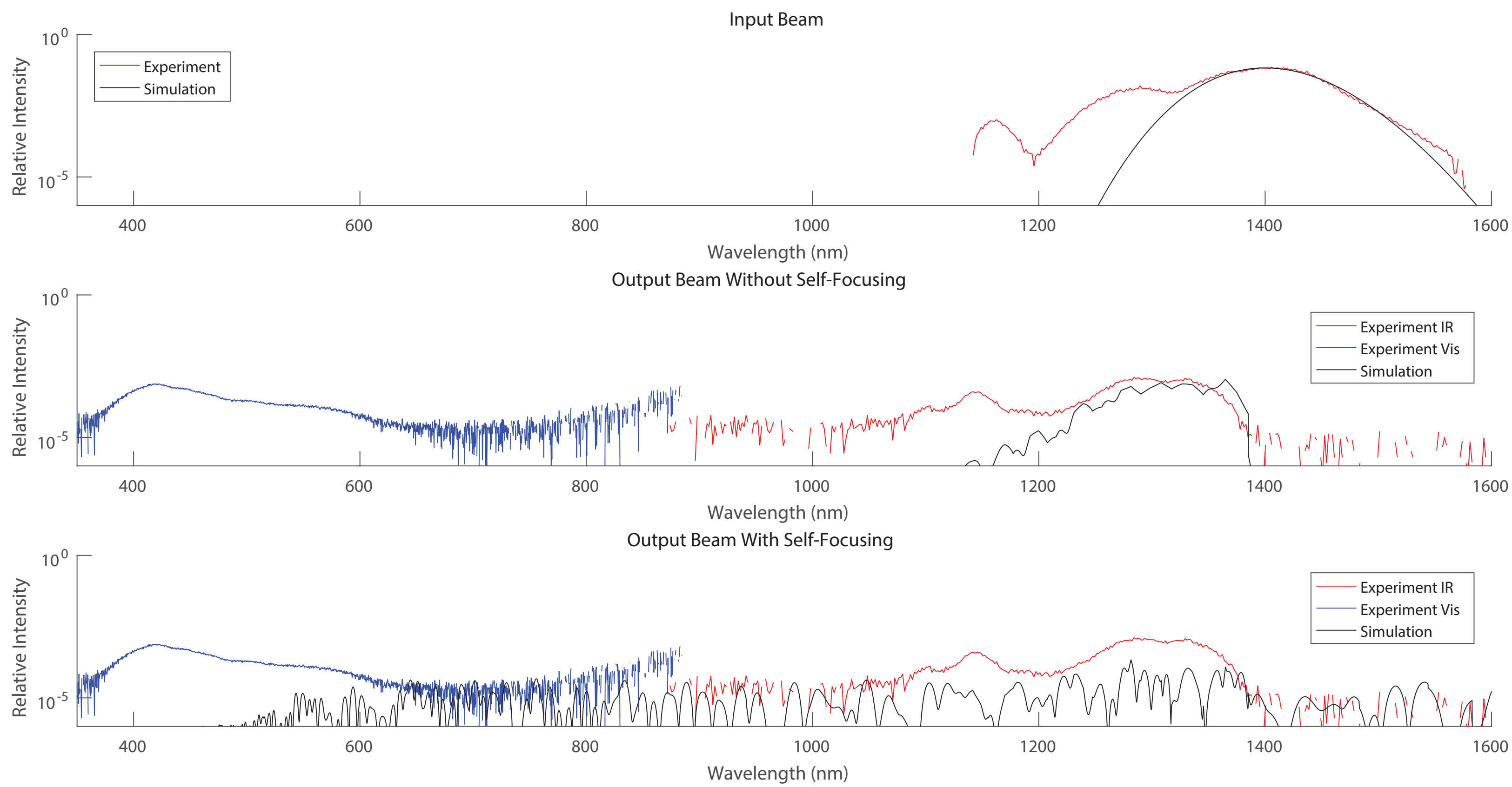

Figure 9. Comparison of "1400 nm" experimental run with a simulated beam at 1400 nm. The top graph compares input beam spectra. The middle graph compares beam spectra after passing through 10.0 mm of water assuming Gaussian beam focusing. The bottom graph compares beam spectra after passing through 10.0 mm of water with Gaussian beam focusing and self-focusing.

4.2 Simulation Of Human Eye

For all wavelengths studied, reducing the pulse duration resulted in a greater pulse energy reaching the retinal plane. Plotting the evolution of a 50 fs, 1375 nm pulse in the spectral domain as it propagates through the eye shows a shift in central wavelength from 1375 nm toward 1300 nm due to strong absorption and SPM (see Figure 10). Plotting the same pulse in the time domain (see Figure 11) shows the effect of dispersion causing the Gaussian pulse to break apart as it propagates, emphasizing the importance of using an envelope model. In Table 4 and Table 5 we list hazards using the system outlined in section 3.5 with the numbers (1) - (4) standing for energy exposure hazards for visible, 800 nm to 1000 nm, 1000 nm to 1200 nm, and 1200+ nm radiation respectively. (5) references the total energy per unit area limits discussed in section 3.5 and (6) references a probable LIB event due to plasma generation prior to the retina (Table 6). Pulses simulated at 500 fs and 1 ps were uniformly under the risk limits set in Table 3 both for simulated runs without and with self-focusing included in the simulation (Table 4 and Table 5 respectively). At 100 fs, it seen that wavelengths between 1300 nm and 1399 nm can reach the retinal plane with energies exceeding the MPE exposures for longer pulse durations (Table 4). Further reducing the pulse duration broadens the pulse bandwidth and increases the maximum intensity resulting in a greater fraction of the pulse energy reaching the retina increasing the severity of the exposure. For 1399 nm pulses with $\beta < 0$, unphysical energy generation occurred (shown as the following tables); however even setting $\beta = 0$ resulted in a severe retinal hazard in all cases of interest. Wavelengths away from the higher ANSI MPE remain retinal safe for simulated wavelengths as short as 35 fs, only becoming hazardous at 10 fs where the broad bandwidth results in some of the initial pulse energy being distributed below 1100 nm (Table 4).

It was observed that self-focusing does not change the retinal hazard designation of any of the simulations. It instead shows that plasma generation will also occur in some of the already severe retinal exposure simulations (Table 5). The location in the eye where plasma generation first occurs is noted in Table 6. In most simulations, plasma generation occurs 1 mm after the retinal plane which is unphysical unless the pulse is pre-focused. In addition to plasma generation risks, self-focusing also changes the pulse area at the retinal plane. The percent change in the pulse area on the retinal plane is shown in Table 7. From Table 7 we observed that the change in area is negligible for most wavelength/time duration combinations that have not already reached the plasma formation threshold prior to the retinal layer. Using the data in Table 5, the hazards simulated against the current ANSI standard for 100 fs pulses (Figure 12) and for 35 fs pulses (Figure 13) are compared.

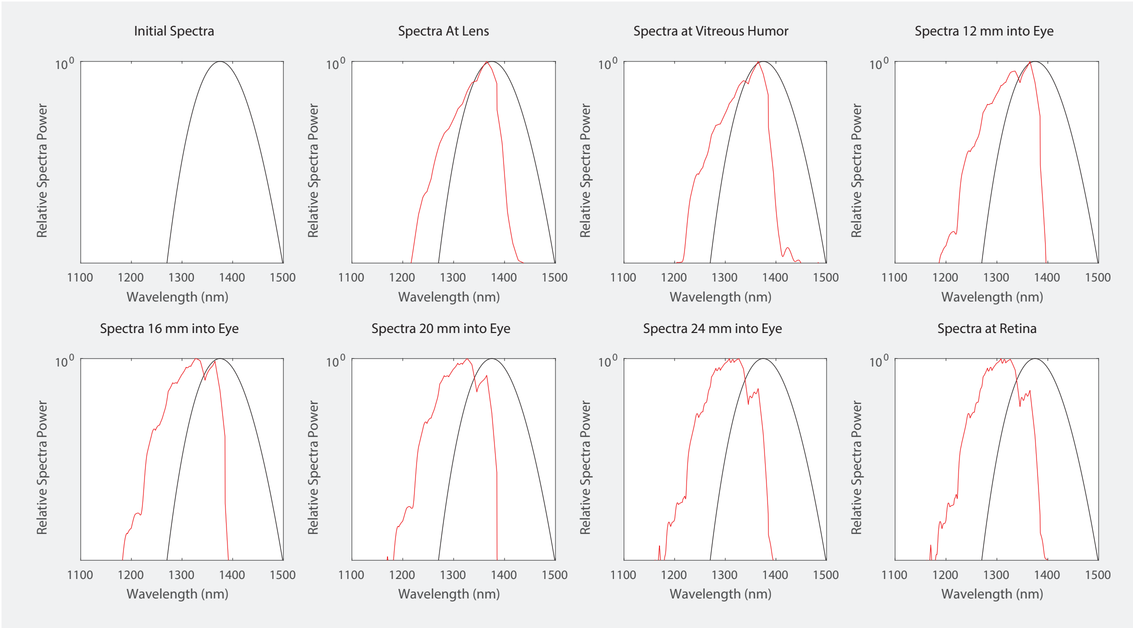

Figure 10. Spectral Distribution of 50 fs, 1375 nm Unchirped Pulse Propagated Through the Eye

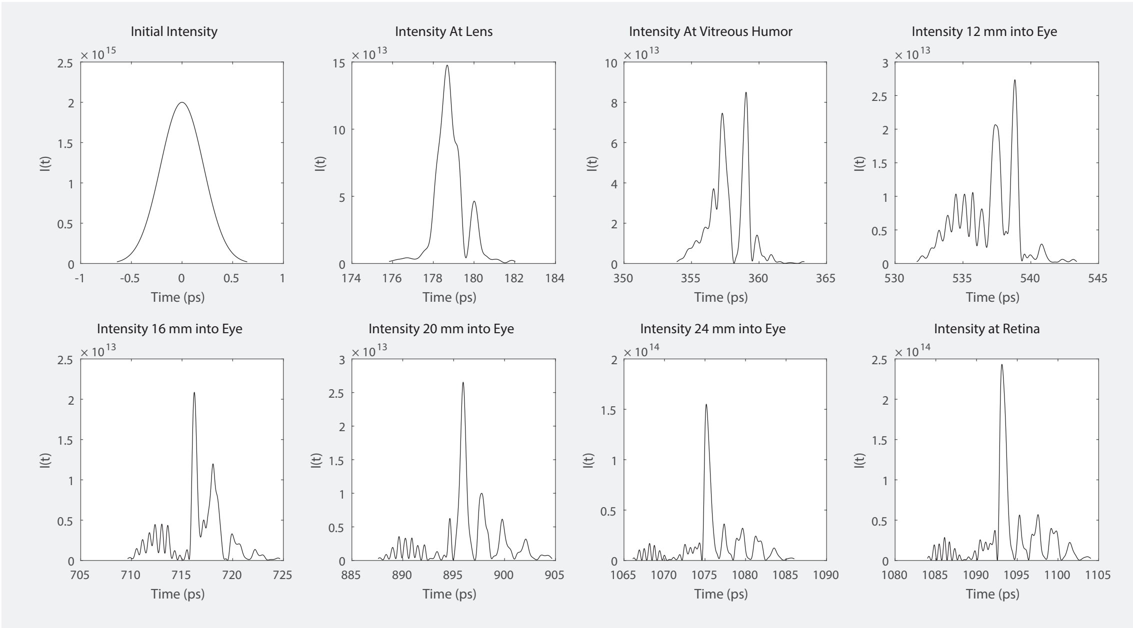

Figure 11. Intensity of 50 fs, 1375 nm Unchirped Pulse Propagated Through the Eye

Table 4. Hazards at MPE Limit Without Self-Focusing

Wavelength (nm)	1200	1250	1300	1350	1375	1399	1399*	1400
10 fs	Haz 3	Con 2,3	Haz 3	Haz 3,4	Sev 2,3	Sev 1-3	X	Haz 3,4
35 fs	Safe	Safe	Con 4,5	Haz 4	Haz 4	Sev 1-4	X	Safe
50 fs	Safe	Safe	Con 4,5	Haz 4	Haz 4	Sev 1-4	X	Safe
100 fs	Safe	Safe	Con 4,5	Haz 4	Con 4,5	Haz 4	Haz 3,4	Safe
500 fs	Safe	Safe	Con 4,5	Con 4	Safe	Safe	Safe	Safe
1000 fs	Safe	Safe	Con 4,5	Con 4	Safe	Safe	Safe	Safe

* Propagated with the saturable absorption reported in [21].
Abbreviations: Concern (Con), Hazard (Haz), Severe (Sev) and Not Simulated (X).

Table 5. Hazards at MPE Limit With Self-Focusing

Wavelength (nm)	1200	1250	1300	1350	1375	1399	1399*	1400
10 fs	Haz 3	Con 2,3	Haz 3	Haz 3,4	Sev 2,3	Sev 6	X	Haz 3,4
35 fs	Safe	Safe	Con 4,5	Haz 4	Haz 4	Sev 6	X	Safe
50 fs	Safe	Safe	Con 4,5	Haz 4	Haz 4	Sev 6	X	Safe
100 fs	Safe	Safe	Con 4,5	Haz 4	Con 4,5	Haz 4	Haz 3,4	Safe
500 fs	Safe	Safe	Con 4,5	Con 4	Safe	Safe	Safe	Safe
1000 fs	Safe	Safe	Con 4,5	Con 4	Safe	Safe	Safe	Safe

* Propagated with the saturable absorption reported in [21].
Abbreviations: Concern (Con), Hazard (Haz), Severe (Sev) and Not Simulated (X).

Table 6. First Point of Plasma Generation in Simulation

Wavelength (nm)	1200	1250	1300	1350	1375	1399	1399*	1400
10 fs	NA	NA	25.46	25.45	24.90	23.94	X	25.56
35 fs	NA	NA	NA	25.48	25.42	24.14	X	NA
50 fs	NA	NA	NA	25.49	25.48	24.48	X	NA
100 fs	NA	NA	25.48	25.52	25.56	25.53	25.34	NA
500 fs	NA	NA	NA	NA	NA	NA	NA	NA
1000 fs	NA	NA	NA	NA	NA	NA	NA	NA

All distances in mm.

Table 7. Change in Area at Retinal Plane from Self-Focusing

Wavelength (nm)	1200	1250	1300	1350	1375	1399	1399*	1400
10 fs	0 %	0 %	0 %	1 %	47 %	Plasma	X	0 %
35 fs	0 %	0 %	0 %	1 %	3 %	Plasma	X	0 %
50 fs	0 %	0 %	0 %	0 %	2 %	Plasma	X	0 %
100 fs	0 %	0 %	0 %	0 %	1 %	4 %	8 %	0 %
500 fs	0 %	0 %	0 %	0 %	0 %	1 %	1 %	0 %
1000 fs	0 %	0 %	0 %	0 %	0 %	0 %	0 %	0 %

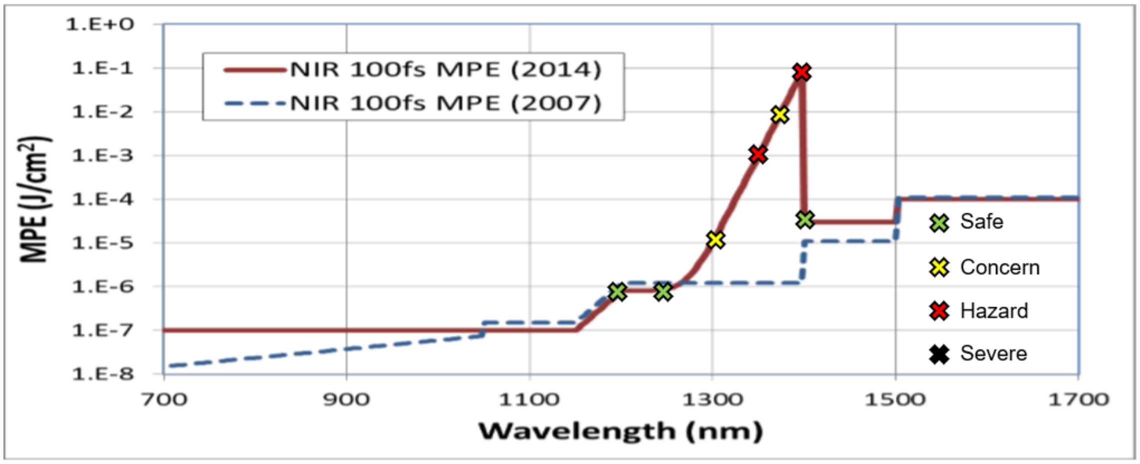

Figure 12. ANSI MPE Limits Versus Simulated Eye Hazards for 100 fs MPE Pulses. The results of the simulation are overlayed on Figure 6.3 in [2].

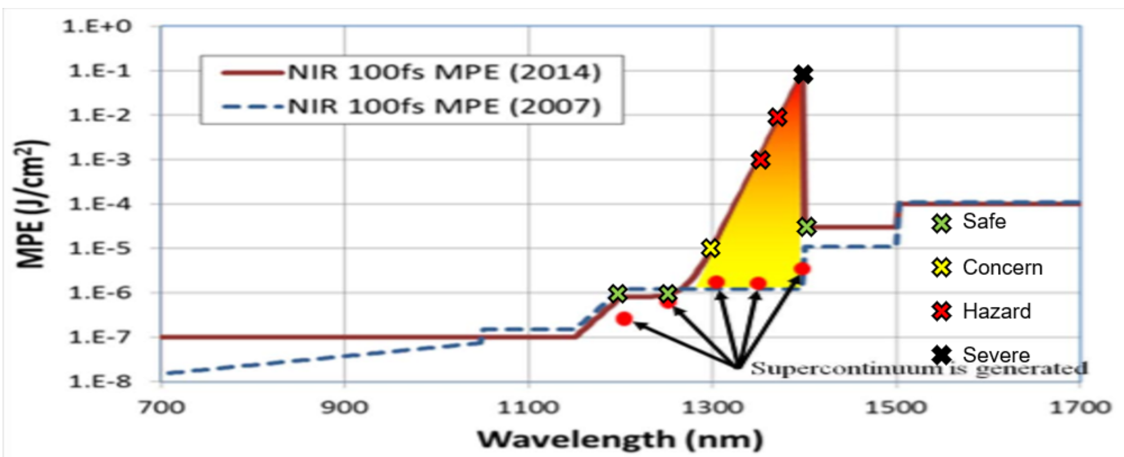

Figure 13. ANSI MPE Limits Versus Simulated Eye Hazards for 35 fs MPE Pulses. The results of the simulation are overlayed on Figure 9.15 in [2]. Note that the experimentally reported supercontinuum thresholds (red circles) are orders of magnitude below the hazards found by simulation. Recall this is most likely due to self-focusing in the water experiment.

The appearance of plasma generation in the post-retinal plane generally occurs near the linear focal point for the wavelength of interest. This suggests that LIB can be induced in the retina if the pulse is pre-focused. Taking the results 1.4 mm behind the retinal plane, Table 8 shows that pre-focusing the pulse so that the focal point is at or near the retinal plane results in more wavelength/time duration combinations where LIB injury is possible. Wavelength/ time duration combinations that do not undergo plasma generation are more intense at the retinal plane resulting in reclassification of risks. For example, 1300 nm exceeds the MPE of a narrowly focused, visible pulse at the retina if it is pre-focused.

Table 8. Hazards at MPE Limit For Pre-Focused Pulses (With Self-Focusing)

Wavelength (nm)	**1200**	**1250**	**1300**	**1350**	**1375**	**1399**	**1399***	**1400**
10 fs	Haz 3	Con 2,3,5	Sev 6	Sev 6	Sev 6	Sev 6	X	Sev 6
35 fs	Con 5	Con 5	Haz 5	Sev 6	Sev 6	Sev 6	X	Con 5
50 fs	Con 5	Con 5	Haz 5	Sev 6	Sev 6	Sev 6	X	Con 5
100 fs	Con 5	Con 5	Sev 6	Sev 6	Sev 6	Sev 6	Sev 6	Safe
500 fs	Con 5	Con 5	Haz 5	Con 4,5	Con 5	Safe	Safe	Safe
1000 fs	Con 5	Con 5	Haz 5	Con 4,5	Con 5	Safe	Safe	Safe

* Propagated with the saturable absorption reported in [21].
Abbreviations: Concern (Con), Hazard (Haz), Severe (Sev) and Not Simulated (X).

Plotting a chirped pulse simulation verifies that the negative chirp given to the pulse at the beginning of the simulation results in the pulse becoming approximately unchirped at the retinal plane (see Figure 14). Unlike pre-focusing the pulse, negatively chirping the pulse to compensate for pulse dispersion at the retinal plane does not enhance the retinal hazard for any time duration/wavelength combination (see Table 9). For wavelengths between 1200 nm and 1300 nm, the low MPE limit precludes supercontinuum generation or self-focusing prior to or at the retinal plane even when the pulse is chirped to compensate for dispersion. For 1375 nm - 1400 nm wavelengths, strong absorption makes the pulse intensity in the cornea, aqueous humor and lens more significant than the pulse intensity near the retinal plane. Chirping the pulse lowers the initial maximum intensity of the pulse which makes long wavelength pulses less likely to undergo SPM and delays plasma generation to a point behind the retinal plane which could only be reached if the pulse was also pre-focused (see Table 10 and Table 11).

Table 9. Hazards at MPE Limit For Negatively Chirped Pulses (With Self-Focusing)

Wavelength (nm)	**1200**	**1250**	**1300**	**1350**	**1375**	**1399**	**1399***	**1400**
10 fs	Haz 3	Con 2,3	Haz 3	Haz 2-4	Sev 2-4	Sev 1-4	X	Haz 3,4
35 fs	Safe	Safe	Con 4,5	Haz 4	Haz 4	Sev 4	X	Safe
50 fs	Safe	Safe	Con 4,5	Haz 4	Haz 4	Haz 4	X	Safe
100 fs	Safe	Safe	Con 4,5	Haz 4	Con 4,5	Con 4	Con 4	Safe
500 fs	Safe	Safe	Con 4,5	Con 4	Safe	Safe	Safe	Safe
1000 fs	Safe	Safe	Con 4,5	Con 4	Safe	Safe	Safe	Safe

* Propagated with the saturable absorption reported in [21].
Abbreviations: Concern (Con), Hazard (Haz), Severe (Sev) and Not Simulated (X).

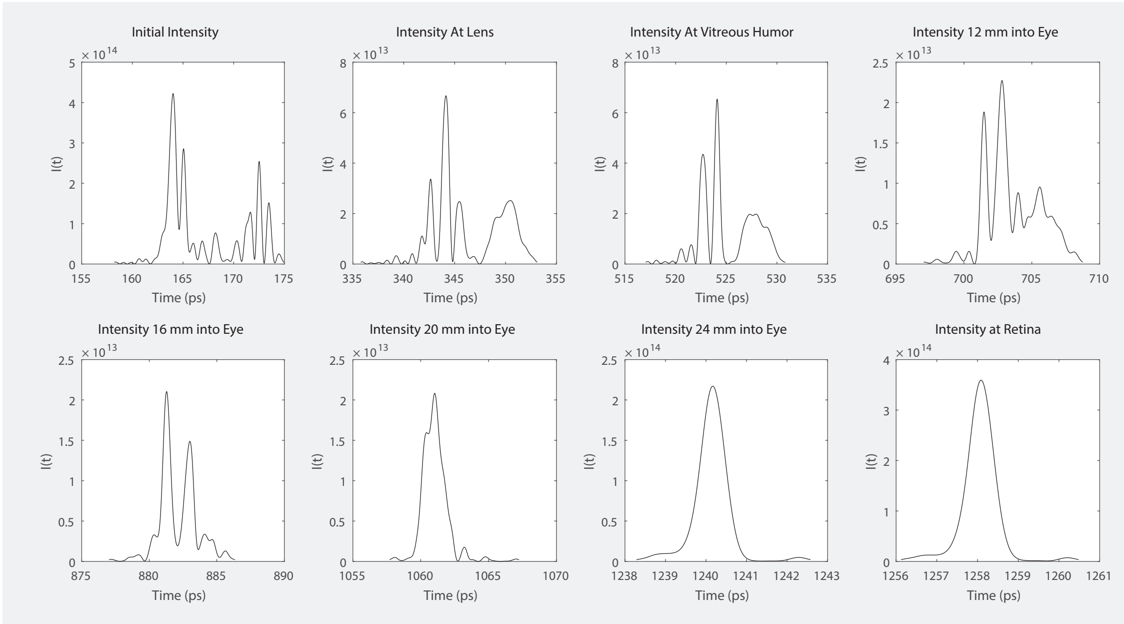

Figure 14. Intensity of 50 fs, 1375 nm Negatively Chirped Pulse Propagated Through the Eye

Table 10. First Point of Plasma Generation in Chirped Pulse Simulation

Wavelength (nm)	1200	1250	1300	1350	1375	1399	1399*	1400
10 fs	25.33	25.40	25.42	25.37	25.04	24.70	X	24.70
35 fs	NA	25.41	25.45	25.45	25.38	25.38	X	NA
50 fs	NA	25.42	25.45	25.48	25.48	24.49	X	NA
100 fs	NA	NA	25.46	25.51	25.55	NA	25.56	NA
500 fs	NA	NA	NA	NA	NA	NA	NA	NA
1000 fs	NA	NA	NA	NA	NA	NA	NA	NA

All distances in mm.

Table 11. Change in Area at Retinal Plane from Self-Focusing of Chirped Pulse

Wavelength (nm)	1200	1250	1300	1350	1375	1399	1399*	1400
10 fs	0 %	0 %	0 %	5 %	24 %	56 %	X	0 %
35 fs	0 %	0 %	0 %	1 %	2 %	6 %	X	0 %
50 fs	0 %	0 %	0 %	0 %	1 %	3 %	X	0 %
100 fs	0 %	0 %	0 %	0 %	1 %	1 %	2 %	0 %
500 fs	0 %	0 %	0 %	0 %	0 %	1 %	1 %	0 %
1000 fs	0 %	0 %	0 %	0 %	0 %	0 %	0 %	0 %

4.3 Results Of Convergence Tests

The total energy, beam radius, and energy in the four wavelength ranges of interest were compared between simulated runs using of a 50 fs, 1375 nm beam. The fractional error was calculated as $|1 - \frac{ErrorRun}{ErrorBestRun}|$ for all runs plotted. In Figure 15, the effect of varying the step size was studied by comparing 50 nm, 80 nm, 100 nm, and 160 nm runs against a "best" run using a 40 nm step size. Comparing the step sizes shows that the total energy, beam radius, and energy at wavelengths above 1000 nm deviate less than 1% from the values reported in the 40 nm run. The energy at wavelengths below 1000 nm was observed to deviate for longer step sizes consistent with expectations that the simulation will fail to simulate wavelengths much shorter than ten times the step size. The plasma generation threshold was reached for all runs at the same point in simulation (to within 1 μm precision) suggesting that changing the step size did not affect self-focusing.

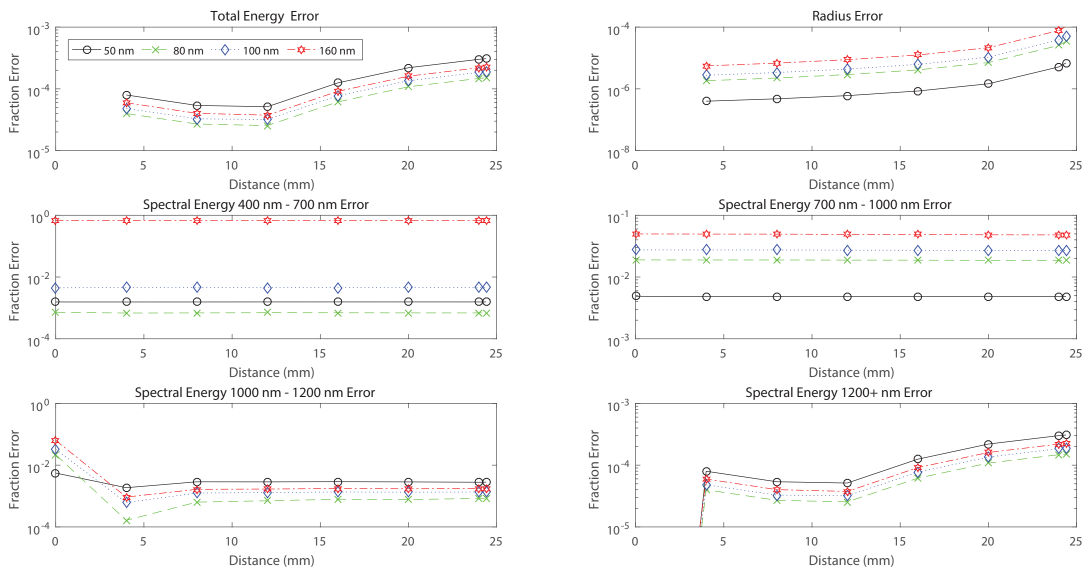

Figure 15. Convergence of Different Step Sizes Compared to a 40 nm Baseline.

The same convergence test was performed where the total simulated time was reduced (see Figure 16). The initial simulated time of $T = 175$ ps was more than sufficient to simulate pulse propagation through the eye. The eye simulation was repeated using a maximum simulated time of $T/2$, $T/4$, $T/8$, and $T/16$. It was noted that reducing the maximum simulated time results in a greater reported error. The largest error is consistently reported for $T/16$ and an error reduction of one order of magnitude is seen by increasing the simulated time to $T/2$. Like the step size study, the plasma generation threshold was consistently reached at the same point in the simulated eye (to within 1 μm precision).

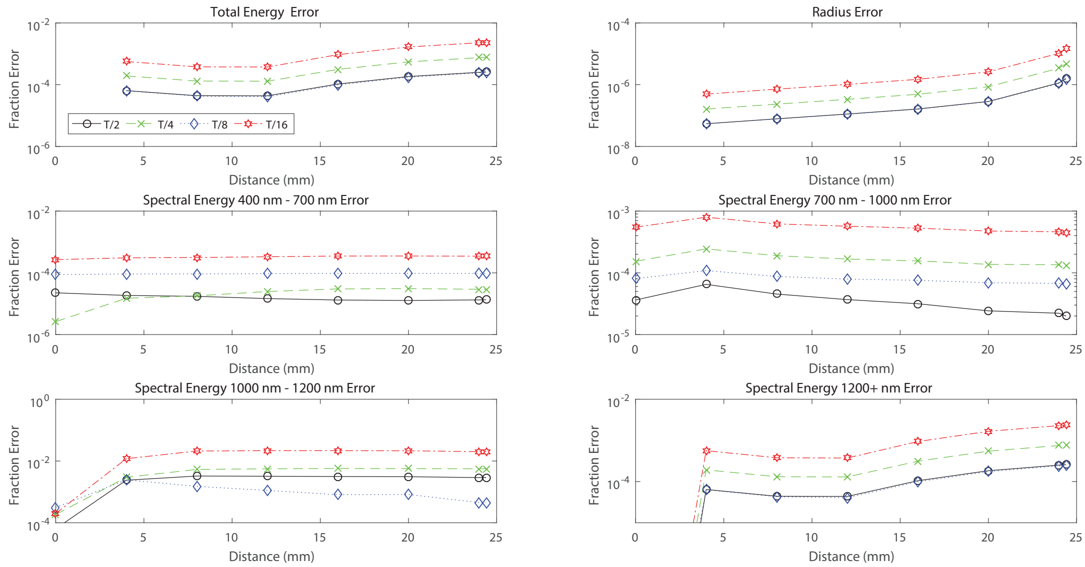

Figure 16. Convergence Test for Different Maximum Simulated Times. Each time plotted is compared to a baseline of maximum time T.

5.0 CONCLUSION

In this report, a one-dimensional nonlinear, femtosecond wave solver was formulated to propagate pulses through a simulated eye. Using the solver, the unusually strong visible light generation reported in [2] was observed to be a result of supercontinuum generation and self-focusing until the water ionized into plasma. Due to limited knowledge of the experimental setup and the absence of plasma propagation calculations in the simulation model, agreement between the simulation and experimental data was not achievable. By applying the simulation to a reduced eye model, it was shown that $<$ 100 fs, 1350 nm to 1399 nm pulses are hazardous to the human eye based on current eye safety standards (see Figure 12 and Figure 13). Increasing the pulse duration to 500 fs decreases the pulse bandwidth resulting in retinal safe pulses consistent with ANSI expectations. Pre-focusing 100 fs, 1300 nm to 1399 nm pulses to focus at the retinal plane results in plasma generation near the retinal plane which poses a severe retinal hazard. Negatively chirping the pulse to correct for dispersion did not appear to increase the risk of a retinal hazard. This study highlights the importance of considering self-focusing effects when considering retinal hazards and provides guidance for future experimental studies of retinal hazards from femtosecond pulses.

6.0 REFERENCES

1. *ANSI, American National Standard for Safe Use of Lasers*, Z136.1-2014, Laser Institute of America, 2014 1, 2.

2. F. J. Echeverria, "Nonlinear optical effects on retinal damage thresholds in the 1200 – 1400 nm wavelength range," PhD thesis, Texas A&M University, May 2015 1–4, 30, 34.

3. A. Bruckner, J. Schurr, and E. Chang, "Biological damage threshold induced by ultrashort 2nd and 4th harmonic light pulses from a mode-locked Nd:glass laser," USAF School of Aerospace Medicine, Brooks AFB, TX 78235, Tech. Rep., 1980, AL-TR-1992-0174 2.

4. C. Cain, G. Noojin, D. Stolarski, R. Thomas, and B. Rockwell, "Near-infrared ultrashort pulse laser bioeffects studies," Optical Radiation Branch, Brooks AFB, TX 78235, Tech. Rep., 2003, AFRL-HE-BR-TR-2003-0029 2.

5. C. Cain, G. Noojin, D. Stolarski, C. Toth, C. DiCarlo, W. Roach, and C. Stein, "Ultrashort pulse laser effects in the primate eye," Optical Radiation Branch, Brooks AFB, TX 78235, Tech. Rep., 1994, AL/OE-TR-1994-0141 2.

6. C. Cain, C. Toth, G. Noojin, V. Carothers, D. Stolarski, and B. Rockwell, "Thresholds for visible lesions in the primate eye produced by ultrashort near-infrared laser pulses," *Investigative Ophthalmology and Visual Science*, vol. 40(100), pp. 2343–2349, Sep. 1999 2.

7. C. Cain, C. Toth, C. DiCarlo, C. Stein, G. Noojin, Stolarski, and W. D. Roach, "Visible retinal lesions from ultrashort laser pulses in the primate eye," *Investigative Ophthalmology and Visual Science*, vol. 36(5), pp. 879–888, Apr. 1995 2.

8. C. Cain, C. Toth, R. Thomas, G. Noojin, V. Carothers, D. Stolarski, and B. Rockwell, "Comparison of macular versus paramacular retinal sensitivity of femtosecond laser pulses," *Journal of Biomedical Optics*, vol. 5(3), pp. 315–320, Jul. 2000 2.

9. C. Cain, C. Toth, G. Noojin, D. Stolarski, R. Thomas, and B. Rockwell, "Thresholds for retinal injury from multiple near-infrared ultrashort laser pulses," *Health Physics*, vol. 82(6), pp. 855–862, Jun. 2002 2.

10. A. Goldman, W. Ham Jr., and H. Mueller, "Mechanisms of retinal damage resulting from the exposure of rhesus monkeys to ultrashort laser pulses," *Experimental Eye Research*, vol. 21(5), pp. 457–469, Nov. 1975 2.

11. A. Goldman, W. Ham Jr., and H. Mueller, "Ocular damage thresholds and mechanisms for ultrashort pulses of both visible and infrared laser radiation in the rhesus monkey," *Experimental Eye Research*, vol. 24(1), pp. 45–56, Jan. 1977 2.

12. J. Taboada and W. Gibbons, “Retinal tissue damage induced by single ultrashort 1060 nm laser light pulses,” *Applied Optics*, vol. 17(18), pp. 2871–2873, Sep. 1978 2.

13. R. Thomas, G. Noojin, D. Stolarski, R. Hall, C. Cain, C. Toth, and B. A. Rockwell, “Comparative study of retinal effects from continuous wave and femtosecond mode-locked lasers,” *Lasers in Surgery and Medicine*, vol. 31(1), pp. 9–17, Jun. 2002 2.

14. C. Toth, C. Cain, C. Stein, G. Noojin, D. Stolarski, J. Zuclich, and W. Roach, “Retinal effects of ultrashort laser pulses in the rabbit eye,” *Investigative Ophthalmology and Visual Science*, vol. 36(9), pp. 1910–1917, Aug. 1995 2.

15. J. Zuclich, W. Elliott, C. Cain, G. Noojin, W. Roach, B. Rockwell, and C. Toth, “Ocular damage induced by ultrashort laser pulses,” USAF Armstrong Laboratory Occupational and Environmental Health Directorate, Brooks AFB, TX 78235, Tech. Rep., 1993 2.

16. J. A. Zuclich, D. J. Lund, and B. E. Stuck, “Wavelength dependence of ocular damage thresholds in the near-IR to far-IR transition region: Proposed revisions to MPEs,” *Health Physics*, vol. 92(1), pp. 15–23, Jan. 2007 2.

17. R. L. Vincelette, B. A. Rockwell, J. W. Oliver, S. S. Kumru, R. J. Thomas, K. J. Schuster, G. D. Noojin, A. D. Shingledecker, D. J. Stolarski, and A. J. Welch, “Trends in retinal damage thresholds from 100 millisecond near-infrared laser radiation exposures: A study at 1,110, 1,130, 1,150, and 1,319 nm,” *Lasers in Surgery and Medicine*, vol. 41, 382–390, Jul. 2009 2.

18. B. Rockwell, W. Roach, M. Rogers, M. Mayo, C. Toth, C. P. Cain, and G. D. Noojin, “Nonlinear refraction in vitreous humor,” *Optics Letters*, vol. 18, pp. 1792–1794, Nov. 1993 2.

19. R. Boyd, *Nonlinear Optics*, 3rd ed. The Institute of Optics at the University of Rochester, Rochester, NY USA, 2008, pp. 207–213, 329–369 4, 7–9.

20. G. M. Hale and M. R. Querry, “Optical constants of water in the 200-nm to 200-µm wavelength region,” *Applied Optics*, vol. 12(3), pp. 555–563, Mar. 1973 5, 6.

21. C. B. Marble, J. E. Clary, G. D. Noojin, S. P. O’Connor, D. T. Nodurft, A. W. Wharmby, B. R. Rockwell, M. O. Scully, and V. V. Yakovlev, “Z-scan measurements of water from 1150 nm to 1400 nm,” *Optics Letters*, Accepted 5, 14, 15, 17, 29, 31, 39, 46, 53, 60.

22. R. L. Vincelette, R. J. Thomas, B. A. Rockwell, C. D. Clark III, and A. J. Welch, “First-order model of thermal lensing in a virtual eye,” *Journal of the Optical Society of America A*, vol. 26(3), pp. 548–558, Mar. 2009 5.

23. R. L. Vincelette, A. J. Welch, R. J. Thomas, B. A. Rockwell, and D. J. Lund, "Thermal lensing in ocular media exposed to continuous-wave near-infrared radiation: The 1150- 1350-nm region," *Journal of Biomedical Optics*, vol. 13(5), 054005, Nov. 2008 5, 17.

24. C. D. Clark III, "Modeling laser damage to the retina," PhD thesis, University of Texas at San Antonio, Aug. 2011 5, 6, 10, 13, 15.

25. E. F. Maher, "Transmission and absorption coefficients for ocular media of the rhesus monkey," USAF School of Aerospace Medicine, Brooks AFB, TX 78235, Tech. Rep., 1978, SAM-TR-78-32 5, 6, 17.

26. R. R. Alfano, *The Supercontinuum Laser Source*. Springer-Verlag, New York, NY USA, 1989 6–8.

27. A. W. Weiner, *Ultrafast Nonlinear Optics*. John Wiley and Sons, Hoboken, NJ USA, 2009 7.

28. B. A. Rockwell, P. K. Kennedy, R. J. Thomas, W. P. Roach, and M. E. Rogers, Eds., *Effect of Nonlinear Optical Phenomena on Retinal Damage*, vol. 2391, SPIE, San Jose, California: Proceedings of the 1995 SPIE, May 1995 8.

29. B. A. Rockwell, R. J. Thomas, and A. Vogel, "Ultrashort laser pulse retinal damage mechanisms and their impact on thresholds," *Medical Laser Application*, vol. 25(10), pp. 84–92, Apr. 2010 8, 14.

30. G. M. Zverev and V. A. Pashkov, "Self-focusing of laser radiation in solid dielectrics," *Soviet Physics JETP*, vol. 30(4), pp. 616–621, Apr. 1970 8.

31. J. A. Dharmadhikari, G. Steinmeyer, G. Gopakumar, D. Mathur, and A. K. Dharmadhikari, "Femtosecond supercontinuum generation in water in the vicinity of absorption bands," *Optics Letters*, vol. 41(15), pp. 3475–3478, Aug. 2016 9, 13, 16.

32. G. Agrawal, *Nonlinear Fiber Optics*, 5th ed. Academic Press, Kidlington, UK, 2013 9–11, 13.

33. A. E. Siegman, *Lasers*. University Science Books, Sausalito, CA USA, 1986 9, 12.

34. R. Trebino, *Frequency-Resolved Optical Gating: The Measurement of Ultrashort Laser Pulses*. Kluwer Academic Publishers, 2001 10.

35. G. Dattoli, L. Giannessi, M. Quattromini, and P. L. Ottaviani, "Symmetric decomposition of exponential operators and evolution problems," *Physics Letters A*, vol. 247, pp. 191–197, Oct. 1998 11.

36. B. E. A. Saleh and M. C. Teich, *Fundamentals of Photonics*, 2nd ed. John Wiley and Sons, Hoboken, NJ USA, 2007 12.

37. M. Sheik-Bahae, T. Said, and E. Van Stryland, “High-sensitivity, single-beam n_2 measurements,” *Optics Letters*, vol. 14(17), pp. 955–957, Sep. 1989 13.

38. J. Hayes, “Thermal blooming of laser beams in fluids,” *Applied Optics*, vol. 11(2), pp. 455–461, Feb. 1972 13.

39. A. Novoa-Lopez J., E. Lopez Lago, M. Dominguez-Perez, J. Troncoso, L. M. Varela, R. de la Fuente, O. Cabeza, H. Michinel, and R. Rodriguez J., “Thermal refraction in ionic liquids induced by a train of femtosecond laser pulses,” *Optics and Laser Technology*, vol. 61, pp. 1–7, Sep. 2014 13.

40. R. M. Williams, A. Flesken-Nikitin, L. H. Ellenson, D. C. Connolly, T. C. Hamilton, A. Y. Nikitin, and W. R. Zipfel, “Strategies for high-resolution imaging of epithelial ovarian cancer by laparoscopic nonlinear microscopy,” *Translational Oncology*, vol. 3(3), pp. 181–194, Jun. 2010 13.

41. N. Olivier, M. A. Luengo-Oroz, L. Duloquin, E. Faure, T. Savy, I. Veilleux, X. Solinas, D. Dóbarre, P. Bourgine, A. Santos, N. Peyriéras, and E. Beaurepaire, “Cell lineage reconstruction of early zebrafish embryos using label-free nonlinear microscopy,” *Science*, vol. 329, 5994, Aug. 2010 13.

42. F. Helmchen and W. Denk, “Deep tissue two-photon microscopy,” *Nature Methods*, vol. 2(12), pp. 932–940, Nov. 2005 13.

43. F. Aptel, N. Olivier, A. Deniset-Besseau, J. M. Legeais, K. Plamann, M. C. Schanne-Klein, and E. Beaurepaire, “Multimodal nonlinear imaging of the human cornea,” *Investigative Ophthalmology and Visual Science*, vol. 51(5), pp. 2459–2465, May 2010 13.

44. Q. Zaidi and J. Pokorny, “Appearance of pulsed infrared light: Second harmonic generation in the eye,” *Applied Optics*, vol. 27(6), pp. 1064–1068, Mar. 1998 13.

APPENDIX A - TABULATED RESULTS FROM EYE SIMULATION

A.1 Unchirped Pulse Simulation Without Self-Focusing

In the following tables, X notes unmeasurable values for pulses that have been totally absorbed in simulation. The 1399* simulations are propagated with the saturable absorption reported in [21] while the 1399 simulations are propagated without nonlinear absorption.

Table A-1. Time Domain Characteristics of Eye Simulation Without Self-Focusing

	Input Pulse			**Output Pulse**			
Wavelength (nm)	**Pulse Duration** (fs)	**Energy** (μJ)	**Power** (MW)	**Pulse Duration** (fs)	**Energy** (μJ)	**Power** (MW)	**Energy / Area vs Limit** (%)
10 fs							
1200	9.8	0.306	30.6	49.7	0.0566	0.0733	0.016
1250	9.8	0.346	34.6	18.5	0.0370	0.0479	0.009
1300	9.8	4.16	416	622	0.252	0.326	0.056
1350	9.8	385	38515	1271	10.4	13.6	2.10
1375	9.8	3848	3.85E5	70.7	129	145	24.9
1399	9.8	38485	3.85E6	217.1	4166	2146	767
1400	9.8	38.5	3848	1271	0.726	0.952	0.134
35 fs							
1200	34.9	0.306	8.73	654	0.0221	0.0274	0.006
1250	34.9	0.346	9.90	791	0.0274	0.0359	0.007
1300	34.9	4.16	119	125	0.201	0.247	0.045
1350	34.9	385	1.10E4	91.1	3.04	3.95	0.616
1375	34.9	3849	1.10E5	92.7	14.4	18.7	2.77
1399	34.9	38485	1.10E6	391	1875	1595	345
1400	34.9	38.5	1100	91.1	0.0159	0.0226	0.003
50 fs							
1200	49.9	0.306	6.11	659	0.0205	0.0268	0.006
1250	49.9	0.346	6.927	799.4	0.0290	0.0371	0.007
1300	49.9	4.16	83.1	119	0.205	0.253	0.046
1350	49.9	385	7703	90.7	1.54	2.16	0.342
1375	49.9	3849	7.70E5	90.1	3.46	4.83	0.668
1399	49.9	38485	7.70E6	333.4	602	576	111
1400	49.9	38.5	770	163	0.00157	0.00220	0.000
100 fs							
1200	99.9	0.306	3.06	1045	0.0198	0.0255	0.006
1250	99.9	0.346	3.46	1187	0.0302	0.0373	0.008
1300	99.9	4.16	41.6	132	0.205	0.348	0.046
1350	99.9	385	3852	198	0.366	0.764	0.074
1375	99.9	3849	38488	838	0.192	0.260	0037
1399	99.9	38485	384848	52.4	0.874	1.15	0.161
1399*	99.9	38485	384848	50.0	15.1	20.9	2.776
1400	99.9	38.5	385	315	3.0E-5	5.1E-5	0.000
500 fs							

Continued on next page

Table A-1 – *Continued from previous page*

	Input Pulse			Output Pulse			
Wavelength (nm)	**Pulse Duration (fs)**	**Energy (μJ)**	**Power (MW)**	**Pulse Duration (fs)**	**Energy (μJ)**	**Power (MW)**	**Energy / Area vs Limit (%)**
1200	499.9	0.306	0.611	715	0.019	0.023	0.005
1250	499.8	0.346	0.693	617	0.031	0.053	0.008
1300	499.8	4.156	8.313	504	0.201	0.400	0.045
1350	499.8	385	770	564	0.078	0.145	0.016
1375	499.8	3849	7698	503	0.037	0.07	0.007
1399	499.8	38484	76970	379	3.96E-7	3.92E-7	0.000
1399*	499.8	38484	76970	372	5.80E-7	6.23E-7	0.000
1400	499.8	38.5	77.0	2311	8.37E-13	1.88E-13	0.000
1 ps							
1200	999.8	0.306	0.306	1079	0.0193	0.0167	0.005
1250	999.8	0.346	0.346	1012	0.0308	0.0308	0.008
1300	999.8	4.16	4.16	1002	0.201	0.201	0.045
1350	999.8	385	385	1005	0.0776	0.0776	0.016
1375	999.8	3849	3849	1019	0.0326	0.0318	0.006
1399	999.8	38485	38485	X	X	X	X
1399*	999.8	38485	38485	X	X	X	X
1400	999.8	38.5	38.5	X	X	X	X

Table A-2. Spectral Characteristics of Eye Simulation Without Self-Focusing

	Input Pulse				Output Pulse			
Wave-length (nm)	**FWHM Spectral Range (nm)**	**RMS Spectral Range (nm)**	10^{-3} **Max (nm)**	10^{-5} **Max (nm)**	**FWHM Spectral Range (nm)**	**RMS Spectral Range (nm)**	10^{-3} **Max (nm)**	10^{-5} **Max (nm)**
10 fs								
1200	1102-1316	1047-1405	938-1664	882-1874	1064-1142	1021-1297	929-1340	873-1373
1250	1145-1377	1085-1474	969-1762	909-2000	1079-1275	1036-1314	957-1345	893-1377
1300	1186-1438	1123-1544	998-1862	935-2131	1094-1301	1053-1324	977-1365	913-1380
1350	1228-1499	1238-1294	1160-1615	961-2268	1238-1294	1093-1325	983-1364	831-1510
1375	1249-1530	1178-1651	1042-2020	974-2340	776-797	713-1309	678-1723	565-2330
1399	1268-1560	1196-1686	1056-2073	985-2410	459-819	421-917	396-2128	366-2595
1400	1269-1561	1196-1687	1056-2075	986-2413	1237-1306	1096-1331	1021-1368	973-1697
35 fs								
1200	1170-1231	1145-1261	1111-1304	1088-1338	1168-1235	1130-1265	1099-1301	1078-1325
1250	1218-1284	1190-1316	1154-1363	1129-1400	1224-1282	1194-1304	1155-1332	1121-1349
1300	1265-1337	1236-1371	1197-1423	1170-1463	1259-1306	1233-1328	1198-1347	1179-1374
1350	1313-1389	1281-1427	1239-1483	1210-1527	1279-1323	1258-1340	1226-1372	1173-1382
1375	1336-1416	1303-1455	1260-1513	1239-1559	1272-1315	1231-1339	1171-1375	1069-1415
1399	1359-1441	1325-1482	1280-1542	1249-1590	738-802	560-1271	527-1839	470-2341
1400	1360-1442	1326-1483	1281-1543	1250-1591	1299-1336	1275-1367	1249-1381	1223-1385
50 fs								
1200	1179-1222	1160-1243	1137-1271	1119-1293	1179-1223	1159-1245	1129-1273	1113-1293
1250	1227-1273	1206-1297	1181-1327	1163-1351	1231-1274	1208-1294	1183-1317	1164-1334
1300	1276-1325	1253-1351	1226-1384	1206-1410	1270-1306	1249-1327	1225-1343	1206-1367
1350	1324-1377	1299-1405	1270-1440	1249-1469	1297-1332	1276-1344	1244-1375	1216-1384
1375	1384-1403	1322-1432	1292-1469	1270-1499	1279-1336	1258-1368	1224-1381	1162-1399
1399	1371-1428	1344-1458	1314-1496	1291-1527	712-795	677-1374	644-1791	502-2341

Continued on next page

Table A-2 – *Continued from previous page*

	Input Pulse				**Output Pulse**			
Wave-length (nm)	**FWHM Spectral Range (nm)**	**RMS Spectral Range (nm)**	10^{-3} **Max (nm)**	10^{-5} **Max (nm)**	**FWHM Spectral Range (nm)**	**RMS Spectral Range (nm)**	10^{-3} **Max (nm)**	10^{-5} **Max (nm)**
1400	1372-1429	1345-1459	1314-1497	1292-1528	1319-1366	1300-1376	1280-1385	1259-1385
100 fs								
1200	1190-1211	1178-1223	1167-1234	1158-1245	1189-1211	1178-1223	1167-1235	1158-1245
1250	1239-1262	1226-1275	1215-1287	1205-1299	1240-1262	1227-1275	1215-1287	1205-1298
1300	1288-1313	1274-1327	1262-1340	1251-1353	1285-1307	1272-1320	1260-1332	1250-1341
1350	1337-1364	1322-1379	1309-1394	1297-1407	1323-1340	1310-1365	1294-1374	1272-1381
1375	1361-1389	1346-1405	1332-1420	1321-1434	1358-1368	1305-1378	1284-1385	1251-1385
1399	1385-1414	1369-1430	1355-1446	1343-1460	1299-1368	1271-1378	1229-1385	1187-1385
1399*	1385-1414	1369-1430	1355-1446	1343-1460	1275-1310	1230-1371	1184-1380	1099-1431
1400	1386-1415	1370-1431	1356-1447	1344-1461	1362-1376	1352-1385	1339-1385	1326-1389
500 fs								
1200	1198-1202	1195-1205	1193-1207	1191-1209	1198-1202	1195-1205	1193-1207	1191-1209
1250	1248-1252	1245-1255	1243-1257	1241-1259	1248-1252	1245-1255	1243-1257	1241-1259
1300	1298-1302	1294-1306	1292-1308	1290-1310	1297-1302	1294-1306	1292-1308	1290-1310
1350	1347-1353	1344-1356	1342-1359	1339-1361	1347-1352	1343-1356	1341-1358	1337-1361
1375	1372-1378	1369-1382	1366-1384	1364-1386	1371-1376	1367-1380	1363-1382	1358-1385
1399	1396-1402	1392-1406	1390-1408	1387-1411	1383-1385	1374-1385	1370-1394	1363-1398
1399*	1396-1402	1392-1406	1390-1408	1387-1411	1383-1385	1374-1385	1369-1392	1362-1398
1400	1397-1403	1393-1407	1391-1409	1388-1412	X	X	X	X
1 ps								
1200	1199-1201	1197-1203	1197-1203	1196-1204	1199-1201	1197-1203	1197-1203	1196-1204
1250	1249-1251	1247-1253	1246-1254	1245-1255	1249-1251	1247-1253	1246-1254	1245-1255
1300	1299-1301	1297-1303	1296-1304	1295-1305	1299-1301	1297-1303	1296-1304	1295-1305
1350	1349-1351	1347-1353	1346-1354	1345-1355	1349-1351	1347-1353	1346-1354	1344-1355

Continued on next page

Table A-2 – *Continued from previous page*

	Input Pulse				Output Pulse			
Wave-length (nm)	**FWHM Spectral Range (nm)**	**RMS Spectral Range (nm)**	10^{-3} **Max (nm)**	10^{-5} **Max (nm)**	**FWHM Spectral Range (nm)**	**RMS Spectral Range (nm)**	10^{-3} **Max (nm)**	10^{-5} **Max (nm)**
1375	1374-1376	1372-1378	1371-1379	1369-1381	1373-1376	1371-1378	1370-1379	1367-1381
1399	1398-1400	1395-1403	1394-1404	1393-1405	X	X	X	X
1399*	1398-1400	1395-1403	1394-1404	1393-1405	X	X	X	X
1400	1399-1401	1396-1399	1395-1405	1394-1406	X	X	X	X

Table A-3. Energy Distribution as a Function of Wavelength for Eye Simulation Without Self-Focusing

Wave-length (nm)	Energy 400 nm to 700 nm (nJ)	Energy 700 nm to 1000 nm (nJ)	Energy 1000 nm to 1200 nm (nJ)	Energy 1200 nm (nJ)	Energy 400 nm to 700 nm (%)	Energy 700 nm to 1000 nm (%)	Energy 1000 nm to 1200 nm (%)	Energy 1200 nm (%)
10 fs								
1200	< 5E-7	0.545	48.2	7.79	0	0.964	85.3	13.8
1250	< 5E-7	0.113	26.4	10.5	0	0.305	71.3	28.4
1300	< 5E-7	0.218	134	118	0	0.087	53.1	46.7
1350	4E-6	12.6	2640	7717	0	0.122	25.5	74.4
1375	421	1.09E5	6621	12781	0.327	84.6	5.14	9.92
1399	3.07E6	1.03E6	42012	19473	73.7	24.8	1.01	0.467
1400	< 5E-7	0.0302	164	562	0	0.004	22.6	77.4
35 fs								
1200	< 5E-7	< 5E-7	11.5	10.7	0	0	51.8	48.2
1250	< 5E-7	< 5E-7	0.733	26.6	0	0	2.68	97.3
1300	< 5E-7	< 5E-7	0.0464	201	0	0	0.023	99.977
1350	< 5E-7	< 5E-7	0.138	3038	0	0	0.005	99.995
1375	< 5E-7	1.59E-4	33.0	14334	0	0	0.230	99.770
1399	7.42E5	1.08E6	32847	24172	38.6	57.4	1.8	1.3
1400	< 5E-7	< 5E-7	5E-6	15.9	0	0	0	100
50 fs								
1200	< 5E-7	< 5E-7	10.2	10.3	0	0	49.8	50.2
1250	< 5E-7	< 5E-7	0.0891	28.9	0	0	0.308	99.7
1300	< 5E-7	< 5E-7	3.47E-5	204	0	0	0	100
1350	< 5E-7	< 5E-7	6.47E-4	1541	0	0	0	100
1375	< 5E-7	< 5E-7	0.146	3462	0	0	0.004	99.996
1399	61210	4.50E5	32026	59206	10.2	74.7	5.32	9.83
1400	< 5E-7	< 5E-7	< 5E-7	1.57	0	0	0	100
100 fs								
1200	< 5E-7	< 5E-7	9.88	9.94	0	0	49.8	50.2
1250	< 5E-7	< 5E-7	1E-6	30.2	0	0	0	100
1300	< 5E-7	< 5E-7	< 5E-7	205	0	0	0	100
1350	< 5E-7	< 5E-7	< 5E-7	366	0	0	0	100
1375	< 5E-7	< 5E-7	< 5E-7	192	0	0	0	100
1399	1E-6	1E-6	6.93E-3	874	0	0	0.001	99.999
1399*	1E-6	2E-6	65.1	15010	0	0	0.432	99.568
1400	< 5E-7	< 5E-7	< 5E-7	0.0300	0	0	0	100
500 fs								
1200	< 5E-7	< 5E-7	9.71	9.69	0	0	50.1	49.9
1250	< 5E-7	< 5E-7	< 5E-7	30.8	0	0	0	100
1300	< 5E-7	< 5E-7	< 5E-7	201	0	0	0	100
1350	< 5E-7	< 5E-7	< 5E-7	78.0	0	0	0	100
1375	< 5E-7	< 5E-7	< 5E-7	37.2	0	0	0	100
1399	< 5E-7	< 5E-7	< 5E-7	3.95E-4	0.047	0.057	0.049	99.8
1399*	< 5E-7	< 5E-7	< 5E-7	5.79E-4	0.032	0.039	0.033	99.869
1400	X	X	X	X	X	X	X	X

Continued on next page

Table A-3 – *Continued from previous page*

Wave-length (nm)	Energy 400 nm to 700 nm (nJ)	Energy 700 nm to 1000 nm (nJ)	Energy 1000 nm to 1200 nm (nJ)	Energy 1200 nm (nJ)	Energy 400 nm to 700 nm (%)	Energy 700 nm to 1000 nm (%)	Energy 1000 nm to 1200 nm (%)	Energy 1200 nm (%)
1 ps								
1200	< 5E-7	< 5E-7	9.71	9.64	0	0	50.2	49.8
1250	< 5E-7	< 5E-7	< 5E-7	30.8	0	0	0	100
1300	< 5E-7	< 5E-7	< 5E-7	201.1	0	0	0	100
1350	< 5E-7	< 5E-7	< 5E-7	77.6	0	0	0	100
1375	< 5E-7	< 5E-7	< 5E-7	32.6	0	0	0	100
1399	X	X	X	X	X	X	X	X
1399*	X	X	X	X	X	X	X	X
1400	X	X	X	X	X	X	X	X

A.2 Unchirped Pulse Simulation With Self-Focusing

In the following tables, X notes unmeasurable values for pulses that have been totally absorbed in simulation. The 1399* simulations are propagated with the saturable absorption reported in [21] while the 1399 simulations are propagated without nonlinear absorption.

Table A-4. Time Domain Characteristics of Eye Simulation with Self-Focusing

	Input Pulse			Output Pulse			
Wavelength (nm)	**Pulse Duration (fs)**	**Energy (μJ)**	**Power (MW)**	**Pulse Duration (fs)**	**Energy (μJ)**	**Power (MW)**	**Energy / Area vs Limit (%)**
10 fs							
1200	9.8	0.306	30.6	49.7	0.0566	0.0733	0.016
1250	9.8	0.346	34.6	18.5	0.0370	0.0479	0.009
1300	9.8	4.156	416	622	0.252	0.326	0.056
1350	9.8	385	38515	1271	10.4	13.6	2.13
1375	9.8	3849	384876	84.6	130	146	46.9
1399	9.8	38485	3.85E6	Plasma	Plasma	Plasma	Plasma
1400	9.8	38.5	3848.5	1271	0.726	0.952	0.134
35 fs							
1200	34.9	0.306	8.73	654	0.0221	0.0274	0.006
1250	34.9	0.346	9.90	791	0.0274	0.0360	0.007
1300	34.9	4.16	119	125	0.201	0.248	0.045
1350	34.9	385	11000	91.1	3.04	3.95	0.619
1375	34.9	3849	110000	92.6	14.4	18.7	2.87
1399	34.9	38485	1.10E6	Plasma	Plasma	Plasma	Plasma
1400	34.9	38.5	1100	91.1	0.0159	0.0226	0.005
50 fs							
1200	49.9	0.306	6.11	659	0.0205	0.0268	0.006
1250	49.9	0.346	6.927	799	0.0290	0.0371	0.007
1300	49.9	4.16	83.1	119	0.205	0.253	0.046
1350	49.9	385	7703	90.7	1.54	2.16	0.314
1375	49.9	3849	7.70E5	90.7	3.46	4.83	1.90
1399	49.9	38485	7.70E6	Plasma	Plasma	Plasma	Plasma
1400	49.9	38.5	770	163	0.00157	0.00220	0.000
100 fs							
1200	99.9	0.306	3.06	1045	0.0198	0.0255	0.006
1250	99.9	0.346	3.46	1187	0.0302	0.0373	0.008
1300	99.9	4.16	41.6	131.8	0.205	0.348	0.046
1350	99.9	385	3852	198	0.366	0.764	0.074
1375	99.9	3849	38488	838	0.192	0.260	0.037
1399	99.9	38485	384848	52.4	0.877	1.16	0.168
1399*	99.9	38485	384848	49.7	15.3	21.2	3.06
1400	99.9	38.5	385	315	3.00E-5	5.09E-5	0.000
500 fs							
1200	499.9	0.306	0.611	715	0.019	0.023	0.005
1250	499.8	0.346	0.693	617	0.031	0.053	0.008

Continued on next page

Table A-4 – *Continued from previous page*

	Input Pulse			Output Pulse			
Wavelength (nm)	**Pulse Duration (fs)**	**Energy (μJ)**	**Power (MW)**	**Pulse Duration (fs)**	**Energy (μJ)**	**Power (MW)**	**Energy / Area vs Limit (%)**
1300	499.8	4.156	8.313	504	0.201	0.4	0.045
1350	499.8	385	770	564	0.078	0.145	0.016
1375	499.8	3849	7698	503	0.037	0.070	0.007
1399	499.8	38484	76970	379	3.96E-7	3.93E-7	0.000
1399*	499.8	38484	76970	371.7	5.80E-7	6.23E-7	0.000
1400	499.8	38.5	77.0	X	X	X	X
1 ps							
1200	999.8	0.306	0.306	1079	0.0193	0.0167	0.005
1250	999.8	0.346	0.346	1012	0.0308	0.0308	0.008
1300	999.8	4.16	4.16	1002	0.201	0.201	0.045
1350	999.8	385	385	1005	0.0775	0.0775	0.016
1375	999.8	3849	3849	1019	0.0326	0.0318	0.006
1399	999.8	38485	38485	X	X	X	X
1399*	999.8	38485	38485	X	X	X	X
1400	999.8	38.5	38.5	X	X	X	X

Table A-5. Spectral Characteristics of Eye Simulation with Self-Focusing

	Input Pulse				**Output Pulse**			
Wave-length (nm)	**FWHM Spectral Range (nm)**	**RMS Spectral Range (nm)**	10^{-3} **Max (nm)**	10^{-5} **Max (nm)**	**FWHM Spectral Range (nm)**	**RMS Spectral Range (nm)**	10^{-3} **Max (nm)**	10^{-5} **Max (nm)**
10 fs								
1200	1103-1316	1047-1405	938-1664	882-1875	1064-1143	1021-1297	929-1340	873-1373
1250	1145-1377	1085-1474	969-1762	909-2000	1079-1275	1036-1314	957-1345	893-1377
1300	1186-1438	1123-1544	998-1862	935-2131	1094-1301	1053-1324	977-1365	913-1380
1350	1228-1499	1160-1615	1028-1967	961-2268	1238-1294	1093-1325	983-1364	831-1510
1375	1249-1530	1178-1651	1042-2020	974-2340	757-1271	712-1337	655-1828	542-2488
1399	1268-1560	1196-1686	1056-2073	985-2410	Plasma	Plasma	Plasma	Plasma
1400	1269-1561	1196-1687	1056-2075	986-2413	1237-1306	1096-1331	1021-1368	973-1697
35 fs								
1200	1170-1231	1145-1261	1111-1304	1088-1338	1168-1235	1130-1265	1099-1301	1078-1325
1250	1218-1284	1190-1316	1154-1363	1129-1400	1224-1282	1194-1304	1155-1332	1121-1349
1300	1265-1337	1236-1371	1197-1423	1170-1463	1259-1306	1233-1328	1198-1347	1170-1374
1350	1313-1389	1281-1427	1239-1483	1210-1527	1279-1323	1258-1340	1226-1372	1173-1382
1375	1336-1416	1303-1455	1260-1513	1230-1559	1272-1315	1231-1339	1171-1375	1069-1416
1399	1359-1441	1325-1482	1280-1542	1249-1590	Plasma	Plasma	Plasma	Plasma
1400	1360-1442	1326-1483	1281-1543	1250-1591	1299-1336	1275-1367	1249-1381	1223-1385
50 fs								
1200	1179-1222	1160-1243	1137-1271	1119-1293	1179-1223	1159-1245	1129-1273	1113-1293
1250	1227-1273	1206-1297	1181-1327	1163-1351	1231-1274	1208-1294	1183-1317	1164-1334
1300	1276-1325	1253-1351	1226-1384	1206-1410	1270-1306	1249-1327	1225-1343	1206-1367
1350	1324-1377	1299-1405	1270-1440	1249-1469	1297-1332	1276-1344	1244-1375	1216-1384
1375	1384-1403	1322-1432	1292-1469	1270-1499	1279-1336	1258-1368	1224-1381	1162-1400
1399	1371-1428	1344-1458	1314-1496	1291-1527	Plasma	Plasma	Plasma	Plasma

Continued on next page

Table A-5 – *Continued from previous page*

	Input Pulse				Output Pulse			
Wave-length (nm)	**FWHM Spectral Range (nm)**	**RMS Spectral Range (nm)**	10^{-3} **Max (nm)**	10^{-5} **Max (nm)**	**FWHM Spectral Range (nm)**	**RMS Spectral Range (nm)**	10^{-3} **Max (nm)**	10^{-5} **Max (nm)**
1400	1372-1429	1345-1459	1314-1497	1292-1528	1319-1366	1300-1376	1280-1385	1259-1385
100 fs								
1200	1190-1211	1178-1223	1167-1234	1158-1245	1189-1211	1178-1223	1167-1235	1158-1245
1250	1239-1262	1226-1275	1215-1287	1205-1299	1240-1262	1227-1275	1215-1287	1205-1298
1300	1288-1313	1274-1327	1262-1340	1251-1353	1285-1307	1272-1320	1260-1332	1250-1341
1350	1337-1364	1322-1379	1309-1394	1297-1407	1323-1340	1310-1365	1294-1374	1272-1381
1375	1361-1389	1346-1405	1332-1420	1321-1434	1358-1368	1305-1378	1284-1385	1251-1385
1399	1385-1414	1369-1430	1355-1446	1343-1460	1299-1368	1271-1378	1229-1385	1187-1385
1399*	1385-1414	1369-1430	1355-1446	1343-1460	1275-1310	1230-1370	1184-1380	1099-1432
1400	1386-1415	1370-1431	1356-1447	1344-1461	1362-1376	1352-1385	1339-1385	1326-1389
500 fs								
1200	1198-1202	1195-1205	1193-1207	1191-1209	1198-1202	1195-1205	1193-1207	1191-1209
1250	1248-1252	1245-1255	1243-1257	1241-1259	1248-1252	1245-1255	1243-1257	1241-1259
1300	1298-1302	1294-1306	1292-1308	1290-1310	1297-1302	1294-1306	1292-1308	1290-1310
1350	1347-1353	1344-1356	1342-1359	1339-1361	1347-1352	1343-1356	1341-1358	1337-1361
1375	1372-1378	1369-1382	1366-1384	1364-1386	1371-1376	1367-1380	1363-1382	1358-1385
1399	1396-1402	1392-1406	1390-1408	1387-1411	1383-1385	1374-1385	1370-1394	1363-1398
1399*	1396-1402	1392-1406	1390-1408	1387-1411	1383-1385	1374-1385	1369-1392	1362-1398
1400	1397-1403	1393-1407	1391-1409	1388-1412	X	X	X	X
1 ps								
1200	1199-1201	1197-1203	1197-1203	1196-1204	1199-1201	1197-1203	1197-1203	1196-1204
1250	1249-1251	1247-1253	1246-1254	1245-1255	1249-1251	1247-1253	1246-1254	1245-1255
1300	1299-1301	1297-1303	1296-1304	1295-1305	1299-1301	1297-1303	1296-1304	1295-1305
1350	1349-1351	1347-1353	1346-1354	1345-1355	1349-1351	1347-1353	1346-1354	1344-1355

Continued on next page

Table A-5 – *Continued from previous page*

	Input Pulse				Output Pulse			
Wave-length (nm)	**FWHM Spectral Range (nm)**	**RMS Spectral Range (nm)**	10^{-3} **Max (nm)**	10^{-5} **Max (nm)**	**FWHM Spectral Range (nm)**	**RMS Spectral Range (nm)**	10^{-3} **Max (nm)**	10^{-5} **Max (nm)**
1375	1374-1376	1372-1378	1371-1379	1369-1381	1373-1376	1371-1378	1370-1379	1367-1381
1399	1398-1400	1395-1403	1394-1404	1393-1405	X	X	X	X
1399*	1398-1400	1395-1403	1394-1404	1393-1405	X	X	X	X
1400	1399-1401	1396-1399	1395-1405	1394-1406	X	X	X	X

Table A-6. Energy Distribution as a Function of Wavelength for Eye Simulation with Self-Focusing

Wave-length (nm)	Energy 400 nm to 700 nm (nJ)	Energy 700 nm to 1000 nm (nJ)	Energy 1000 nm to 1200 nm (nJ)	Energy 1200 nm (nJ)	Energy 400 nm to 700 nm (%)	Energy 700 nm to 1000 nm (%)	Energy 1000 nm to 1200 nm (%)	Energy 1200 nm (%)
10 fs								
1200	< 5E-7	0.545	48.2	7.79	0	0.964	85.3	13.8
1250	< 5E-7	0.113	26.4	10.5	0	0.305	71.3	28.4
1300	< 5E-7	0.218	134	118	0	0.087	53.1	46.8
1350	4.0E-6	12.6	2639	7715	0	0.122	25.5	74.4
1375	737	110226	5522	13500	0.567	84.8	4.25	10.4
1399	Plasma	Plasma	Plasma	Plasma	Plasma	Plasma	Plasma	Plasma
1400	< 5E-7	0.0302	164	562	0.000	0.004	22.6	77.3
35 fs								
1200	< 5E-7	< 5E-7	11.5	10.7	0	0	51.8	48.2
1250	< 5E-7	< 5E-7	0.733	26.6	0	0	2.68	97.32
1300	< 5E-7	< 5E-7	0.0464	201	0	0	0.023	99.977
1350	< 5E-7	< 5E-7	0.137	3038	0	0	0.005	99.995
1375	< 5E-7	1.60E-4	33.0	14300	0	0	0.230	99.770
1399	Plasma	Plasma	Plasma	Plasma	Plasma	Plasma	Plasma	Plasma
1400	< 5E-7	< 5E-7	4.7E-6	15.9	0	0	0	100
50 fs								
1200	< 5E-7	< 5E-7	10.2	10.3	0	0	49.8	50.2
1250	< 5E-7	< 5E-7	0.089	28.9	0	0	0.308	99.692
1300	< 5E-7	< 5E-7	3.48E-5	205	0	0	0	100
1350	< 5E-7	< 5E-7	6.47E-4	1541	0	0	0	100
1375	< 5E-7	< 5E-7	0.147	3463	0	0	0.004	99.996
1399	Plasma	Plasma	Plasma	Plasma	Plasma	Plasma	Plasma	Plasma
1400	< 5E-7	< 5E-7	< 5E-7	1.57	0	0	0	100
100 fs								
1200	< 5E-7	< 5E-7	9.88	9.94	0	0	49.8	50.2
1250	< 5E-7	< 5E-7	1.13E-6	30.2	0	0	0	100
1300	< 5E-7	< 5E-7	< 5E-7	205	0	0	0	100
1350	< 5E-7	< 5E-7	< 5E-7	366	0	0	0	100
1375	< 5E-7	< 5E-7	< 5E-7	192	0	0	0	100
1399	< 5E-7	1.06E-6	0.00704	877	0	0	0.001	99.999
1399*	1.02E-6	1.86E-6	68.32	15243	0	0	0.446	99.554
1400	< 5E-7	< 5E-7	< 5E-7	0.0300	0	0	0	100
500 fs								
1200	< 5E-7	< 5E-7	9.71	9.69	0	0	50.1	49.9
1250	< 5E-7	< 5E-7	< 5E-7	30.8	0	0	0	100
1300	< 5E-7	< 5E-7	< 5E-7	201	0	0	0	100
1350	< 5E-7	< 5E-7	< 5E-7	78.0	0	0	0	100
1375	< 5E-7	< 5E-7	< 5E-7	37.2	0	0	0	100
1399	< 5E-7	< 5E-7	< 5E-7	3.95E-4	0.047	0.057	0049	99.8
1399*	< 5E-7	< 5E-7	< 5E-7	5.79E-4	0.032	0.039	0.033	99.869
1400	X	X	X	X	X	X	X	X
1 ps								

Continued on next page

Table A-6 – *Continued from previous page*

Wave-length (nm)	**Energy 400 nm to 700 nm (nJ)**	**Energy 700 nm to 1000 nm (nJ)**	**Energy 1000 nm to 1200 nm (nJ)**	**Energy 1200 nm (nJ)**	**Energy 400 nm to 700 nm (%)**	**Energy 700 nm to 1000 nm (%)**	**Energy 1000 nm to 1200 nm (%)**	**Energy 1200 nm (%)**
1200	< 5E-7	< 5E-7	9.71	9.64	0	0	50.2	49.8
1250	< 5E-7	< 5E-7	< 5E-7	30.8	0	0	0	100
1300	< 5E-7	< 5E-7	< 5E-7	201	0	0	0	100
1350	< 5E-7	< 5E-7	< 5E-7	77.6	0	0	0	100
1375	< 5E-7	< 5E-7	< 5E-7	32.6	0	0	0	100
1399	X	X	X	X	X	X	X	X
1399*	X	X	X	X	X	X	X	X
1400	X	X	X	X	X	X	X	X

A.3 Pre-Focused Pulse Simulation

In the following tables, X notes unmeasurable values for pulses that have been totally absorbed in simulation. The 1399* simulations are propagated with the saturable absorption reported in [21] while the 1399 simulations are propagated without nonlinear absorption.

Table A-7. Time Domain Characteristics of Pre-Focused Eye Simulation with Self-Focusing

	Input Pulse			Output Pulse			
Wavelength (nm)	Pulse Duration (fs)	Energy (μJ)	Power (MW)	Pulse Duration (fs)	Energy (μJ)	Power (MW)	Energy / Area vs Limit (%)
10 fs							
1200	9.8	0.306	30.6	145.9	0.0514	0.0643	43.8
1250	9.8	0.346	34.6	117.1	0.0330	0.0416	27.8
1300	9.8	4.156	416	Plasma	Plasma	Plasma	Plasma
1350	9.8	385	38515	Plasma	Plasma	Plasma	Plasma
1375	9.8	3849	384876	Plasma	Plasma	Plasma	Plasma
1399	9.8	38485	3.85E6	Plasma	Plasma	Plasma	Plasma
1400	9.8	38.5	3848.5	Plasma	Plasma	Plasma	Plasma
35 fs							
1200	34.9	0.306	8.73	789.5	0.0186	0.0230	12.5
1250	34.9	0.346	9.90	1151	0.0230	0.0280	15.0
1300	34.9	4.16	119	136.4	0.160	0.193	192
1350	34.9	385	11000	Plasma	Plasma	Plasma	Plasma
1375	34.9	3849	110000	Plasma	Plasma	Plasma	Plasma
1399	34.9	38485	1.10E6	Plasma	Plasma	Plasma	Plasma
1400	34.9	38.5	1100	94.2	0.0122	0.0159	5.95
50 fs							
1200	49.9	0.306	6.11	786	0.0172	0.0208	11.4
1250	49.9	0.346	6.927	1172	0.0245	0.0282	15.7
1300	49.9	4.16	83.1	117	0.160	0.190	226
1350	49.9	385	7703	Plasma	Plasma	Plasma	Plasma
1375	49.9	3849	7.70E5	Plasma	Plasma	Plasma	Plasma
1399	49.9	38485	7.70E6	Plasma	Plasma	Plasma	Plasma
1400	49.9	38.5	770	172	0.00106	0.00138	0.479
100 fs							
1200	99.9	0.306	3.06	1153	0.0166	0.0191	10.6
1250	99.9	0.346	3.46	1218	0.0257	0.0304	15.7
1300	99.9	4.16	41.6	Plasma	Plasma	Plasma	Plasma
1350	99.9	385	3852	Plasma	Plasma	Plasma	Plasma
1375	99.9	3849	38488	Plasma	Plasma	Plasma	Plasma
1399	99.9	38485	384848	Plasma	Plasma	Plasma	Plasma
1399*	99.9	38485	384848	Plasma	Plasma	Plasma	Plasma
1400	99.9	38.5	385	318	1.56E-5	2.51E-5	0.007
500 fs							
1200	499.9	0.306	0.611	758	0.016	0.018	10.2
1250	499.8	0.346	0.693	631	0.026	0.045	16.0

Continued on next page

Table A-7 – *Continued from previous page*

	Input Pulse			Output Pulse			
Wavelength (nm)	**Pulse Duration** (fs)	**Energy** (μJ)	**Power** (MW)	**Pulse Duration** (fs)	**Energy** (μJ)	**Power** (MW)	**Energy / Area vs Limit** (%)
1300	499.8	4.156	8.313	519	0.156	0.308	125
1350	499.8	385	770	577	0.044	0.082	25.0
1375	499.8	3849	7698	504	0.018	0.034	10.5
1399	499.8	38484	76970	406	1.55E-7	1.52E-7	0.000
1399*	499.8	38484	76970	394	2.28E-7	2.44E-7	0.000
1400	499.8	38.5	77.0	X	X	X	X
1 ps							
1200	999.8	0.306	0.306	1091	0.0162	0.0137	10.2
1250	999.8	0.346	0.346	1017	0.0263	0.0262	15.6
1300	999.8	4.16	4.16	1015	0.162	0.160	102
1350	999.8	385	385	1012	0.0445	0.0444	23.4
1375	999.8	3849	3849	1020	0.0156	0.0152	8.01
1399	999.8	38485	38485	X	X	X	X
1399*	999.8	38485	38485	X	X	X	X
1400	999.8	38.5	38.5	X	X	X	X

Table A-8. Spectral Characteristics of Pre-Focused Eye Simulation with Self-Focusing

	Input Pulse				Output Pulse			
Wave-length (nm)	**FWHM Spectral Range (nm)**	**RMS Spectral Range (nm)**	10^{-3} **Max (nm)**	10^{-5} **Max (nm)**	**FWHM Spectral Range (nm)**	**RMS Spectral Range (nm)**	10^{-3} **Max (nm)**	10^{-5} **Max (nm)**
10 fs								
1200	1103-1316	1047-1405	938-1664	882-1875	1069-1142	1019-1294	925-1341	868-1543
1250	1145-1377	1085-1474	969-1762	909-2000	1085-1273	1034-1314	953-1342	881-1610
1300	1186-1438	1123-1544	998-1862	935-2131	Plasma	Plasma	Plasma	Plasma
1350	1228-1499	1160-1615	1028-1967	961-2268	Plasma	Plasma	Plasma	Plasma
1375	1249-1530	1178-1651	1042-2020	974-2340	Plasma	Plasma	Plasma	Plasma
1399	1268-1560	1196-1686	1056-2073	985-2410	Plasma	Plasma	Plasma	Plasma
1400	1269-1561	1196-1687	1056-2075	986-2413	Plasma	Plasma	Plasma	Plasma
35 fs								
1200	1170-1231	1145-1261	1111-1304	1088-1338	1169-1234	1128-1265	1099-1299	1074-1332
1250	1218-1284	1190-1316	1154-1363	1129-1400	1225-1282	1195-1305	1153-1336	1121-1365
1300	1265-1337	1236-1371	1197-1423	1170-1463	1267-1298	1235-1327	1197-1365	1147-1415
1350	1313-1389	1281-1427	1239-1483	1210-1527	Plasma	Plasma	Plasma	Plasma
1375	1336-1416	1303-1455	1260-1513	1230-1559	Plasma	Plasma	Plasma	Plasma
1399	1359-1441	1325-1482	1280-1542	1249-1590	Plasma	Plasma	Plasma	Plasma
1400	1360-1442	1326-1483	1281-1543	1250-1591	1297-1336	1275-1365	1248-1379	1220-1385
50 fs								
1200	1179-1222	1160-1243	1137-1271	1119-1293	1179-1223	1158-1246	1128-1274	1113-1298
1250	1227-1273	1206-1297	1181-1327	1163-1351	1231-1274	1209-1293	1183-1319	1155-1347
1300	1276-1325	1253-1351	1226-1384	1206-1410	1270-1298	1248-1322	1220-1363	1182-1400
1350	1324-1377	1299-1405	1270-1440	1249-1469	Plasma	Plasma	Plasma	Plasma
1375	1384-1403	1322-1432	1292-1469	1270-1499	Plasma	Plasma	Plasma	Plasma
1399	1371-1428	1344-1458	1314-1496	1291-1527	Plasma	Plasma	Plasma	Plasma

Continued on next page

Table A-8 – *Continued from previous page*

	Input Pulse				**Output Pulse**			
Wave-length (nm)	**FWHM Spectral Range (nm)**	**RMS Spectral Range (nm)**	10^{-3} **Max (nm)**	10^{-5} **Max (nm)**	**FWHM Spectral Range (nm)**	**RMS Spectral Range (nm)**	10^{-3} **Max (nm)**	10^{-5} **Max (nm)**
1400	1372-1429	1345-1459	1314-1497	1292-1528	1318-1340	1299-1375	1279-1385	1257-1385
100 fs								
1200	1190-1211	1178-1223	1167-1234	1158-1245	1189-1211	1178-1223	1167-1235	1157-1245
1250	1239-1262	1226-1275	1215-1287	1205-1299	1240-1262	1227-1275	1216-1287	1205-1305
1300	1288-1313	1274-1327	1262-1340	1251-1353	Plasma	Plasma	Plasma	Plasma
1350	1337-1364	1322-1379	1309-1394	1297-1407	Plasma	Plasma	Plasma	Plasma
1375	1361-1389	1346-1405	1332-1420	1321-1434	Plasma	Plasma	Plasma	Plasma
1399	1385-1414	1369-1430	1355-1446	1343-1460	Plasma	Plasma	Plasma	Plasma
1399*	1385-1414	1369-1430	1355-1446	1343-1460	Plasma	Plasma	Plasma	Plasma
1400	1386-1415	1370-1431	1356-1447	1344-1461	1362-1375	1352-1385	1338-1385	1325-1388
500 fs								
1200	1198-1202	1195-1205	1193-1207	1191-1209	1198-1202	1195-1205	1193-1207	1191-1209
1250	1248-1252	1245-1255	1243-1257	1241-1259	1248-1252	1245-1255	1243-1258	1241-1259
1300	1298-1302	1294-1306	1292-1308	1290-1310	1297-1302	1294-1306	1290-1309	1285-1314
1350	1347-1353	1344-1356	1342-1359	1339-1361	1347-1352	1343-1356	1341-1359	1337-1363
1375	1372-1378	1369-1382	1366-1384	1364-1386	1371-1376	1367-1380	1363-1382	1357-1385
1399	1396-1402	1392-1406	1390-1408	1387-1411	1383-1385	1374-1385	1369-1389	1063-1397
1399*	1396-1402	1392-1406	1390-1408	1387-1411	1383-1385	1373-1385	1368-1389	1362-1397
1400	1397-1403	1393-1407	1391-1409	1388-1412	X	X	X	X
1 ps								
1200	1199-1201	1197-1203	1197-1203	1196-1204	1199-1201	1197-1203	1197-1203	1196-1204
1250	1249-1251	1247-1253	1246-1254	1245-1255	1249-1251	1247-1253	1246-1254	1245-1255
1300	1299-1301	1297-1303	1296-1304	1295-1305	1299-1301	1297-1303	1296-1304	1293-1307
1350	1349-1351	1347-1353	1346-1354	1345-1355	1349-1351	1347-1353	1346-1354	1344-1356

Continued on next page

Table A-8 – *Continued from previous page*

	Input Pulse				Output Pulse			
Wave-length (nm)	**FWHM Spectral Range (nm)**	**RMS Spectral Range (nm)**	10^{-3} **Max (nm)**	10^{-5} **Max (nm)**	**FWHM Spectral Range (nm)**	**RMS Spectral Range (nm)**	10^{-3} **Max (nm)**	10^{-5} **Max (nm)**
1375	1374-1376	1372-1378	1371-1379	1369-1381	1373-1376	1371-1378	1370-1379	1367-1381
1399	1398-1400	1395-1403	1394-1404	1393-1405	X	X	X	X
1399*	1398-1400	1395-1403	1394-1404	1393-1405	X	X	X	X
1400	1399-1401	1396-1399	1395-1405	1394-1406	X	X	X	X

Table A-9. Energy Distribution as a Function of Wavelength for Pre-Focused Eye Simulation with Self-Focusing

Wave-length (nm)	Energy 400 nm to 700 nm (nJ)	Energy 700 nm to 1000 nm (nJ)	Energy 1000 nm to 1200 nm (nJ)	Energy 1200 nm (nJ)	Energy 400 nm to 700 nm (%)	Energy 700 nm to 1000 nm (%)	Energy 1000 nm to 1200 nm (%)	Energy 1200 nm (%)
10 fs								
1200	< 5E-7	0.539	44.4	6.46	0	1.048	86.394	12.558
1250	< 5E-7	0.130	24.1	8.69	0	0.393	73.239	26.367
1300	Plasma	Plasma	Plasma	Plasma	Plasma	Plasma	Plasma	Plasma
1350	Plasma	Plasma	Plasma	Plasma	Plasma	Plasma	Plasma	Plasma
1375	Plasma	Plasma	Plasma	Plasma	Plasma	Plasma	Plasma	Plasma
1399	Plasma	Plasma	Plasma	Plasma	Plasma	Plasma	Plasma	Plasma
1400	Plasma	Plasma	Plasma	Plasma	Plasma	Plasma	Plasma	Plasma
35 fs								
1200	< 5E-7	< 5E-7	9.68	8.96	0	0	51.9	48.1
1250	< 5E-7	< 5E-7	0.619	22.4	0	0	2.685	97.315
1300	< 5E-7	< 5E-7	0.0859	160	0	0	0.054	99.946
1350	Plasma	Plasma	Plasma	Plasma	Plasma	Plasma	Plasma	Plasma
1375	Plasma	Plasma	Plasma	Plasma	Plasma	Plasma	Plasma	Plasma
1399	Plasma	Plasma	Plasma	Plasma	Plasma	Plasma	Plasma	Plasma
1400	< 5E-7	< 5E-7	3.84e-6	12.2	0	0	0	100
50 fs								
1200	< 5E-7	< 5E-7	8.56	8.65	0	0	49.7	50.3
1250	< 5E-7	< 5E-7	0.0777	24.4	0	0	0.317	99.683
1300	< 5E-7	< 5E-7	3.00E-3	160	0	0	0.002	99.998
1350	Plasma	Plasma	Plasma	Plasma	Plasma	Plasma	Plasma	Plasma
1375	Plasma	Plasma	Plasma	Plasma	Plasma	Plasma	Plasma	Plasma
1399	Plasma	Plasma	Plasma	Plasma	Plasma	Plasma	Plasma	Plasma
1400	< 5E-7	< 5E-7	< 5E-7	1.06	0	0	0	100
100 fs								
1200	< 5E-7	< 5E-7	8.28	8.33	0	0	49.8	50.2
1250	< 5E-7	< 5E-7	2.77E-5	25.7	0	0	0	100
1300	Plasma	Plasma	Plasma	Plasma	Plasma	Plasma	Plasma	Plasma
1350	Plasma	Plasma	Plasma	Plasma	Plasma	Plasma	Plasma	Plasma
1375	Plasma	Plasma	Plasma	Plasma	Plasma	Plasma	Plasma	Plasma
1399	Plasma	Plasma	Plasma	Plasma	Plasma	Plasma	Plasma	Plasma
1399*	Plasma	Plasma	Plasma	Plasma	Plasma	Plasma	Plasma	Plasma
1400	< 5E-7	< 5E-7	< 5E-7	0.0156	0	0	0	100
500 fs								
1200	< 5E-7	< 5E-7	8.13	8.10	0	0	50.1	49.9
1250	< 5E-7	< 5E-7	< 5E-7	26.2	0	0	0	100
1300	< 5E-7	< 5E-7	< 5E-7	156	0	0	0	100
1350	< 5E-7	< 5E-7	< 5E-7	44.3	0	0	0	100
1375	< 5E-7	< 5E-7	< 5E-7	18.1	0	0	0	100
1399	< 5E-7	< 5E-7	< 5E-7	1.54E-4	0.121	0.143	0.119	99.5
1399*	< 5E-7	< 5E-7	< 5E-7	2.27E-4	0.082	0.097	0.081	99.673
1400	X	X	X	X	X	X	X	X

Continued on next page

Table A-9 – *Continued from previous page*

Wave-length (nm)	**Energy 400 nm to 700 nm (nJ)**	**Energy 700 nm to 1000 nm (nJ)**	**Energy 1000 nm to 1200 nm (nJ)**	**Energy 1200 nm (nJ)**	**Energy 400 nm to 700 nm (%)**	**Energy 700 nm to 1000 nm (%)**	**Energy 1000 nm to 1200 nm (%)**	**Energy 1200 nm (%)**
1 ps								
1200	< 5E-7	< 5E-7	8.12	8.07	0	0	50.2	49.8
1250	< 5E-7	< 5E-7	< 5E-7	26.3	0	0	0	100
1300	< 5E-7	< 5E-7	< 5E-7	162	0	0	0	100
1350	< 5E-7	< 5E-7	< 5E-7	44.5	0	0	0	100
1375	< 5E-7	< 5E-7	< 5E-7	15.6	0	0	0	100
1399	X	X	X	X	X	X	X	X
1399*	X	X	X	X	X	X	X	X
1400	X	X	X	X	X	X	X	X

A.4 Chirped Pulse Simulation

In the following tables, X notes unmeasurable values for pulses that have been totally absorbed in simulation. The 1399* simulations are propagated with the saturable absorption reported in [21] while the 1399 simulations are propagated without nonlinear absorption.

Table A-10. Time Domain Characteristics of Chirped Eye Simulation with Self-Focusing

	Input Pulse			Output Pulse			
Wavelength (nm)	**Pulse Duration (fs)**	**Energy (μJ)**	**Power (MW)**	**Pulse Duration (fs)**	**Energy (μJ)**	**Power (MW)**	**Energy / Area vs Limit (%)**
10 fs							
1200	624	0.306	30.6	12.7	0.056	167.3	0.016
1250	648	0.346	34.6	12.8	0.037	104	0.009
1300	840	4.16	416	13.2	0.249	681	0.056
1350	704	385	38515	9.2	6.36	3465	1.36
1375	680	3849	384876	64.9	66.8	12313	17.0
1399	680	38485	3848482	872	573	39665	240
1400	680	38.5	3848.5	14.5	0.740	1714	0.136
35 fs							
1200	654	0.306	8.73	31.0	0.0221	16.6	0.006
1250	796	0.346	9.90	39.4	0.0273	15.5	0.007
1300	84.7	4.16	119	58.7	0.200	91.0	0.045
1350	142	385	11004	55.2	2.92	1030	0.595
1375	986	3849	109965	53	8.57	1431	1.70
1399	891	38485	1099566	251	32.4	606	6.34
1400	890	38.5	1100	60.0	0.0159	3.89	0.003
50 fs							
1200	660	0.306	6.11	47.0	0.0205	6.53	0.006
1250	798	0.346	6.93	53.4	0.0290	8.47	0.007
1300	86.9	4.16	83.1	63.2	0.204	50.8	0.046
1350	164	385	7703	70.5	1.51	264	0.307
1375	908	3849	76975	70.4	2.17	154	0.423
1399	911	38485	769696	56.5	5.29	63.4	1.00
1400	908	38.5	770	71.4	0.00157	0.122	0.000
100 fs							
1200	1047	0.306	3.06	98.7	0.0198	1.56	0.006
1250	1186	0.346	3.46	101	0.0302	2.42	0.008
1300	113	4.16	41.6	108	0.205	11.0	0.046
1350	974	385	3852	110	0.360	15.4	0.073
1375	176	3839	38488	109	0.174	4.98	0.034
1399	185	38485	384848	132	0.043	0.478	0.008
1399*	185	38485	384848	107	0.0567	0.625	0.011
1400	955	38.5	385	182	3.00E-5	9.80E-4	0.000
500 fs							
1200	716	0.306	0.611	499	0.0194	0.0668	0.005
1250	618	0.346	0.693	500	0.0308	0.0717	0.008

Continued on next page

Table A-10 – *Continued from previous page*

	Input Pulse			Output Pulse			
Wavelength	**Pulse Duration**	**Energy**	**Power**	**Pulse Duration**	**Energy**	**Power**	**Energy / Area vs Limit**
(nm)	**(fs)**	**(μJ)**	**(MW)**	**(fs)**	**(μJ)**	**(MW)**	**(%)**
1300	502	4.16	8.31	502	0.201	0.399	0.045
1350	549	385	770	490	0.0779	0.166	0.016
1375	501	3849	7698	498	0.0372	0.0700	0.007
1399	551	38485	76970	388	4.94E-8	3.77E-8	0.000
1399*	551	38485	76970	391	8.09E-8	6.91E-8	0.000
1400	552	38.5	77.0	X	X	X	X
1 ps							
1200	1080	0.306	0.306	999	0.0193	0.0225	0.005
1250	1012	0.346	0.346	1000	0.0308	0.0309	0.008
1300	1000	4.16	4.16	1002	0.201	0.201	0.045
1350	1001	385	385	1004	0.0776	0.0775	0.016
1375	1000	3849	3849	1018	0.0326	0.0319	0.006
1399	1002	38485	38485	X	X	X	X
1399*	1002	38485	38485	X	X	X	X
1400	1001	38.5	38.5	X	X	X	X

Table A-11. Spectral Characteristics of Chirped Eye Simulation with Self-Focusing

	Input Pulse				Output Pulse			
Wave-length (nm)	**FWHM Spectral Range (nm)**	**RMS Spectral Range (nm)**	10^{-3} **Max (nm)**	10^{-5} **Max (nm)**	**FWHM Spectral Range (nm)**	**RMS Spectral Range (nm)**	10^{-3} **Max (nm)**	10^{-5} **Max (nm)**
10 fs								
1200	1103-1316	1047-1405	938-1664	882-1875	1064-1143	1021-1297	929-1341	875-1376
1250	1145-1377	1085-1474	969-1762	909-2000	1078-1275	1035-1314	957-1346	895-1382
1300	1186-1438	1123-1544	998-1862	935-2131	1093-1302	1053-1325	974-1367	905-1544
1350	1228-1499	1160-1615	1028-1967	961-2268	1246-1319	1001-1385	777-1706	697-2079
1375	1249-1530	1178-1651	1042-2020	974-2340	1249-1300	742-1385	675-1794	604-2398
1399	1268-1560	1196-1686	1056-2073	985-2410	1102-1315	710-1777	597-2239	470-2622
1400	1269-1561	1196-1687	1056-2075	986-2413	1236-1308	1094-1333	1007-1377	922-1707
35 fs								
1200	1170-1231	1145-1261	1111-1304	1088-1338	1168-1235	1130-1265	1099-1301	1078-1325
1250	1218-1284	1190-1316	1154-1363	1129-1400	1224-1282	1194-1304	1155-1333	1121-1350
1300	1265-1337	1236-1371	1197-1423	1170-1463	1259-1305	1233-1328	1197-1348	1169-1374
1350	1313-1389	1281-1427	1239-1483	1210-1527	1282-1328	1254-1340	1218-1370	1179-1423
1375	1336-1416	1303-1455	1260-1513	1230-1559	1290-1333	1256-1346	1203-1397	1164-1459
1399	1359-1441	1325-1482	1280-1542	1249-1590	1281-1314	1199-1364	1121-1374	1049-1491
1400	1360-1442	1326-1483	1281-1543	1250-1591	1299-1336	1276-1366	1249-1381	1227-1385
50 fs								
1200	1179-1222	1160-1243	1137-1271	1119-1293	1179-1223	1159-1245	1129-1273	1113-1293
1250	1227-1273	1206-1297	1181-1327	1163-1351	1231-1274	1208-1294	1183-1317	1164-1335
1300	1276-1325	1253-1351	1226-1384	1206-1410	1270-1306	1249-1327	1225-1343	1205-1367
1350	1324-1377	1299-1405	1270-1440	1249-1469	1299-1332	1279-1344	1253-1372	1225-1399
1375	1348-1403	1322-1432	1292-1469	1270-1499	1309-1337	1283-1367	1253-1381	1214-1410
1399	1371-1428	1344-1458	1314-1496	1291-1527	1282-1332	1257-1368	1194-1385	1161-1423

Continued on next page

Table A-11 – *Continued from previous page*

	Input Pulse				Output Pulse			
Wave-length (nm)	**FWHM Spectral Range (nm)**	**RMS Spectral Range (nm)**	10^{-3} **Max (nm)**	10^{-5} **Max (nm)**	**FWHM Spectral Range (nm)**	**RMS Spectral Range (nm)**	10^{-3} **Max (nm)**	10^{-5} **Max (nm)**
1400	1372-1429	1345-1459	1314-1497	1292-1528	1319-1366	1300-1376	1281-1385	1265-1385
100 fs								
1200	1190-1211	1178-1223	1167-1234	1158-1245	1189-1211	1178-1223	1167-1235	1158-1245
1250	1239-1262	1226-1275	1215-1287	1205-1299	1240-1262	1227-1275	1215-1287	1205-1298
1300	1288-1313	1274-1327	1262-1340	1251-1353	1285-1307	1272-1320	1260-1332	1250-1341
1350	1337-1364	1322-1379	1309-1394	1297-1407	1323-1340	1311-1364	1301-1374	1279-1383
1375	1361-1389	1346-1405	1332-1420	1321-1434	1355-1368	1325-1378	1306-1385	1276-1385
1399	1385-1414	1369-1430	1355-1446	1343-1460	1360-1364	1351-1385	1298-1385	1281-1387
1399*	1385-1414	1369-1430	1355-1446	1343-1460	1360-1364	1351-1385	1298-1385	1276-1387
1400	1386-1415	1370-1431	1356-1447	1344-1461	1362-1376	1352-1385	1339-1385	1326-1389
500 fs								
1200	1198-1202	1195-1205	1193-1207	1191-1209	1198-1202	1195-1205	1193-1207	1191-1209
1250	1248-1252	1245-1255	1243-1257	1241-1259	1248-1252	1245-1255	1243=1257	1241-1259
1300	1298-1302	1294-1306	1292-1308	1290-1310	1297-1302	1294-1306	1292-1308	1290-1310
1350	1347-1353	1344-1356	1342-1359	1339-1361	1347-1352	1343-1356	1341-1358	1338-1361
1375	1372-1378	1369-1382	1366-1384	1364-1386	1371-1376	1367-1380	1362-1382	1358-1385
1399	1396-1402	1392-1406	1390-1408	1387-1411	1384-1385	1377-1385	1374-1396	1367-1399
1399*	1396-1402	1392-1406	1390-1408	1387-1411	1384-1385	1376-1385	1373-1396	1366-1399
1400	1397-1403	1393-1407	1391-1409	1388-1412	X	X	X	X
1 ps								
1200	1199-1201	1197-1203	1197-1203	1196-1204	1199-1201	1197-1203	1197-1203	1196-1204
1250	1249-1251	1247-1253	1246-1254	1245-1255	1249-1251	1247-1253	1246-1254	1245-1255
1300	1299-1301	1297-1303	1296-1304	1295-1305	1299-1301	1297-1303	1296-1304	1295-1305
1350	1349-1351	1347-1353	1346-1354	1345-1355	1349-1351	1347-1353	1346-1354	1345-1355

Continued on next page

Table A-11 – *Continued from previous page*

	Input Pulse				Output Pulse			
Wave-length (nm)	**FWHM Spectral Range (nm)**	**RMS Spectral Range (nm)**	10^{-3} **Max (nm)**	10^{-5} **Max (nm)**	**FWHM Spectral Range (nm)**	**RMS Spectral Range (nm)**	10^{-3} **Max (nm)**	10^{-5} **Max (nm)**
1375	1374-1376	1372-1378	1371-1379	1369-1381	1373-1376	1371-1378	1370-1379	1367-1381
1399	1398-1400	1395-1403	1394-1404	1393-1405	X	X	X	X
1399*	1398-1400	1395-1403	1394-1404	1393-1405	X	X	X	X
1400	1399-1401	1396-1404	1395-1405	1394-1406	X	X	X	X

Table A-12. Energy Distribution as a Function of Wavelength for Chirped Eye Simulation with Self-Focusing

Wave-length (nm)	Energy 400 nm to 700 nm (nJ)	Energy 700 nm to 1000 nm (nJ)	Energy 1000 nm to 1200 nm (nJ)	Energy 1200 nm (nJ)	Energy 400 nm to 700 nm (%)	Energy 700 nm to 1000 nm (%)	Energy 1000 nm to 1200 nm (%)	Energy 1200 nm (%)
10 fs								
1200	< 5E-7	0.539	48.1	7.76	0	0.956	85.3	13.8
1250	< 5E-7	0.112	26.3	10.5	0	0.304	71.3	28.4
1300	< 5E-7	0.245	132	117	0	0.098	53.1	46.8
1350	0.0673	592	1866	3904	0.001	9.30	29.3	61.4
1375	282	17995	13397	35130	0.422	26.9	20.1	52.6
1399	18439	300808	126238	127833	3.22	52.5	22.0	22.3
1400	< 5E-7	0.162	175	565	0	0.022	23.7	76.3
35 fs								
1200	< 5E-7	< 5E-7	11.5	10.7	0	0	51.8	48.2
1250	< 5E-7	< 5E-7	0.731	26.6	0	0	2.68	97.3
1300	< 5E-7	< 5E-7	0.0482	200	0	0	0.024	99.976
1350	< 5E-7	< 5E-7	0.0957	2915	0	0	0.003	99.997
1375	< 5E-7	< 5E-7	0810	8570	0	0	0.009	99.991
1399	< 5E-7	6.46E-3	667	31760	0	0	2.06	97.94
1400	< 5E-7	< 5E-7	< 5E-7	15.9	0	0	0	100
50 fs								
1200	< 5E-7	< 5E-7	10.2	10.3	0	0	49.8	50.2
1250	< 5E-7	< 5E-7	0.0886	28.9	0	0	0.306	99.694
1300	< 5E-7	< 5E-7	6.35E-5	204	0	0	0	100
1350	< 5E-7	< 5E-7	3.13E-5	1508	0	0	0	100
1375	< 5E-7	< 5E-7	1.97E-3	2171	0	0	0	100
1399	< 5E-7	< 5E-7	2.24	5287	0	0	0.0423	99.958
1400	< 5E-7	< 5E-7	< 5E-7	1.57	0	0	0	100
100 fs								
1200	< 5E-7	< 5E-7	9.88	9.94	0	0	49.8	50.2
1250	< 5E-7	< 5E-7	1.07E-6	30.2	0	0	0	100
1300	< 5E-7	< 5E-7	< 5E-7	205	0	0	0	100
1350	< 5E-7	< 5E-7	< 5E-7	360	0	0	0	100
1375	< 5E-7	< 5E-7	< 5E-7	174	0	0	0	100
1399	< 5E-7	< 5E-7	< 5E-7	43.0	0	0	0	100
1399*	< 5E-7	< 5E-7	< 5E-7	56.7	0	0	0	100
1400	< 5E-7	< 5E-7	< 5E-7	0.03000	0	0	0	100
500 fs								
1200	< 5E-7	< 5E-7	9.71	9.69	0	0	50.1	49.9
1250	< 5E-7	< 5E-7	< 5E-7	30.9	0	0	0	100
1300	< 5E-7	< 5E-7	< 5E-7	201	0	0	0	100
1350	< 5E-7	< 5E-7	< 5E-7	77.9	0	0	0	100
1375	< 5E-7	< 5E-7	< 5E-7	37.2	0	0	0	100
1399	< 5E-7	< 5E-7	< 5E-7	4.94E-5	0	0	0	100
1399*	< 5E-7	< 5E-7	< 5E-7	8.09E-5	0	0	0	100
1400	X	X	X	X	X	X	X	X

Continued on next page

Table A-12 – *Continued from previous page*

Wave-length (nm)	Energy 400 nm to 700 nm (nJ)	Energy 700 nm to 1000 nm (nJ)	Energy 1000 nm to 1200 nm (nJ)	Energy 1200 nm (nJ)	Energy 400 nm to 700 nm (%)	Energy 700 nm to 1000 nm (%)	Energy 1000 nm to 1200 nm (%)	Energy 1200 nm (%)
1 ps								
1200	$<$ 5E-7	$<$ 5E-7	9.71	9.64	0	0	50.2	49.8
1250	$<$ 5E-7	$<$ 5E-7	$<$ 5E-7	30.8	0	0	0	100
1300	$<$ 5E-7	$<$ 5E-7	$<$ 5E-7	201	0	0	0	100
1350	$<$ 5E-7	$<$ 5E-7	$<$ 5E-7	77.6	0	0	0	100
1375	$<$ 5E-7	$<$ 5E-7	$<$ 5E-7	32.6	0	0	0	100
1399	X	X	X	X	X	X	X	X
1399*	X	X	X	X	X	X	X	X
1400	X	X	X	X	X	X	X	X

APPENDIX B - SIMULATION CODE

B.1 Simulation Of Water Experiment

```
%% Simple Nonlinear-1D Propagator Model
% Chris Marble
% 06/12/2018
% Last Update: 07/09/2018
% Simulation of Frank's water experiment
% Only simulating 10 mm of water, no cuvette or interface effects are
   simulated
% All units in SI (mks) unless specified otherwise (ie X_nm
% means variable X in nm units)

%% Step 0: Initialize program parameters
% Physical Constants
c=2.998e8;  % Speed of light (m/s)
mu=1;       % Permeability of free space
epsilon0 = 8.85418782e-12; % Permittivity of free space (F/m)
X = 524288; % Number of time steps simulated
dx = 50e-9; % Spatial step simulated (m)
dt = dx/c;  % Time step (s)

% Beam parameters & Simulation parameters
StartDist = 0e-3; % Where to start nonlinear simulation
Stop =  200000;      % Choose how far to propagate nonlinearly
EndDist = 0e-3;       % Choose how far to propagate linearly
                      % after nonlinear section
                      % (In general no distance)

%{
%lambda0    % Wavelength claimed in experiment
lambda0     % Actual wavelength simulated
Tau_t       % Initial FWHM pulse duration (seconds)
n2          % Nonlinear refractive index (m^2/W)
beta        % Nonlinear absorption coefficient (m/W)
R0          % Beam radius entering cuvette (meters)
%Energy     % Minimum energy for spectral broadening in
            % experiment
Energy      % Energy in experiment to simulate against
Rret        % Beam radius in water
DistRet     % Distance to focus in water
xR          % Rayleigh range in water
%Rret       % Beam radius in air
%DistRet    % Distance to focus in air
%xR         % Rayleigh range in air
n0_Est      % n0 from Sellmeier fit from Rockwell's paper
RStop       % Minimum radius due to plasma effects

%lambda0 = 1200e-9;
lambda0 = 1185e-9;
Tau_t = 35e-15;
n2 = 4.45e-20;
beta = 9.26e-14;
```

```
R0 = 363.4e-6;
%Energy = 0.158e-6;
Energy = 1.928e-6;
Rret = 34.1e-6; % Focal radius in water
DistRet = 7.781e-3; % Distance to focus in water
xR = 3.049e-3; % Rayleigh range in water
%Rret = 25.6e-6; % Focal radius in air
%DistRet = 5.837e-3; % Distance to focus in air
%xR = 1.716e-3;  % Rayleigh Range in air
n0_Est = 1.31699314;
RStop = 7e-6;

%lambda0 = 1250e-9;
lambda0 = 1225e-9;
Tau_t = 35e-15;
n2 = 9.26e-20;
beta = 12.9e-14;
R0 = 331.4e-6;
%Energy = 0.306e-6;
Energy = 1.653e-6;
Rret = 34.1e-6;
DistRet = 7.103e-3; % Distance to focus in water
xR = 2.927e-3;  % Rayleigh Range in Water
%Rret = 25.6e-6; % Focal radius in air
%DistRet = 5.329e-3; % Distance to focus in air
%xR = 1.647e-3;  % Rayleigh Range in air
n0_Est = 1.31606318;
RStop = 7e-6;

%lambda0 = 1300e-9;
lambda0 = 1310e-9;
Tau_t = 35e-15;
n2 = 6.8e-20;
beta = 8.2e-14;
R0 = 339.2e-6;
%Energy = 0.578e-6;
Energy = 1.616e-6;
Rret = 34.1e-6;
DistRet = 7.273e-3; % Distance to focus in water
xR = 2.814e-3;  % Rayleigh Range in Water
%Rret = 25.6e-6; % Focal radius in air
%DistRet = 5.456e-3; % Distance to focus in air
%xR = 1.584e-3;  % Rayleigh Range in air
n0_Est = 1.31513385;
RStop = 5e-6;

lambda0 = 1350e-9;
Tau_t = 35e-15;
n2 = 9.0e-20;
beta = 16e-14;
R0 = 276.0e-6;
%Energy = 0.404e-6;
```

```
Energy = 1.994e-6;
Rret = 34.3e-6;
DistRet = 5.918e-3; % Distance to focus in water
xR = 2.731e-3;  % Rayleigh Range in Water
%Rret = 25.7e-6; % Focal radius in air
%DistRet = 4.44e-3; % Distance to focus in air
%xR = 1.537e-3;  % Rayleigh Range in air
n0_Est = 1.31420093;
RStop = 5e-6;

lambda0 = 1400e-9;
Tau_t = 35e-15;
n2 = 7.5e-20;
beta = -7.7e-14;
R0 = 346.5e-6;
%Energy = 1.956e-6;
Energy = 3.661e-6;
Rret = 34.3e-6;
DistRet = 7.442e-3; % Distance to focus in water
xR = 2.634e-3;  % Rayleigh Range in Water
%Rret = 25.7e-6; % Focal radius in air
%DistRet = 5.583e-3; % Distance to focus in air
%xR = 1.482e-3;  % Rayleigh Range in air
n0_Est = 1.31326094;
RStop = 2e-6;
%}

% Choose wavelength to test here & wavelength parameteres
lambda0 = 1350e-9;
Tau_t = 35e-15;
n2 = 9.0e-20;
beta = 16e-14;
R0 = 276.0e-6;
%Energy = 0.404e-6;
Energy = 1.994e-6;
Rret = 34.3e-6;
DistRet = 5.918e-3; % Distance to focus in water
xR = 2.731e-3;  % Rayleigh Range in Water
%Rret = 25.7e-6; % Focal radius in air
%DistRet = 4.44e-3; % Distance to focus in air
%xR = 1.537e-3;  % Rayleigh Range in air
n0_Est = 1.31420093;
RStop = 5e-6;

% Now compute other values
w0=2*pi()*c/lambda0; % Calculate central frequency

%% Step 1. Initialize n0/k0 values
% Lookup Table: Look up n0, k0, for each wavelength fft
% generates
% Format of input: Omega, Lambda, n0, k0, n2, beta, n2_Unc, beta_Unc;
```

```
% Call data from CSV file
Values = csvread('LookupTable_V2.csv',1,0);

% Pull the data we need for simulation
Omega_V = Values(:,1);
n0_V = Values(:,3);
k0_V = Values(:,4);

clear Values % Don't need all these values anymore

% Build vectors to recieve data for simulation
Omega = transpose(2*pi()/dt*(-X/2:X/2-1)/X); % Find sim. frequencies
% Note: Sim. Frequencies dictated by dt, X and FFT function (see
   MATLAB documentation on FFT for more details
n0 = zeros(X,1);
k0 = zeros(X,1);

% For first set of wavelengths (the negative wavelengths from the FFT)
for i = (1:X/2)
    % Find position in table and interpolate between nearest table
    % values
    % Find position relative to tabulated frequencies
    Pos = find(abs(Omega(i)) > Omega_V,1);
    % Interpolate between values in the table
    % Slope parameter of interpolation: m
    m(i) = (abs(Omega(i))-Omega_V(Pos))/(Omega_V(Pos-1)-Omega_V(Pos));
    % Compute n/k for each frequency of interest
    n0(i) = n0_V(Pos)+(n0_V(Pos-1)-n0_V(Pos))*m(i); %Refractive
                                                     %Index
    k0(i) = k0_V(Pos)+(k0_V(Pos-1)-k0_V(Pos))*m(i); %Extinction
                                                     %Coefficient
end

% For Omega(X/2+1) -> 0 then look up value... don't really matter
   anyway since this frequency should be zero in simulation
    n0(X/2+1) = 8.8486;
    k0(X/2+1) = 6.931E-03;
    m(X/2+1) = 0;

% Continue looping through the rest of the simulated frequencies
for i = (X/2+2:X)
    Pos = find(abs(Omega(i)) > Omega_V,1);
    m(i) = (abs(Omega(i))-Omega_V(Pos))/(Omega_V(Pos-1)-Omega_V(Pos));
    n0(i) = n0_V(Pos)+(n0_V(Pos-1)-n0_V(Pos))*m(i);
    k0(i) = k0_V(Pos)+(k0_V(Pos-1)-k0_V(Pos))*m(i);
end

% Clear what we no longer need...
clear Omega_V n0_V alpha0_V m

%% Step 2: Start with a Gaussian pulse in time, discretize it
% Start with large vector of zeros for the electric field
```

```
Efield = zeros(X,1);

% Build a vector for all moments of time simulated
TimeVec = transpose(0:(X-1));
TimeVec = TimeVec*dt;
% I have now built my initial timespace, shift it so the pulse is not
   cut off
TimeVec = TimeVec - 3*Tau_t;

% Now setup the initial Efield of the pulse
Efield = exp(-2*log(2)/Tau_t^2*TimeVec.^2).*exp(1i*w0*TimeVec);

%% Step 3: Find area of the beam
% Starting point at water/glass interface
% And for all points in the nonlinear solver
Area0 = pi()*R0^2; % Initial area

R = zeros(1,Stop+1);
% Frank's assumption:
% Assume Gaussian beam focusing behavior at all points in the media
for (x = 1:1:Stop+1)
    dist = StartDist + (x-1)*dx;
    R(x) = Rret*sqrt(1+(dist-DistRet)^2/xR^2);
end

% Find area at each point in eye
Area = pi()*R.^2;

%% Step 4: Calculate intensity and normalize it to value of interest

% Set-up step only: Normalize I to peak intensity of problem
I = 0.5*c*n0_Est*epsilon0.*abs(Efield).^2/Area0;
IPeak = Energy/Tau_t/pi()/(R0)^2;

% Now adjust amplitude of electric field acordingly
Efield = sqrt(IPeak)/sqrt(max(I))*Efield;
I = 0.5*c*n0_Est*epsilon0.*abs(Efield).^2/Area0;

% Save initial values for comparison
I0 = I*Area0/Area(1); % Save for comparison
IPeak = max(I0); % Save for self-focusing
E0 = Efield; % Save for Comparison

%% Step 6: Convert to frequency domain
EfieldFreq = fftshift(fft(Efield));

%% Set up graphs
% ___Parameters for graphs___
Lambda_nm = 2*pi()*c*1e9./Omega;
E0Freq = fftshift(fft(E0));

% Choose which frequencies you want to plot and record for analysis
```

```
ViewVec = (X/2+10000):(X/2+131100);

%pathTempOmega = ['OmegaTemp_' num2str(lambda0*1e9) 'nm.csv' ];
%csvwrite(pathTempOmega,Omega);

% Constants for the for loops (improves compuational speed to
    initialize here)
IConst = 0.5*c*n0_Est*epsilon0; % Constant part of intensity calc.
DVec = -1i*Omega.*n0*dx/c -abs(Omega).*k0*dx/c; % Constant part of
    linear propagator term
ExpDVec = exp(DVec); % Faster to pre-compute this value
NConst = -1i*w0*n2*(dx/2)/c - beta*(dx/2)/2; % Constant part of
    nonlinear propagator
AreaNow = Area0; % Initialize variable here
R4 = zeros(Stop,1);
R4(1) = R(1);

% Start waitbar for user to see code is running
%f = waitbar(0,'Please wait...');

% Save initial information
% Path files output CSV files that can be analyzed or made into videos
pathB = ['Spectra_In_' num2str(lambda0*1e9) 'nm.csv' ];
csvwrite(pathB,abs(E0Freq(ViewVec)/X).^2);

pathD = ['Lambda.csv' ];
csvwrite(pathD,Lambda_nm(ViewVec));

%% Propagate forward:
for(PositionCtrA = 1:1000) % This is the large "step"
    for(PositionCtrB = 1:Stop/1000) % This is the small "step"
        % Skip Step 0 - 2 which were only for code initialization

        % Step 3: Get the area

        % Find where you are in the simulation
        PositionCtr = (PositionCtrA-1)*Stop/1000+PositionCtrB;
        % Find angle of descent linear & nonlinear
        Theta_Linear = abs(tan((R(PositionCtr+1)-R(PositionCtr))/dx));
        Theta_Nonlinear = sqrt(2*n2*IPeak/n0_Est);

        % Find self-focusing corrected radius
        if(PositionCtr == 1)     % If just starting simulation
            R4(PositionCtr) = R(1);
        elseif(PositionCtr*dx < DistRet)     % If before focal point
            R4(PositionCtr) = max(R4(PositionCtr-1) - atan(sqrt(
                Theta_Linear^2 + Theta_Nonlinear^2))*dx,RStop);
        else                                    % After focal point
            if(Theta_Linear < Theta_Nonlinear) % && Nonlinear focusing
                dominates
                R4(PositionCtr) = max(R4(PositionCtr-1) - atan(sqrt(-
                    Theta_Linear^2 + Theta_Nonlinear^2))*dx,RStop);
```

```
            else                                % && Linear de-focusing
                 dominates
                R4(PositionCtr) = max(R4(PositionCtr-1) + atan(sqrt(+
                    Theta_Linear^2 - Theta_Nonlinear^2))*dx,RStop);
            end
        end

        % Find area
        AreaNow = pi*R4(PositionCtr)^2; % The self-focused area
        %AreaNow = pi*R(PositionCtr)^2; % Uncomment for simulation
            without self-focusing

        % Step 4: Calculate intensity
        I = IConst.*abs(Efield).^2/AreaNow;
        IPeak = max(I); % Keep to calc self-focusing next step

        % Step 5: Split-step nonlinear term
        Efield = Efield.*exp(NConst*I);

        % Step 6: Convert to frequency domain
        EfieldFreq = fftshift(fft(Efield));

        % Step 7: Propagate dx forward in space
        %EfieldFreq = EfieldFreq.*exp(DVec);
        EfieldFreq = EfieldFreq.*ExpDVec; % Faster method

        % Step 8: Convert back to time domain
        Efield = ifft(ifftshift(EfieldFreq));

        % Step 9: Split-step nonlinear term
        I = IConst.*abs(Efield).^2/AreaNow;
        Efield = Efield.*exp(NConst*I);     % Time cost 0.02 sec
    end

    % Update the waitbar so the user can see progress
    %waitbar(((PositionCtrA)/1000),f);

    % Every mm plot
    if(mod(PositionCtrA,100) == 0)

        pathF = ['IntensityAt_' num2str(PositionCtrA/100) ' mm_'
            num2str(lambda0*1e9) 'nm.csv' ];
        csvwrite(pathF,I);

        pathG = ['SpectraAt_' num2str(PositionCtrA/100) ' mm_' num2str
            (lambda0*1e9) 'nm.csv' ];
        csvwrite(pathG,abs(EfieldFreq(ViewVec)/X).^2/Area((
            PositionCtrA)*Stop/1000));


        % Plot time domain
        figure;
```

```
        plot(TimeVec*10e12, I0, 'k')
        hold on
        plot(TimeVec*10e12, I, 'r')
        hold off

        title(['Intensity at ' num2str(PositionCtrA/100) ' mm for '
           num2str(lambda0*1e9) ' nm beam'])
        xlabel('Time (ps)')
        ylabel('I(t)')
        legend({'Input Pulse','Pulse at Position'},'Location','
           northeast')

        % Plot the frequency domain
        figure;
        semilogy(Lambda_nm(ViewVec), abs(E0Freq(ViewVec)/X).^2/Area(1)
           ,'k')
        hold on
        semilogy(Lambda_nm(ViewVec), abs(EfieldFreq(ViewVec)/X).^2/
           Area((PositionCtrA)*Stop/1000),'r--')
        hold off
        title(['Power Spectral Density at ' num2str(PositionCtrA/100)
           ' mm for ' num2str(lambda0*1e9) ' nm beam'])
        xlabel('Wavelength (nm)')
        ylabel('|E|^2/Area')
        legend({'Input Pulse','Pulse at Position'},'Location', '
           northeast')
    end
end

%% Calculate resulting pulse at end of simulation
% Calculate I at end of simulation:
REnd = Rret*sqrt(1+(StartDist+Stop*dx+EndDist-DistRet)^2/xR^2);
AEnd = pi()*REnd^2;
I = 0.5*c*n0_Est*epsilon0.*abs(Efield).^2/AEnd;


% Looking in the time domain
plot(TimeVec*10e12, I0, 'k')
hold on
plot(TimeVec*10e12, I, 'r')
hold off
title(['Intensity at ' num2str(1000*Stop*dx) ' mm in Time Domain for '
     num2str(lambda0*1e9) ' nm beam'])
xlabel('Time (ps)')
ylabel('I(t)')
legend({'Input Pulse','Pulse Exiting Simulation'},'Location','
    northeast')
figure;


% Looking in the frequency domain

```

```
figure;
semilogy(Lambda_nm(ViewVec),abs(E0Freq(ViewVec)/X).^2/Area(1),'k')
hold on
semilogy(Lambda_nm(ViewVec),abs(EfieldFreq(ViewVec)/X).^2/AEnd,'r--')
hold off
%plot(2*pi()*c*1e9./Omega,abs(EfieldFreq(1:(X/2+1))/X).^2)
title(['Power Spectral Density out of cuvette for ' num2str(lambda0*1
    e9) ' nm beam'])
xlabel('Wavelength (nm)')
ylabel('|E|^2/Area')
legend({'Input Pulse','Pulse Exiting Simulation'},'Location','
    northeast')
ylim([1e-6 1e14])

% Plot Beam Radius
figure;
plot(dx*(1:Stop),1e+6*R4,'k')
%plot(2*pi()*c*1e9./Omega,abs(EfieldFreq(1:(X/2+1))/X).^2)
title(['Beam Radius ' num2str(lambda0*1e9) ' nm beam'])
xlabel('Distance in the Material')
ylabel('Radius (um)')


% Close waitbar now that we are done
%close(f)

% Save all the things we want for later analysis
pathB = ['Efield_Out_' num2str(lambda0*1e9) 'nm.csv' ];
csvwrite(pathB,Efield);

%% Use same area for normalization since we are seeing output
%  at spectrometer
pathC = ['Spectra_Out_' num2str(lambda0*1e9) 'nm.csv' ];
csvwrite(pathC,abs(EfieldFreq(ViewVec)/X).^2);

% Save the calculated radius too
pathE = ['Radius_'  num2str(lambda0*1e9) 'nm.csv' ];
csvwrite(pathE,1e6*R4);
```

B.2 Simulation Of Unchirped/Negatively Chirped Pulses In The Reduced Eye Model

```
%% Simple Nonlinear-1D Propagator Model
% Chris Marble
% 06/12/2018
% Last Update: 07/19/2018
% Simulate a Gaussian laser strike to the eye
% Treat lens like water with 40% the absorbance of water
% Code for full eye simulation for the paper
% Includes self-focusing effects
% All units in SI (mks) unless specified otherwise
% Times of interest: 10 fs, 35 fs, 50 fs, 100 fs, 1000 fs
```

```
% Enable or disable chirping by commenting chirp section in
% initialization oode

%% Step 0: Initialize program parameters
% Physical Constants
c=2.998e8;
mu=1;
epsilon0 = 8.85418782e-12;
% Choose Number of time elements Tfinal = dt*X - Shift
X = 1048576; % 26 mm propagation
dx = 50e-9; % Choose a spatial step size less than 0.1*Lambda_min
dt = dx/c;  % "Golden Timestep"

% Wavelength dependent data here
%{
lambda0     % Central wavelength of pulse (meters)
MPE_H0_ANSI % ANSI MPE in uJ/cm^2 for wavelength of interest
Tau_t       % Initial FWHM pulse duration (seconds)
n2          % Nonlinear refractive index (m^2/W)
beta        % Nonlinear absorption coefficient (m/W)
n0_Est      % n0 from Sellmeier fit for humor from Rockwell's
            % paper for focusing calcuation using reduced eye
            % model (REM)
R0          % Beam radius entering the eye (meters). Current
            % assumption: 7 mm diameter pupil

lambda0 = 1200e-9;
MPE_H0_ANSI = 0.794;
Tau_t = 50e-15;
n2 = 4.45e-20;
beta = 9.26e-14;
n0_Est = 1.31699314;
R0 = 3.5e-3;

lambda0 = 1250e-9;
MPE_H0_ANSI = 0.9; % uJ/cm^2
Tau_t = 50e-15;
n2 = 9.26e-20;
beta = 12.9e-14;
n0_Est = 1.31606318;
R0 = 3.5e-3;

lambda0 = 1300e-9;
MPE_H0_ANSI = 10.8; % uJ/cm^2
Tau_t = 50e-15;
n2 = 6.8e-20;
beta = 8.2e-14;
n0_Est = 1.31513385;
R0 = 3.5e-3;

lambda0 = 1350e-9;
MPE_H0_ANSI = 1000.8; % uJ/cm^2
```

```
Tau_t = 50e-15;
n2 = 9.0e-20;
beta = 16e-14;
n0_Est = 1.31420093;
R0 = 3.5e-3;

lambda0 = 1375e-9;
MPE_H0_ANSI = 10000.8; % uJ/cm^2
Tau_t = 50e-15;
n2 = 8.3e-20;
beta = 0;
n0_Est = 1.31373201;
R0 = 3.5e-3;

lambda0 = 1399e-9;
MPE_H0_ANSI = 100000.8; % uJ/cm^2
Tau_t = 50e-15;
n2 = 7.5e-20;
beta = 0;
n0_Est = 1.31327983;
R0 = 3.5e-3;

lambda0 = 1400e-9;
MPE_H0_ANSI = 100.0; % uJ/cm^2
Tau_t = 50e-15;
n2 = 7.5e-20;
beta = -7.7e-14;
n0_Est = 1.31326094;
R0 = 3.5e-3;
%}

% Choose wavelength to test here & wavelength parameteres
lambda0 = 1375e-9;
MPE_H0_ANSI = 10000.8; % uJ/cm^2
Tau_t = 50e-15;
n2 = 8.3e-20;
beta = 0;
n0_Est = 1.31373201;
R0 = 3.5e-3;

RStop = 1e-8;   % Stop R from going to zero if self focusing dominates

% Now compute other values of interest
Energy = MPE_H0_ANSI*1e-6*(pi()*(100*R0)^2);    % Convert MPE to pulse
    energy (Joules)
w0=2*pi()*c/lambda0; % Find central pulse frequency
RadCurve = 6.1E-3; % Radius of curvature of reduced eye model (REM)
focalLength = RadCurve*n0_Est/(n0_Est-1);   % Focal length of REM
   hemisphere lens

% Eye constants
Rfoc = 2*lambda0*focalLength/(pi()*(2*R0)); % Find the radius at the
```

```
    focal point;
DistFocus = focalLength; % Distance to focal point
xR = pi()*Rfoc^2/lambda0;   % Rayleigh range assuming Gaussian beam
    focusing

% Beam parameters & Simulation parameters
% Variables to change
StopA =   80000;    % Propagate 4 mm to lens of eye (4 mm)
StopB =   StopA;    % Propagate 4 mm of lens to vitreous humor
                    % (to 8 mm)
StopC =  328000;    % Propagate 16.4 mm to the retina
                    % (to 24.4 mm)
StopD =   28000;    % Propagate beyond the retina past the
                    % nonlinear region (to 25.8 mm)
StopTotal = StopA + StopB + StopC + StopD; % Total propagation
                                           % distance
Steps_Per_100um = 2000; % Relate steps to mm in vitreous to
                        % capture images

%% Step 1. Initialize n0/k0 values
% Lookup Table: Look up n0, k0, for each wavelength fft generates
% Lookup Table based on Segelsteins' thesis
% Format of table: Omega, Lambda, n0, k0, n2, beta, n2_Unc, beta_Unc;

% Call data from CSV file
Values = csvread('LookupTable_V2.csv',1,0);

% Pull the data we need for simulation
Omega_V = Values(:,1);
n0_V = Values(:,3);
k0_V = Values(:,4);

clear Values % Don't need anymore

% Build vectors to recieve data for simulation
Omega = transpose(2*pi()/dt*(-X/2:X/2-1)/X); % Find simulation
                                             % frequencies
% Note: Sim. Frequencies dictated by dt, X and FFT function (see
    MATLAB
% documentation on FFT for more details)
n0 = zeros(X,1);
k0 = zeros(X,1);

% For first set of wavelengths (the negative wavelengths from the FFT)
for i = (1:X/2)
    % Find position in table and interpolate between nearest
    % table values
    % Find position relative to tabulated frequencies
    Pos = find(abs(Omega(i)) > Omega_V,1);
    % Interpolate between values in the table
    % Slope parameter of interpolation: m
    m(i) = (abs(Omega(i))-Omega_V(Pos))/(Omega_V(Pos-1)-Omega_V(Pos));
```

```
    % Compute n/k for each frequency of interest
    n0(i) = n0_V(Pos)+(n0_V(Pos-1)-n0_V(Pos))*m(i); %Refractive
                                                     %Index
    k0(i) = k0_V(Pos)+(k0_V(Pos-1)-k0_V(Pos))*m(i); %Extinction
                                                     %Coeffecient
end

% For Omega(X/2+1) -> 0 then look up value... don't really matter
   anyway
% since this frequency should be zero in simulation
    n0(X/2+1) = 8.8486;
    k0(X/2+1) = 6.931E-03;
    m(X/2+1) = 0;

% Same thing, just for the positive wavelengths
for i = (X/2+2:X)
    Pos = find(abs(Omega(i)) > Omega_V,1);
    m(i) = (abs(Omega(i))-Omega_V(Pos))/(Omega_V(Pos-1)-Omega_V(Pos));
    n0(i) = n0_V(Pos)+(n0_V(Pos-1)-n0_V(Pos))*m(i);
    k0(i) = k0_V(Pos)+(k0_V(Pos-1)-k0_V(Pos))*m(i);
end

% Clear what we no longer need
clear Omega_V n0_V alpha0_V m


%% Step 2: Start with a Gaussian pulse in time, discretize it
% Start with large vector of zeros for the electric field
Efield = zeros(X,1);

% Build a vector for all moments of time simulated
TimeVec = transpose(0:(X-1));
TimeVec = TimeVec*dt;
% I have now built my initial timespace, shift it so the pulse is not
   cut off
TSHIFT = 3*Tau_t; % Unchirped pulse
%TSHIFT = 20e-12; % Negatively chirped pulse
TimeVec = TimeVec - TSHIFT;

% Now setup the initial Efield of the pulse
Efield = exp(-2*log(2)/Tau_t^2*TimeVec.^2).*exp(1i*w0*TimeVec);

%% Step 3: Find area of the beam
% Starting point at Surface of the eye
% And for all points in the nonlinear solver
Area0 = pi()*R0^2; % Initial area

R = zeros(1,StopTotal); % Initialize
% Assume Gaussian beam focusing behavior at all points in the eye
for (x = 1:1:StopTotal)
    dist = (x-1)*dx;
    R(x) = Rfoc*sqrt(1+(dist-DistFocus)^2/xR^2);
```

```
end

% Find area at each point in eye
Area = pi()*R.^2;

%% Step 4: Calculate intensity and normalize it to value of interest ( and chirp the pulse if desired)

% Set-up step only: Normalize I to peak intensity of problem
I = 0.5*c*n0_Est*epsilon0.*abs(Efield).^2/Area(1);
IPeak = Energy/Tau_t/Area(1);

% Now adjust amplitude of electric field acordingly
Efield = sqrt(IPeak)/sqrt(max(I))*Efield;
I = 0.5*c*n0_Est*epsilon0.*abs(Efield).^2/Area(1);

% Comment off if you are not chirping the pulse
%{
% How to chirp the pulse:
%   I chirp the pulse by shifting the constituent waves by exp(iwnz/c) .
%   A side effect of chirping the pulse this way is that is in now " located" at a different point in time
%   I then move the pulse location back in time toward t = 0 sec without changing the pulse characteristics by multiplying by exp(iw (-1.3)z/c).

% To chirp the pulse (negatively chirped to counter GVD at retina):
% Go to frequency domain
EfieldFreq = fftshift(fft(Efield));
% Chirp and shift back in time towards the origin (t = 0)
EfieldFreq = EfieldFreq.*exp(+1i*Omega.*(n0-1.3)*0.0244/c);
% Go back to time domain
Efield = ifft(ifftshift(EfieldFreq));
% Update intensity
I = 0.5*c*n0_Est*epsilon0.*abs(Efield).^2/Area(1);
IPeak = max(I);
%}
% End of pulse chirping --------------------------------------------------

% Save initial values for comparison
I0 = I; % Save for comparison
E0 = Efield; % Save for Comparison
E0Freq = fftshift(fft(E0)); % Save for comparison

%% Set up graphs
% ___Parameters for graphs___
Lambda_nm = 2*pi()*c*1e9./Omega;
ViewVec = (X/2+20000):(X/2+275000); % Long run view from 200 nm
                                    % to 2500 nm
```

```
% Constants for the for loops (improves compuational speed to initialize here)
IConst = 0.5*c*n0_Est*epsilon0; % Constant part of intensity calc.
DVec = -1i*Omega.*n0*dx/c -abs(Omega).*k0*dx/c; % Constant part of linear propagator term
DVec_Lens = -1i*Omega.*n0*dx/c - 0.4*abs(Omega).*k0*dx/c;   % Constant part of linear propagator (Reduced absorption)
ExpDVec = exp(DVec); % Faster to pre-compute this value
ExpDVec_Lens = exp(DVec_Lens); % Faster to pre-compute this value (Reduced absorption)
NConst = -1i*w0*n2*(dx/2)/c - beta*(dx/2)/2;    % Constant part of nonlinear propagator
AreaNow = Area(1);  % Initialize variable here
R4 = zeros(StopTotal,1);
R4(1) = R(1);
PlasmaFlag = 0; % No plasma generated yet

%% Plot/Save initial behavior
%{
% Time plot
figure;
plot(TimeVec*10e12, I0, 'k')
title(['Intensity at 0 mm for ' num2str(lambda0*1e9) ' nm beam'])
xlabel('Time (ps)')
ylabel('I(t)')
legend({'Input Pulse'},'Location','northeast')

% Looking in the frequency domain
figure;
semilogy(Lambda_nm(ViewVec),abs(E0Freq(ViewVec)/X).^2/Area(1),'k')
title(['Power Spectral Density at 0 mm for ' num2str(lambda0*1e9)...
    ' nm beam'])
xlabel('Wavelength (nm)')
ylabel('|E|^2/Area')
legend({'Input Pulse'},'Location','northeast')
ylim([1e-5 1e15])
%}

% Path files are output CSV files that can be analyzed
% or made into videos
pathA = ['Lambda.csv' ];
csvwrite(pathA,Lambda_nm(ViewVec));

pathB = ['Intensity_In_' num2str(lambda0*1e9) 'nm.csv' ];
csvwrite(pathB,I0);

pathC = ['Spectra_In_' num2str(lambda0*1e9) 'nm.csv' ];
csvwrite(pathC,abs(E0Freq(ViewVec)/X).^2/Area(1));

%% Propagate from cornea to lens through aqueous humor:
for(PositionCtrA = 1:StopA)
    % Steps 0 - 2 are only needed for set up.
```

```
% Step 3: Get the area
% Find where you are
PositionCtr = PositionCtrA;

% Find self-focusing corrected radius
if(PositionCtr == 1)                    % If just starting simulation
    R4(PositionCtr) = R(1);
elseif((PositionCtr-1)*dx < DistFocus)     % If before focal point
    % Find angle of descent linear & nonlinear
    Theta_Linear = abs(tan((R(PositionCtr)-R(PositionCtr-1))/dx));
    Theta_Nonlinear = sqrt(2*n2*IPeak/n0_Est);

    R4(PositionCtr) = max(R4(PositionCtr-1) - atan(sqrt(Theta_Linear^2 + Theta_Nonlinear^2))*dx,RStop);
else                                    % If after focal point
    % Find angle of descent linear & nonlinear
    Theta_Linear = abs(tan((R(PositionCtr)-R(PositionCtr-1))/dx));
    Theta_Nonlinear = sqrt(2*n2*IPeak/n0_Est);

    if(Theta_Linear < Theta_Nonlinear) % && Nonlinear focusing
                                       % dominates
        R4(PositionCtr) = max(R4(PositionCtr-1) - atan(sqrt(-Theta_Linear^2 + Theta_Nonlinear^2))*dx,RStop);
    else                               % && Linear de-focusing dominates
        R4(PositionCtr) = max(R4(PositionCtr-1) + atan(sqrt(+Theta_Linear^2 - Theta_Nonlinear^2))*dx,RStop);
    end
end

% Find area
AreaNow = pi*R4(PositionCtr)^2;
%AreaNow = pi*R(PositionCtr)^2; % Uncomment to disable self-focusing

% Step 4: Calc intensity
I = IConst.*abs(Efield).^2/AreaNow;

% Step 5: Split step nonlinear term
Efield = Efield.*exp(NConst*I);

% Step 6: Convert to frequency domain
EfieldFreq = fftshift(fft(Efield));

% Step 7: Propagate dx forward in space
EfieldFreq = EfieldFreq.*ExpDVec;

% Step 8: Convert back to time domain
Efield = ifft(ifftshift(EfieldFreq));

% Step 9: Split step nonlinear term
I = IConst.*abs(Efield).^2/AreaNow;
```

```
    Efield = Efield.*exp(NConst*I);

    % Step 10: Calc intensity for self-focusing in next step
    I = IConst.*abs(Efield).^2/AreaNow;
    IPeak = max(I);

    % Check for plamsa generation
    if(IPeak > 2e17)
       if(PlasmaFlag == 0)
           PlasmaFlag = 1; % Plasma has been formed
           pathP = ['PlasmaWarningAt_' num2str(PositionCtr*dx) ' mm_'
               num2str(lambda0*1e9) 'nm.csv' ];
           csvwrite(pathP,1e6*R4(PositionCtr));
       end
    end
end

%% Record result at lens
pathD = ['IntensityAt_' num2str((StopA)*1000*dx) ' mm_' num2str(
    lambda0*1e9) 'nm.csv' ];
csvwrite(pathD,I);

pathE = ['SpectraAt_' num2str((StopA)*1000*dx) ' mm_' num2str(lambda0
    *1e9) 'nm.csv' ];
csvwrite(pathE,abs(EfieldFreq(ViewVec)/X).^2/Area(StopA));

% Plot values at lens (4 mm)
%{
    I = 0.5*c*n0_Est*epsilon0.*abs(Efield).^2/Area(StopA);
    figure;
    plot(TimeVec*10e12, I0, 'k')
    hold on
    plot(TimeVec*10e12, I,'r')
    hold off

    title(['Intensity at ' num2str(StopA*1000*dx) ' mm for ' num2str(
       lambda0*1e9) ' nm beam'])
    xlabel('Time (ps)')
    ylabel('I(t)')
    legend({'Input Pulse','Pulse at Position'},'Location','northeast')

    % Looking in the frequency domain
    figure;
    semilogy(Lambda_nm(ViewVec),abs(E0Freq(ViewVec)/X).^2/Area0,'k')
    hold on
    semilogy(Lambda_nm(ViewVec),abs(EfieldFreq(ViewVec)/X).^2/Area(
       StopA),'r--')
    hold off

    title(['Power Spectral Density at ' num2str(StopA*1000*dx) ' mm
       for ' num2str(lambda0*1e9) ' nm beam'])
    xlabel('Wavelength (nm)')
```

```
    ylabel('|E|^2/Area')
    legend({'Input Pulse','Pulse at Position'},'Location','northeast')
%}

%% Propagate through the lens

% Let's assume that the lens acts like water but with only 40 the
    absorbance of water

for(PositionCtrB = 1:StopB)

    % Step 3: Get the area
    % Find where you are
    PositionCtr = StopA + PositionCtrB;

    % Find angle of descent linear & nonlinear
    Theta_Linear = abs(tan((R(PositionCtr)-R(PositionCtr-1))/dx));
    Theta_Nonlinear = sqrt(2*n2*IPeak/n0_Est);

    % Find self-focusing corrected radius
    if((PositionCtr-1)*dx < DistFocus)     % If before focal point
       R4(PositionCtr) = max(R4(PositionCtr-1) - atan(sqrt(
           Theta_Linear^2 + Theta_Nonlinear^2))*dx,RStop);
    else                                   % If after focal point
        if(Theta_Linear < Theta_Nonlinear) % && Nonlinear focusing
            dominates
            R4(PositionCtr) = max(R4(PositionCtr-1) - atan(sqrt(-
                Theta_Linear^2 + Theta_Nonlinear^2))*dx,RStop);
        else                               % && Linear de-focusing
            dominates
            R4(PositionCtr) = max(R4(PositionCtr-1) + atan(sqrt(+
                Theta_Linear^2 - Theta_Nonlinear^2))*dx,RStop);
        end
    end

    % Find area
    AreaNow = pi*R4(PositionCtr)^2;
    %AreaNow = pi*R(PositionCtr)^2; % Uncomment to disable self-
        focusing

    % Step 4: Calc intensity
    I = IConst.*abs(Efield).^2/AreaNow;

    % Step 5: Split step nonlinear term
    Efield = Efield.*exp(NConst*I);

    % Step 6: Convert to frequency domain
    EfieldFreq = fftshift(fft(Efield));

    % Step 7: Propagate dx forward in space
    EfieldFreq = EfieldFreq.*ExpDVec_Lens;
```

```
    % Step 8: Convert back to time domain
    Efield = ifft(ifftshift(EfieldFreq));

    % Step 9: Split step nonlinear term
    I = IConst.*abs(Efield).^2/AreaNow;
    Efield = Efield.*exp(NConst*I);

    % Step 10: Calc intensity for self-focusing in next step
    I = IConst.*abs(Efield).^2/AreaNow;
    IPeak = max(I);

    % Check for plamsa generation
    if(IPeak > 2e17)
        if(PlasmaFlag == 0)
            PlasmaFlag = 1; % Plasma has been formed
            pathP = ['PlasmaWarningAt_' num2str(PositionCtr*dx) ' mm_'
                num2str(lambda0*1e9) 'nm.csv' ];
            csvwrite(pathP,1e6*R4(PositionCtr));
        end
    end

end

%% Record the value at the vitreous humor (8 mm)
pathD = ['IntensityAt_' num2str((StopA + StopB)*1000*dx) ' mm_'
    num2str(lambda0*1e9) 'nm.csv' ];
csvwrite(pathD,I);

pathE = ['SpectraAt_' num2str((StopA + StopB)*1000*dx) ' mm_' num2str(
    lambda0*1e9) 'nm.csv' ];
csvwrite(pathE,abs(EfieldFreq(ViewVec)/X).^2/Area(StopA + StopB));

% Plot values at vitreous humor (8 mm)
%{
    I = 0.5*c*n0_Est*epsilon0.*abs(Efield).^2/Area((StopA + StopB));
    figure;
    plot(TimeVec*10e12, I0, 'k')
    hold on
    plot(TimeVec*10e12, I,'r')
    hold off

    title(['Intensity at ' num2str((StopA + StopB)*1000*dx) ' mm for '
        num2str(lambda0*1e9) ' nm beam'])
    xlabel('Time (ps)')
    ylabel('I(t)')
    legend({'Input Pulse','Pulse at Position'},'Location','northeast')

    % Looking in the frequency domain
    figure;
    semilogy(Lambda_nm(ViewVec),abs(E0Freq(ViewVec)/X).^2/Area0,'k')
    hold on
    semilogy(Lambda_nm(ViewVec),abs(EfieldFreq(ViewVec)/X).^2/Area((
```

```
        StopA + StopB)),'r--')
    hold off

    title(['Power Spectral Density at ' num2str((StopA + StopB)*1000*dx) ' mm for ' num2str(lambda0*1e9) ' nm beam'])
    xlabel('Wavelength (nm)')
    ylabel('|E|^2/Area')
    legend({'Input Pulse','Pulse at Position'},'Location','northeast')
%}

%% Propagate from end of lens to retinal plane

for(PositionCtrC1 = 1:StopC/Steps_Per_100um)
    for(PositionCtrC2 = 1:Steps_Per_100um)

        % Step 3: Get the area
        % Find where you are
        PositionCtr = StopA + StopB + (PositionCtrC1-1)*Steps_Per_100um+PositionCtrC2;

        % Find angle of descent linear & nonlinear
        Theta_Linear = abs(tan((R(PositionCtr)-R(PositionCtr-1))/dx));
        Theta_Nonlinear = sqrt(2*n2*IPeak/n0_Est);

        % Find self-focusing corrected radius
        if((PositionCtr-1)*dx < DistFocus)     % If before focal point
            R4(PositionCtr) = max(R4(PositionCtr-1) - atan(sqrt(Theta_Linear^2 + Theta_Nonlinear^2))*dx,RStop);
        else                                 % If after focal point
            if(Theta_Linear < Theta_Nonlinear) % && Nonlinear focusing dominates
                R4(PositionCtr) = max(R4(PositionCtr-1) - atan(sqrt(-Theta_Linear^2 + Theta_Nonlinear^2))*dx,RStop);
            else                             % && Linear de-focusing dominates
                R4(PositionCtr) = max(R4(PositionCtr-1) + atan(sqrt(+Theta_Linear^2 - Theta_Nonlinear^2))*dx,RStop);
            end
        end

        % Find area
        AreaNow = pi*R4(PositionCtr)^2;
        %AreaNow = pi*R(PositionCtr)^2; % Uncomment to disable self-focusing

        % Step 4: Calc intensity
        I = IConst.*abs(Efield).^2/AreaNow;

        % Step 5: Split step nonlinear term
        Efield = Efield.*exp(NConst*I);

        % Step 6: Convert to frequency domain
```

```
        EfieldFreq = fftshift(fft(Efield));

        % Step 7: Propagate dx forward in space
        EfieldFreq = EfieldFreq.*ExpDVec;

        % Step 8: Convert back to time domain
        Efield = ifft(ifftshift(EfieldFreq));

        % Step 9: Split step nonlinear term
        I = IConst.*abs(Efield).^2/AreaNow;
        Efield = Efield.*exp(NConst*I);

        % Step 10: Calc intensity for self-focusing in next step
        I = IConst.*abs(Efield).^2/AreaNow;
        IPeak = max(I);

        % Check for plamsa generation
        if(IPeak > 2e17)
            if(PlasmaFlag == 0)
                PlasmaFlag = 1; % Plasma has been formed
                pathP = ['PlasmaWarningAt_' num2str(PositionCtr*dx) '
                    mm_' num2str(lambda0*1e9) 'nm.csv' ];
                csvwrite(pathP,1e6*R4(PositionCtr));
            end
        end

    end

    % Record information every 4 mm
    if(mod(PositionCtrC1,40)==0)
        %{
        figure;
        plot(TimeVec*10e12, I0, 'k')
        hold on
        plot(TimeVec*10e12, I,'r')
        hold off

        title(['Intensity at ' num2str((StopA + StopB + PositionCtrC1*
            Steps_Per_100um)*1000*dx) ' mm for ' num2str(lambda0*1e9) '
             nm beam'])
        xlabel('Time (ps)')
        ylabel('I(t)')
        legend({'Input Pulse','Pulse at Position'},'Location','
            northeast')

        % Looking in the frequency domain
        figure;
        semilogy(Lambda_nm(ViewVec),abs(E0Freq(ViewVec)/X).^2/Area0,'k
            ')
        hold on
        semilogy(Lambda_nm(ViewVec),abs(EfieldFreq(ViewVec)/X).^2/Area
            ((StopA + StopB + PositionCtrC1*Steps_Per_100um)),'r--')
```

```
        hold off

        title(['Power Spectral Density at ' num2str((StopA + StopB + PositionCtrC1*Steps_Per_100um)*1000*dx)
        xlabel('Wavelength (nm)')
        ylabel('|E|^2/Area')
        legend({'Input Pulse','Pulse at Position'},'Location','northeast')
        %}


        pathD = ['IntensityAt_' num2str((StopA + StopB + PositionCtrC1*Steps_Per_100um)*1000*dx) ' mm_' num2str(lambda0*1e9) 'nm.csv' ];
        csvwrite(pathD,I);

        pathE = ['SpectraAt_' num2str((StopA + StopB + PositionCtrC1*Steps_Per_100um)*1000*dx) ' mm_' num2str(lambda0*1e9) 'nm.csv' ];
        csvwrite(pathE,abs(EfieldFreq(ViewVec)/X).^2/Area((StopA + StopB + PositionCtrC1*Steps_Per_100um)));
    end
end

%% Calculate resulting pulse at retina
% Calculate I at retina:
%REnd = Rfoc*sqrt(1+((StopA+StopB+StopC)*dx-DistFocus)^2/xR^2);
%AEnd = pi()*REnd^2;
AEnd = pi()*R4(StopA+StopB+StopC)^2;
I = 0.5*c*n0_Est*epsilon0.*abs(Efield).^2/AEnd;

% Save results
pathF = ['Intensity_Retina_' num2str(lambda0*1e9) 'nm.csv' ];
csvwrite(pathF,I);

pathG = ['Spectra_Retina_' num2str(lambda0*1e9) 'nm.csv' ];
csvwrite(pathG,abs(EfieldFreq(ViewVec)/X).^2/AEnd);

%{
% Looking in the time domain
plot(TimeVec*10e12, I0, 'k')
hold on
plot(TimeVec*10e12, I, 'r')
hold off
title(['Intensity at ' num2str(1000*Stop*dx) ' mm in Time Domain for ' num2str(lambda0*1e9) ' nm beam'])
xlabel('Time (ps)')
ylabel('I(t)')
legend({'Input Pulse','Pulse at Retina'},'Location','northeast')
figure;
%}
```

```
%{
% Looking in the frequency domain
figure;
semilogy(Lambda_nm(ViewVec),abs(E0Freq(ViewVec)/X).^2/Area0,'k')
hold on
semilogy(Lambda_nm(ViewVec),abs(EfieldFreq(ViewVec)/X).^2/AEnd,'r--')
hold off
%plot(2*pi()*c*1e9./Omega,abs(EfieldFreq(1:(X/2+1))/X).^2)
title(['Power Spectral Density out of cuvette for ' num2str(lambda0*1
    e9) ' nm beam'])
xlabel('Wavelength (nm)')
ylabel('|E|^2/Area')
legend({'Input Pulse','Pulse at Retina'},'Location','northeast')
ylim([1e-6 1e14])
%}

%% Now propagate past nonlinear region in eye tissue. Assume
% same linear/nonlinear properties as water.
for(PositionCtrD = 1:StopD)

    % Step 3: Get the area
    % Find where you are
    PositionCtr = StopA + StopB + StopC + PositionCtrD;

    % Find angle of descent linear & nonlinear
    Theta_Linear = abs(tan((R(PositionCtr)-R(PositionCtr-1))/dx));
    Theta_Nonlinear = sqrt(2*n2*IPeak/n0_Est);

    % Find self-focusing corrected radius
    if((PositionCtr-1)*dx < DistFocus)    % If before focal point
        R4(PositionCtr) = max(R4(PositionCtr-1) - atan(sqrt(
            Theta_Linear^2 + Theta_Nonlinear^2))*dx,RStop);
    else                                 % If after focal point
        if(Theta_Linear < Theta_Nonlinear) % && Nonlinear focusing
                                           % dominates
            R4(PositionCtr) = max(R4(PositionCtr-1) - atan(sqrt(-
                Theta_Linear^2 + Theta_Nonlinear^2))*dx,RStop);
        else                               % && Linear de-focusing
                                           % dominates
            R4(PositionCtr) = max(R4(PositionCtr-1) + atan(sqrt(+
                Theta_Linear^2 - Theta_Nonlinear^2))*dx,RStop);
        end
    end

    % Find area
    AreaNow = pi*R4(PositionCtr)^2;
    %AreaNow = pi*R(PositionCtr)^2; % Uncomment to disable self-
        focusing

    % Step 4: Calc intensity
    I = IConst.*abs(Efield).^2/AreaNow;
```

```
    % Step 5: Split step nonlinear term
    Efield = Efield.*exp(NConst*I);

    % Step 6: Convert to frequency domain
    EfieldFreq = fftshift(fft(Efield));

    % Step 7: Propagate dx forward in space
    EfieldFreq = EfieldFreq.*ExpDVec;

    % Step 8: Convert back to time domain
    Efield = ifft(ifftshift(EfieldFreq));

    % Step 9: Split step nonlinear term
    I = IConst.*abs(Efield).^2/AreaNow;
    Efield = Efield.*exp(NConst*I);

    % Step 10: Calc intensity for self-focusing in next step
    I = IConst.*abs(Efield).^2/AreaNow;
    IPeak = max(I);

    % Check for plamsa generation
    if(IPeak > 2e17)
        if(PlasmaFlag == 0)
            PlasmaFlag = 1; % Plasma has been formed
            pathP = ['PlasmaWarningAt_' num2str(PositionCtr*dx) ' mm_'
                num2str(lambda0*1e9) 'nm.csv' ];
            csvwrite(pathP,1e6*R4(PositionCtr));
        end
    end

end

% Calculate intensity at end of simulation
%REnd2 = Rfoc*sqrt(1+((StopA+StopB+StopC+StopD)*dx-DistFocus)^2/xR^2);
%AEnd2 = pi()*REnd2^2;
AEnd2 = pi()*R4(StopA+StopB+StopC+StopD)^2;
I = 0.5*c*n0_Est*epsilon0.*abs(Efield).^2/AEnd2;

% Save values
pathF = ['Intensity_BeyondRetina_' num2str(lambda0*1e9) 'nm.csv' ];
csvwrite(pathF,I);

pathG = ['Spectra_BeyondRetina_' num2str(lambda0*1e9) 'nm.csv' ];
csvwrite(pathG,abs(EfieldFreq(ViewVec)/X).^2/AEnd2);

pathH = ['Radius_'  num2str(lambda0*1e9) 'nm.csv' ];
csvwrite(pathH,1e6*R4);
```

LIST OF SYMBOLS, ABBREVIATIONS, AND ACRONYMS

β	nonlinear absorption
α_0	linear absorption
n_0	linear refractive index
n_2	nonlinear refractive index
AFRL	Air Force Research Laboratory
ANSI	American National Standards Institute
fs	femtosecond
GNLSE	generalized nonlinear Schrödinger equation
GVD	group velocity dispersion
LIB	laser induced breakdown
MPE	Maximum Permissible Exposure
near-IR	near-infrared
NLSE	nonlinear Schrödinger equation
nm	nanometer
REM	reduced eye model
SBS	stimulated Brillouin scattering
SPM	Self-phase modulation
SRS	stimulated Raman scattering
XPM	cross-phase modulation